

2005

Nanofiber-crack interaction in a carbon nanofiber reinforced composite

Anis Gawandi
University of Dayton

Follow this and additional works at: https://ecommons.udayton.edu/graduate_theses

Recommended Citation

Gawandi, Anis, "Nanofiber-crack interaction in a carbon nanofiber reinforced composite" (2005). *Graduate Theses and Dissertations*. 2840.

https://ecommons.udayton.edu/graduate_theses/2840

This Dissertation is brought to you for free and open access by the Theses and Dissertations at eCommons. It has been accepted for inclusion in Graduate Theses and Dissertations by an authorized administrator of eCommons. For more information, please contact mschlange1@udayton.edu, ecommons@udayton.edu.

NANOFIBER - CRACK INTERACTION IN A CARBON NANOFIBER
REINFORCED COMPOSITE

Dissertation submitted to,
The School of Engineering of the
UNIVERSITY OF DAYTON

In partial fulfillment of the requirement for
The degree
Doctor of Philosophy in Materials Engineering


By
Anis A. Gawandi


UNIVERSITY OF DAYTON
Dayton, Ohio

October 2005


NANOFIBER – CRACK INTERACTION IN A CARBON NANOFIBER REINFORCED COMPOSITE

APPROVED BY:

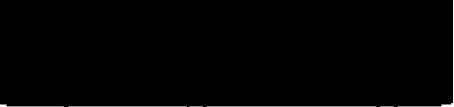

James M. Whitney, Ph.D.
Professor, Civil and Environmental Engineering and
Engineering Mechanics
Committee Chairman



Robert A. Brockman, Ph.D.
Professor, Civil and Environmental
Engineering and Engineering
Mechanics
Committee Member



Daniel Eylon, Ph.D.
Professor and Chair
Department of Materials Engineering
Committee Member


Youssef Roffoul, Ph.D.
Professor, Department of Mathematics
Committee Member


G. P. Tandon, Ph.D.
Distinguished Research Engineer
University of Dayton Research Institute
Committee Member


Thomas J. Whitney, Ph.D., P.E.
Research Engineer
University of Dayton Research Institute
Committee Member


Joseph E. Saliba, Ph.D., P.E.
Dean, School of Engineering


Donald L. Moon, Ph. D.
Associate Dean
Graduate Engineering Programs and Research
School of Engineering

ABSTRACT

NANOFIBER – CRACK INTERACTION IN A CARBON NANOFIBER REINFORCED COMPOSITE

Name: Anis Gawandi
University of Dayton

Advisor: Dr. James M. Whitney

The fracture behavior of a nanocomposite reinforced with carbon nanofibers is characterized by considering the interactions between a propagating matrix crack and nanofibers. The nanofibers considered in the study have a hollow structure and transversely isotropic elastic properties. The nanoscale dimensions of these fibers render the experimental measurement of elastic properties very difficult. At the same time, the elastic properties are likely to show a significant variation with a lack of controllability. The nanofiber wall thickness is not constant and instead shows a range of values. The fracture characterization of nanofiber-reinforced composites needs to account for the influence of nanofiber hollow geometry and the interphase between the nanofiber and matrix. However, research work reported to date has been mostly empirical. Analytical studies that consider nanofiber hollow geometry in conjunction with fracture behavior have not been reported.

In the present work, an insight is gained into the energetics of a matrix crack propagating towards a nanofiber using an analytical approach. Two-dimensional and three-dimensional studies are performed to compute energy release rates. Mixed mode configurations are also incorporated to evaluate mode II behavior. Additionally, secondary failure mechanisms are investigated by computing the maximum values of interface tractions and their locations. The results of the investigation indicate that the nanofiber wall thickness can have a significant influence on crack energetics. Also, the presence of an interphase between a nanofiber and matrix alters the crack energetics considerably.

ACKNOWLEDGEMENTS

I would like to thank my committee members for their guidance in the fulfillment of this work. First of all, I thank my doctoral study advisor Dr. James Whitney for his support and guidance throughout this effort. Thank you for all the help and encouragement that led to my growth and accomplishments. I would also like to thank Dr. Robert Brockman for his immense help and guidance with the finite element analysis work. Dr. Brockman, I am grateful to you for all those enlightening discussions despite your busy schedule. To Dr. G. P. Tandon, thank you for your insight from time to time, and for making sure that this work shaped up the way it has. To Dr. Danny Eylon, thank you, this Ph D study would not have been possible without your help. Thanks to Dr. Tom Whitney for giving me the opportunity to be a part of the Ohio Aerospace Institute project, which resulted in this thesis work. Thanks also to Dr. Yossuf Raffoul, the mathematical concepts I learned from your classes have been great help.

This work would not have been possible without the support and sacrifices of my wife Shakira and my children Aariz and Shifa. You are the light of my life, my strength, and every reason of enchantment in my life. To my parents and brothers, thanks for your support all these years. I am indebted to Dayton Area Graduate Studies Institue (DAGSI) for the financial support that made this endeavor possible. Thanks are also due to Ohio Supercomputer Center (OSC) for the computational support. Thanks to Dr. Joseph Saliba for encouraging me to pursue doctoral studies, and to Cheryl Seitz of the Materials Engineering Department for all the help.

TABLE OF CONTENTS

ABSTRACT	iii
ACKNOWLEDGEMENTS.....	iv
LIST OF FIGURES.....	vii
LIST OF TABLES.....	xiii
LIST OF SYMBOLS/ABBREVIATIONS.....	xiv
CHAPTER	
I.	
INTRODUCTION.....	1
Problem Statement	
Objectives	
II. LITERATURE REVIEW.....	4
Carbon Nanofiber Reinforced Composites	
Fracture Characterization of Nanofiber Reinforced Composites	
Toughening Mechanisms	
Crack – Inclusion Interaction	
Summary	
III. ANALYSIS APPROACH.....	26
Assumptions	
Analysis Tool	
Two-Dimensional Problem	
Three-Dimensional Problem	
IV. CHARACTERIZATION OF THE INFLUENCE OF NANAFIBER MODULI AND POISSON'S RATIO.....	46
Characterization of the Influence of Nanofiber Moduli	
Characterization of the Influence of Nanofiber Poisson's Ratio	
V. CHARACTERIZATION OF THE INFLUENCE OF NANOFIBER WALL THICKNESS.....	79
Characterization Approach	

Influence of Nanofiber Wall Thickness on Mode I Behavior	
Influence of Nanofiber Wall Thickness on Mode II Behavior	
Influence of Nanofiber Wall Thickness on Interface Traction	
Influence of Nanofiber Wall Thickness on the Locations of Maximum Traction	
VI. CHARACTERIZATION OF THE INFLUENCE OF AN INTERPHASE BETWEEN THE NANOFIBER AND MATRIX.....	100
Influence of Interphase Elastic Modulus	
Influence of Interphase Thickness	
VII. CHARACTERIZATION OF THE INFLUENCE OF NANOFIBER DIAMETER.....	113
Influence of Nanofiber Diameter on Mode I Behavior	
Influence of Nanofiber Diameter on Mode II Behavior	
VIII. CONCLUSIONS AND RECOMMENDATIONS.....	120
Summary of Variables	
Significant Results	
Recommendations for Experimental Validation	
Desirable Nanofiber Properties for Fracture	
Recommendations for Future Work	
Recommendations for Material Scientists	
REFERENCES.....	129

LIST OF FIGURES

Figure 1. Single nanofiber.....	8
Figure 2. Nanofiber bundle.....	8
Figure 3. Carbon nanofiber graphitic structure	9
Figure 4. Schematic of the nanofiber-crack interaction problem.....	28
Figure 5. Two-dimensional finite element model.....	28
Figure 6. Details of finite element mesh showing hollow fiber and crack oriented at..... $\theta = 0$	29
Figure 7. Mesh details near crack-tip L.....	29
Figure 8. Schematic of the three-dimensional problem.....	36
Figure 9. Schematic of the portion to be modeled.....	36
Figure 10. Schematic showing nanofiber longitudinal section.....	37
Figure 11. Geometric parameters in three-dimensional study.....	37
Figure 12. Successive crack positions.....	38
Figure 13. Coarse Model.	39
Figure 14. Submodel.....	39
Figure 15. Variation of energy release rate for a propagating crack.....	48
Figure 16. Influence of E_R on G_I/G_{I0} , $\theta = 0$	50
Figure 17. Influence of E_R on G_I/G_{I0} , $\theta = 22.5$	50
Figure 18. Influence of E_R on G_I/G_{I0} , $\theta = 45$	51
Figure 19. Influence of E_R on G_I/G_{I0} , $\theta = 45$ and $t_w = 20\text{nm}$	51
Figure 20. Influence of E_R on G_{II}/G_{II0} , $\theta = 22.5$	52
Figure 21. Influence of E_R/E_m on G_{II}/G_{II0} , $\theta = 45$	52
Figure 22. Influence of E_R/E_m on G_{II}/G_{II0} , $\theta = 22.5$ and $t_w = 20\text{nm}$	53

Figure 23. Energy release rate along the crack front	55
Figure 24. Energy release rate along all crack fronts.....	55
Figure 25. Variation of G_I at closest and farthest points on the crack front.....	57
Figure 26. Mode I energy release rate at $\theta = 90$ (point c) at successive crack positions for various fiber orientations.....	57
Figure 27. Mode I energy release rate along the farthest crack front position for various nanofiber orientations	58
Figure 28. Mode I energy release rate along the closest crack front position for various nanofiber orientations.....	58
Figure 29. Mode I energy release rate for various nanofiber anisotropy ratios	59
Figure 30. Mode I energy release rate for various nanofiber anisotropy ratios.....	59
Figure 31. Mode I energy release rate for various nanofiber anisotropy ratios.....	60
Figure 32. Normal and shear components of interface traction.....	62
Figure 33. Measurement of location of maximum normal and shear tractions at the nanofiber-matrix interface.....	62
Figure 34. Influence of E_f/E_m on maximum interface normal traction.....	63
Figure 35. Influence of E_f/E_m on maximum interface normal traction.....	63
Figure 36. Influence of E_f/E_m on maximum interface shear traction.....	64
Figure 37. Influence of E_f/E_m on maximum interface shear traction.....	64
Figure 38. Location of maximum normal traction as a function of the nanofiber transverse modulus	66
Figure 39. Location of maximum normal traction as a function of the nanofiber transverse modulus	66
Figure 40. Location of maximum normal traction as a function of the crack orientation.....	67
Figure 41. Location of maximum shear traction as a function of the nanofiber modulus.....	67
Figure 42. Location of maximum shear traction as a function of the nanofiber modulus	68
Figure 43. Location of maximum shear traction as a function of the crack orientation	68
Figure 44. Influence of Poisson's ratio mismatch of nanofiber and matrix on G_I/G_{I0} , $t_w = 10$ nm.....	71
Figure 45. Influence of Poisson's ratio mismatch of nanofiber and matrix on G_I/G_{I0} , $t_w = 20$ nm.....	71

Figure 46. Influence of Poisson's ratio mismatch of nanofiber and matrix on G_I/G_{I0} , $t_w = 35$ nm.....	72
Figure 47. Influence of Poisson's ratio mismatch of nanofiber and matrix on G_I/G_{I0} , $t_w = 50$ nm.....	72
Figure 48. Influence of Poisson's ratio mismatch of nanofiber and matrix on G_I/G_{I0} , $\theta = 45$	73
Figure 49. Influence of Poisson's ratio mismatch of nanofiber and matrix on G_{II}/G_{II0} , $\theta = 22.5$	74
Figure 50. Influence of Poisson's ratio mismatch of nanofiber and matrix on G_{II}/G_{II0} , $\theta = 45$	74
Figure 51. Influence of Poisson's ratio mismatch of nanofiber and matrix on maximum interfacial normal traction, $\theta = 0$	76
Figure 52. Influence of Poisson's ratio mismatch of nanofiber and matrix on maximum interfacial normal traction, $\theta = 22.5$	76
Figure 53. Influence of Poisson's ratio mismatch of nanofiber and matrix on maximum interfacial normal traction, $\theta = 45$	77
Figure 54. Influence of Poisson's ratio mismatch of nanofiber and matrix on maximum interfacial shear traction, $\theta = 0$	77
Figure 55. Influence of Poisson's ratio mismatch of nanofiber and matrix on maximum interfacial shear traction, $\theta = 22.5$	78
Figure 56. Influence of Poisson's ratio mismatch of nanofiber and matrix on maximum interfacial shear traction, $\theta = 45$	78
Figure 57. Influence of the nanofiber wall thickness on G_I/G_{I0}	81
Figure 58. Influence of the nanofiber wall thickness on G_I/G_{I0}	82
Figure 59. Influence of the nanofiber wall thickness on G_I/G_{I0}	82
Figure 60. Influence of the nanofiber wall thickness on G_I/G_{I0}	83
Figure 61. Influence of the nanofiber wall thickness on G_I/G_{I0}	83
Figure 62. Influence of the nanofiber wall thickness on G_I/G_{I0}	84
Figure 63. Influence of the nanofiber wall thickness on G_I/G_{I0}	84
Figure 64. Mode I energy release rate at point 'c' ($\theta=90$) for successive crack front positions.....	85
Figure 65. Mode I energy release rate at point 'c' ($\theta=90$) for successive crack front positions.....	85

Figure 66. Influence of nanofiber wall thickness on Mode I energy release rate along the crack front.....	86
Figure 67. Influence of nanofiber wall thickness on Mode I energy release rate along the crack front	86
Figure 68. Influence of the nanofiber wall thickness on G_{II}/G_{IIO}	88
Figure 69. Influence of the nanofiber wall thickness on G_{II}/G_{IIO}	88
Figure 70. Influence of the nanofiber wall thickness on G_{II}/G_{IIO}	89
Figure 71. Influence of the nanofiber wall thickness on G_{II}/G_{IIO}	89
Figure 72. Influence of the nanofiber wall thickness on the behavior of maximum interface normal traction.....	92
Figure 73. Influence of the nanofiber wall thickness on the behavior of maximum interface shear traction	92
Figure 74. Influence of the nanofiber wall thickness on maximum interface normal traction.....	93
Figure 75. Influence of the nanofiber wall thickness on maximum interface normal traction.....	93
Figure 76. Influence of the nanofiber wall thickness on maximum interface shear traction.....	94
Figure 77. Influence of the nanofiber wall thickness on maximum interface shear traction.....	94
Figure 78. Influence of the nanofiber wall thickness on maximum interface shear traction.....	95
Figure 79. Influence of the nanofiber wall thickness on the location of maximum interface normal traction.....	97
Figure 80. Location of maximum interface normal traction for various values of nanofiber wall thickness (t_w).....	98
Figure 81. Location of maximum interface normal traction for various values of nanofiber wall thickness (t_w).....	98
Figure 82. Location of maximum interface shear traction for various values of nanofiber wall thickness (t_w).....	99
Figure 83. Influence of interphase elastic properties on mode I crack behavior.....	103
Figure 84. Influence of a stiff and a compliant interphase on G_I/G_{IO}	104
Figure 85. Influence of a stiff and compliant interphase on the mode I energy release rate.....	104

Figure 86. Influence of a stiff and compliant interphase on the mode I energy release rate at the farthest crack position.....	105
Figure 87. Influence of a stiff and compliant interphase on the mode I energy release rate at the closest crack position.....	105
Figure 88. Influence of a stiff and a compliant interphase on G_{II}/G_{II0}	107
Figure 89. Schematic of the results for the investigation of the Influence of the interphase thickness on G_I/G_{I0}	110
Figure 90. Influence of the interphase thickness on G_I/G_{I0} when the interphase is compliant than the matrix	112
Figure 91. Influence of the interphase thickness on G_I/G_{I0} when the interphase is stiffer than the matrix.....	112
Figure 92. Influence of the nanofiber diameter on G_I/G_{I0}	114
Figure 93. Influence of the nanofiber diameter on G_I/G_{I0}	114
Figure 94. Influence of the nanofiber diameter on G_I/G_{I0}	115
Figure 95. Influence of the nanofiber diameter on G_I/G_{I0}	115
Figure 96. Influence of nanofiber diameter on Mode I energy release rate along the crack front	118
Figure 97. Influence of nanofiber diameter on Mode I energy release rate along the crack front.....	118
Figure 98. Influence of the nanofiber diameter on G_{II}/G_{II0}	119
Figure 99. Influence of the nanofiber diameter on G_{II}/G_{II0}	119

LIST OF TABLES

Table 1. Selected values of normalized mode I stress intensity factors.....	34
Table 2. Isolated influence of interphase.....	101
Table 3. Incorporation of the effect of a stiff nanofiber.....	101
Table 4. Reference cases.....	101
Table 5. Details of the models considered to investigate the influence of the interphase thickness.....	109

LIST OF SYMBOLS/ABBREVIATIONS

a	Half crack length
θ	Crack orientation
ϕ	Orientation of the nanofiber longitudinal axis with respect to the stress axis
r_i	Nanofiber inner radius
r_o	Nanofiber outer radius
r	Distance of left crack-tip from the center of the fiber along global x axis
K_{IL}	Mode-I stress intensity factor at the left crack-tip
K_{IR}	Mode-I stress intensity factor at the right crack-tip
K_{IIL}	Mode-II stress intensity factor at the left crack-tip
K_{IIR}	Mode-II stress intensity factor at the right crack-tip
SR_{max}	Maximum normal traction at fiber-matrix interface
SRT_{max}	Maximum shear traction at fiber-matrix interface
S	Applied uniaxial stress
E_m	Matrix elastic modulus
E_{fL}	Nanofiber longitudinal modulus
E_{ft}	Nanofiber transverse modulus
ν_{ft}	Nanofiber transverse Poisson's ratio
ν_{fl}	Nanofiber longitudinal Poisson's ratio
ν_m	Matrix Poisson's ratio
t_w	Nanofiber wall thickness
E_i	Elastic modulus of the interphase between the nanofiber and matrix
ν_i	Poisson's ratio of the interphase between the nanofiber and matrix

t_i	Thickness of the interphase between the nanofiber and matrix
NDE	Nodal Displacement Extrapolation
APDL	ANSYS Parametric Design Language

CHAPTER I

INTRODUCTION

Nanocomposites are new kind of composite materials that comprise resin reinforced with nanometer-sized reinforcement. The discovery of carbon nanotubes in the nineties and other nanoscale materials subsequently has made it possible to reinforce the matrix material at nanoscale. Exceptional mechanical properties have been reported for nanoscale materials. As a result, it is expected that there will be substantial improvement in stiffness, strength and other thermo-mechanical properties of a composite containing very small weight percent of nanoscale reinforcement. Also, the presence of nanofiller may be helpful with regard to traditionally 'weak links' in composites like through the thickness properties and matrix-dominated properties (like fracture toughness).

One type of above mentioned nanoscale materials is vapor grown carbon nanofibers (VGCNF). Carbon nanofibers have recently attracted much attention as a potential resin reinforcement material. These fibers are hollow and at a diameter range of 100 to 200 nanometer, considerably larger than nanotubes. From the mechanics standpoint, the nanofiber properties are orthotropic (transversely isotropic). Carbon nanofibers are expected to offer an economical alternative to conventional fibers and other potential nanoscale reinforcement materials like nanotubes without sacrificing mechanical properties. Also, due to their relatively larger dimensions, nanofibers are expected to offer much better controllability.

Problem Statement

Although materials like carbon nanofibers seem to be promising as potential composite reinforcement, analytical characterization work on the same is still in its infancy. Fracture characterization is one such area. Although there has been some empirical work reported in

conjunction with the fracture characterization of nanofiber reinforced composite, there are hardly any analytical fracture studies reported to date. On the other hand, nanofibers, when studied from the perspective of their influence on fracture behavior of composite, make it necessary to consider various new aspects. Nanofibers have hollow cylindrical geometry, and as a consequence a certain wall thickness. A hollow geometry has not been considered to date when evaluating the influence of the stiff reinforcement on a matrix crack. Also, there is expected to be a dominant interphase region in a nanofiber-reinforced matrix material due to the nanoscale dimensions of nanofibers.

The other challenge presented by nanofibers when it comes to fracture characterization, is the lack of controllability as compared to conventional fibers. As a result the nanofiber structure shows a large variation and as a consequence significant variations in their geometry and probably elastic properties. All the aforementioned variables need consideration when characterizing the fracture behavior. The first step towards understanding the fracture behavior for a nanofiber-reinforced matrix is to consider interaction between a crack and nanofiber.

The interaction between a stiff or compliant inclusion (or fiber) and a crack has been an active area of research, especially since the advent of composite materials. Although various configurations and inclusion shapes have been considered, no effort has considered the interaction between a material like nanofiber and a matrix crack. Especially, hollow fiber geometry has not been considered and an interphase region between the fiber and matrix has not received much attention when it comes to a crack-inclusion interaction problem. The present study considers these issues and characterizes the fracture behavior in a nanofiber-reinforced composite by investigating the nanofiber-crack interaction.

Objectives

The objective of this study is to investigate the fracture behavior of a carbon nanofiber-reinforced composite. To this end, the nanofiber-crack interaction is considered . To include

maximum possible material and geometric parameters in the analysis, both two-dimensional and three dimensional finite element studies are performed.

Mixed mode energy release rates are computed for various parametric configurations. Especially, the influence of the nanofiber anisotropy and its hollow structure on the crack energetics is studied. Besides the fracture parameter like energy release rate nanofiber-matrix interface tractions are investigated for a secondary failure mechanism. Maximum values of the normal and shear components of the interface tractions and their corresponding locations are obtained.

CHAPTER II

LITERATURE REVIEW

Reinforcing matrix at nanometer scale is a new challenge for composites technology. But doing so has a potential to cause a dramatic enhancement in thermo-mechanical properties of composite materials. Uniform dispersion of nanoscale reinforcement in a matrix means a tremendous increase in surface area and surface energy. The interfacial area between the constituents per volume of the material can be compared to having a football field within a raindrop [1]. The nanoscale size of material means little probability of having a defect. Thus, one expects that nanoscale materials will exhibit exceptional mechanical properties, and research work reported to date corroborates the expectation. Various nano-reinforcements being investigated today include equiaxed (Carbon Black, Silica), tubular (Carbon Nanofibers, Carbon Nanotubes, Silicate Nanotubes), and platelets (Nano-clay).

Above are the examples of potential nano-reinforcement in zero, one, and two dimensions respectively. As mentioned above, excellent thermo-mechanical properties have been reported for some of the above materials. For example, elastic modulus values of up to 1 TPa and 600 GPa respectively, have been reported for single wall carbon nanotubes and vapor grown carbon nanofibers [2]. If these materials can be incorporated into matrix, the benefits of nanoscale reinforcement can be combined with the traditional composite structure to yield a multi-scale hybrid micro/nanocomposite [2].

Although nanocomposites offer dramatic potential property enhancements, there are various challenges with their processing and characterization that must be overcome to realize this potential. So far, dispersing nanofillers uniformly in matrix, and controlling their orientation has proved to be a significant challenge. Another major challenge has been that of

fiber wetting by the matrix. Observed composite stiffness and strength values have been significantly less than predicted [3]. This has been attributed to poor fiber-matrix adhesion.

One type of nanofillers currently being explored is vapor grown carbon nanofibers (VGCNF). With strong mechanical properties [4], these nanofibers are a promising class of nano-reinforcement materials. Like other nanoscale reinforcement types, carbon nanofibers have presented processing challenges in terms of uniform dispersion and adhesion with resin. In the absence of reasonable degree of either or both of these, stiffness and strength values reported have been lower than predicted [5]. Recently, fiber surface functionalization techniques have been reported [6], which add to the fiber surface, functional groups (like amine group) that improve adhesion with matrix. Also, improved mixing techniques have largely alleviated the problem of uniform dispersion of the nanofibers in the matrix [7].

It is well known that composite materials offer great advantage owing to their specific stiffness (stiffness per weight) and specific strength (strength per weight). But due to the preferential direction (orthotropic material properties) of property enhancement, a lamina has poor transverse and through the thickness thermo-mechanical properties, which are typically matrix dominated. Reinforcing the weak matrix phase by nano-sized filler material is expected to dramatically improve these weak links. Theoretically, if nanofibers can be oriented in the through the thickness direction, the properties in that direction will be significantly improved. One of the matrix-dominated properties that may also be significantly affected is fracture toughness. Effect of nano-reinforcement on the fracture toughness of resin with or without the presence of conventional fibers is an important area to explore.

Fracture in composite materials is a complex phenomenon owing to its inherent multiphase structure. Delamination and matrix cracking are the primary fracture phenomena observed in composite materials. Being the main life limiting damage modes, their characterization and possible toughening mechanisms has attracted considerable research effort. Fracture toughness of a composite has, thus come to be identified with the resistance to the above phenomena. Nanosized reinforcement of resin is expected to improve its

thermo-mechanical properties. But, fracture characterization of nanofiller-reinforced composite is still in its infancy with most of the work reported being empirical in nature.

As one considers fracture behavior in the presence of nanoscale constituent, it is important to study basic toughening or weakening mechanisms by considering an interaction between a nanoscale flaw and the nanofiller. The first challenge here would be that of the analytical approach. A crack problem can be considered at any scale. But, at nano scale the structure may resemble a lattice structure more than a continuum. Whether continuum mechanics is valid and if it is not, at what scale does it ceases to be applicable is a question still being investigated. A bottom up approach like molecular dynamics can accurately simulate the atomic nature of the materials, but is still subject to severe length and time scale limitations [8]. On the other hand continuum mechanics is not subject to length and time limitations, but is phenomenological and may be inaccurate at nanoscale. At the same time recent research based on the experimental work and molecular dynamics simulations has indicated that materials like nanofibers can be considered within the framework of continuum mechanics as anisotropic homogeneous inclusions with large aspect ratio [9]. Odegard [10] predicted the elastic modulus of a single wall nanotube reinforce composite by modeling the single wall nanotube (SWNT), local polymer near the nanotube, and nanotube-polymer interface as an effective continuum fiber. Bulk properties were assumed for the polymer surrounding the fiber and a perfect bond was assumed between the nanotube and the polymer. In another work, Odegard [11] developed a method to serve as a link between computational chemistry and solid mechanics by substituting discrete molecular structures with equivalent continuum models. The various contributions to atomic potential were summed and the system was modeled as a truss with the truss members substituting for the atomic bonds. Equating the strain energy of the truss members to that of the total atomic potential expressions for elastic properties was developed. Wei [12] et al. developed a general analytic expression for the Young's modulus of a range of carbon nanofibers with single or multishell nanocone or cone-stacked structures from the continuum elastic theory.

One field in which the continuum and atomistic approaches depend on each other quite essentially is that of fracture mechanics [13]. As one surveys the literature for fracture characterization of resins or composites reinforced with nanofillers in general and carbon nanofibers in particular, one can't help but notice overwhelmingly empirical nature of the approach and may be as a consequence, lack of analytical studies. The literature review presented below is divided into five categories that broadly describe vapor grown carbon nanofiber reinforced composites and their fracture characterization. Various toughening mechanisms are then discussed. Finally, crack-fiber interaction and common approaches to analyze this problem are discussed.

Carbon Nanofiber Reinforced Composites

Vapor grown carbon nanofibers are currently being explored as potential composite reinforcement. The fibers are grown from hydrocarbons in the gas phase using metallic particles as catalysts [14]. Nanofibers are hollow with an outer diameter in the range of 100 nm to 200 nm (figure 1). Like the overall diameter, the wall thickness of a nanofiber also shows a range of values and can be as small as ten percent of the fiber diameter [15]. This wall comprises layers of Graphene sheets slightly inclined with respect to the fiber longitudinal axis (figure 3). Nanofibers are approximately 150 times smaller than conventional carbon fibers but significantly larger than nanotubes (1 to 10 nm diameter). The length of the fibers is 30,000 nm to 100,000 nm [4] giving them an aspect ratio of greater than 100. But, as the fibers are not straight (figure 2), the effective aspect ratio may be less [7]. The geometry of nanofibers can be measured using microscopy techniques like transmission electron microscopy (TEM, to measure inner and outer diameter) and tests like bulk density (to measure length).

On the other hand, due to their very small dimensions, mechanical properties of nanofibers are extremely difficult to measure experimentally. Although the elastic properties are reported to be orthotropic [9], the values are not very well known. At the same time, in the

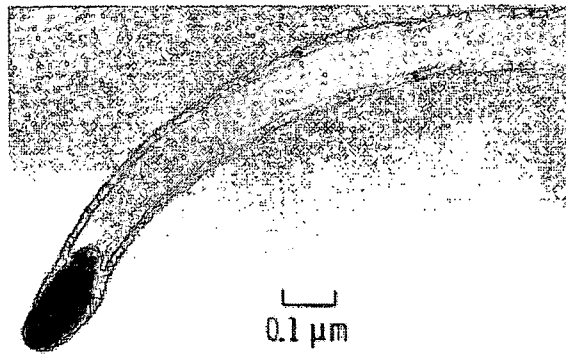


Figure 1. Carbon nanofiber

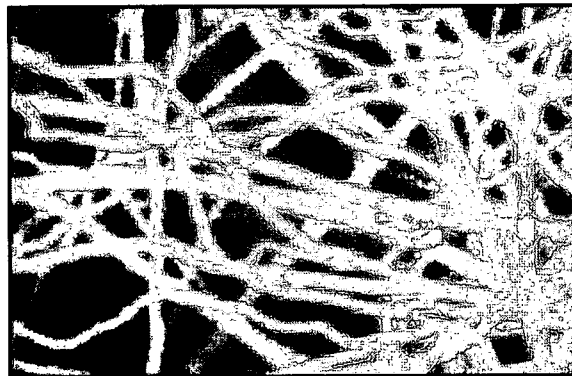


Figure 2. Carbon nanofibers in a bundle

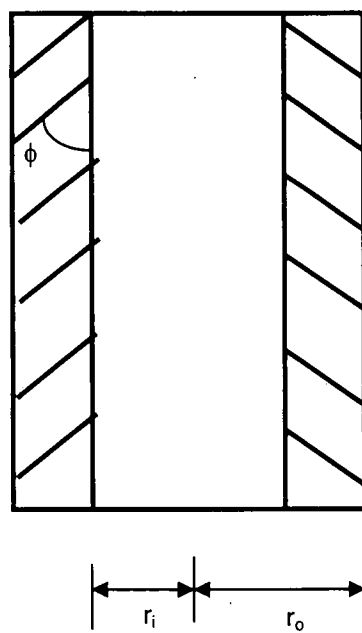


Figure 3. Carbon nanofiber graphitic structure

absence of controllability of nanofiber structure, the nanofiber elastic properties are likely to show a significant variation. As mentioned above, a nanofiber wall comprises graphite layers (figure 3). As the orientation of these layers changes, the nanofiber properties like elastic moduli and Poisson's ratio are likely to vary [12].

The use of carbon fibers in composites is restricted by its high production cost, which is about \$23 per pound. Carbon nanofibers can provide a cost-effective alternative to conventional fibers for both military and commercial applications [16]. Though they cannot be produced by standard techniques, with new processing methods, they can be much less expensive to produce. The Air Force Research Laboratory (AFRL) expects their cost to be at approximately \$ 3 per pound. The cost effectiveness can come with additional but not less important benefits like high stiffness and thermal conductivity without the need for high temperature treatment.

Fracture Characterization of Nanofiber-Reinforced Composites

The fracture behavior of the advanced composite materials is considerably different from and more complex than that of metals. Although composite materials are statically brittle they show no propensity for the nucleation and growth of a through crack as exhibited in metals [17]. Cracks can be arrested before growing to catastrophic proportion due to laminate geometry. Composites are inherently multiphase materials and as a result have interfaces/interphase that may affect the energy release rate. Also, the cracks can be diverted along certain structural features in such a way that crack surfaces may retain traction by the way of frictional contact between the two fracture surfaces [18].

Fracture characterization in nanocomposites in general is still in its infancy. Most of the work on mechanical properties seems to be related with the stiffness and strength of the nano-fillers themselves. Fracture characterization so far seems to be overwhelmingly empirical and most of it is focused on nanoparticles as nano-reinforcement. With regards to

nanofiber-reinforced composite, not much is reported on any analytical modeling, although literature survey does yield a few empirical studies.

Tandon [7] used vapor grown carbon nanofibers (PR24-PS) in Epon862 epoxy resin and IM7 carbon fibers. He developed SEM/TEM technique to determine nanofiber lengths representing in-situ values. Compact tension tests on resin with nanofibers gave K_{IC} 20 to 23 percent higher than that for the neat resin. The enhancement seemed to be more with the higher percentage of nanofibers. The mode-I and mode-II fracture toughness data was obtained from the double cantilever and end notch flexure tests on the unidirectional specimen that included nanomatrix and IM7 regular carbon fibers. The fracture toughness values obtained however showed no significant change due to the addition of nanofibers, indicating that the behavior in the presence of both regular fibers and nanofibers is dominated by considerably larger regular fibers.

Shofner et al. [19] considered fracture behavior of ABS resin reinforced with up to ten percent vapor grown carbon nanofibers. Tensile tests were conducted and fracture surface studied. Results indicated that carbon nanofibers change the fracture behavior of the ABS polymer from ductile to brittle, as bonding at the fiber-matrix interface is not ideal. The fracture behavior was observed to be similar to that of tightly cross-linked resins where molecular network was unable to deform sufficiently.

Wu [20] performed experimental and analytical work on the edge effects in conjunction with the concept of suppression of delamination based on nanofiber reinforcement of interfaces between plies in advanced laminated composites. The nanofiber used had a diameter of 300 nm. Laminate lay-up was designed to induce maximum free-edge stresses using a modified numerical scheme based on semi-analytic Lekhnitski stress potentials. Static and fatigue tension test results showed statistically significant improvements in edge-delamination onset stress. DCB and ENF tests were carried to assess rate effects on mode-I and II fracture. A phenomenological fracture model was developed based on thermal activation concept. Substantial improvement in interlaminar fracture toughness was recorded

as a result of nanofiber reinforcement. An improvement in mode-I and II dynamic fracture toughness was also reported based on dynamic finite element analyses. Results also showed that the presence of nanofibers resulted in substantial delays in crack initiation.

As evident from the above literature review, nanofibers seem to influence the fracture behavior of the composite. As we try to link the experimental observations to analytical reasoning it is worthwhile to look at some of toughening mechanisms in composites. These mechanisms can be the consequence of the inherent structure of the composite or can be induced.

Toughening Mechanisms

Like the plastic zone at the crack tip in a ductile metal that requires energy dissipation and enhances fracture toughness, various phenomena take place in a fiber reinforced composite materials that provide resistance to crack driving force and thus increase the critical energy release rate thereby enhancing the fracture toughness. The toughening mechanisms in composites can exist as a consequence of their inherent structure or can be introduced by adding a second phase.

Toughening by second phase particles

Since the fracture toughness of a composite is a matrix dominant property, significant effort has been directed towards improving the fracture toughness of the resin itself [21]. Especially, if the matrix is brittle like commonly used epoxy, one of the most widely studied techniques is the addition of elastomeric toughening agent to the resin. The elastomeric additive forms a dispersed phase of soft inclusions in the brittle resin, which increases the fracture toughness of the neat resin through a crack blunting mechanism. The improvement in the fracture toughness occurs primarily because of a dilatational deformation of the soft inclusions in the triaxial stress field at the crack tip. As a result, large crack-tip plastic deformation zones develop in the elastomer-modified resin. However, the relative increase in

the toughness of a composite is not as high as bulk resin. The presence of the fibers in a composite restricts the size of the deformation zones reducing the degree of load distribution away from the crack tip [21]. Therefore, the increase in the interlaminar fracture toughness of composites is much smaller fraction of their neat resin fracture toughness.

Toughening by Adhesion Control

Another technique to increase the fracture toughness in composites is to control the adhesion between fiber and matrix. It has been shown [22] that the translation of the resin toughness to mode I delamination composite toughness is highly dependent on fiber-matrix adhesion. In case of a weak bond between the two, resin participation in the fracture resistance is restricted. Increasing the level of adhesion between the fiber and the matrix or tailoring the interface results in significant improvement in the fracture toughness.

Fiber Bridging

Fiber bridging is a toughening mechanism wherein the propagating crack leaves fibers intact [23]. The unbroken fibers exert a traction force on the crack surfaces similar to the Dugdale-Barenblatt [24, 25] yield strip model. As a result, crack propagation is met with an increased resistance. Thus the energy release rate increases with the crack length. This is known as the R-curve effect. The higher fracture energy is associated with de-bonding of the surface area of bridged fibers and breaking of these fibers. Several analytical models have been presented in literature to describe fiber crack bridging. Most of them consider an array of parallel fibers bridging the crack based on the assumption that the action of the bridging fibers can be well approximated by closing pressure acting on crack faces [26]. Also, most models assume that energy dissipation mechanism is through fiber-matrix debonding and frictional sliding. In some models the closing pressure is derived using shear lag analysis, while in others a constant bridging stress is assumed. In other works closing tractions are related to crack opening displacement.

Matrix dominated fracture represents minimum value of fracture toughness [27]. Fiber bridging causes expenditure of energy to overcome bridging traction in the process of crack extension. Thus, one over-estimates the fracture toughness. If fiber bridging can't be guaranteed in the structure the fracture toughness value associated with fiber bridging will be unconservative.

The toughening mechanisms discussed above are associated with macro-scale fracture behavior. The dimensions of the rubber particles used as second phase for toughening are on the order of few micrometers. The fiber-bridging models are associated with conventional fibers that are micrometer sized and may be present in as high a volume fraction as 65 percent. It is not clear if these toughening mechanisms will be present when size of the toughening agent is on the nanometer scale and volume fraction is low.

Although enhancement of properties of metals by adding a second phase and of resins by adding fibers have been established technologies, analytical studies considering the interaction between an inclusion (or a fiber) and a crack received attention only around late sixty to early seventies. Initial works on this problem were those by Tamate [28] and Erdogan [29]. There has since been steady although not considerable research effort expended on the same. Following section presents literature review on crack-inclusion interaction.

Crack-Inclusion Interaction

The initial work on the subject of an interaction between a crack and an inclusion was more from the perspective of a metallic inclusion in a matrix. With the advent and growing application of composite materials, the area of the research work broadened to be relevant to the toughening mechanisms related with a crack in a polymer or ceramic matrix interacting with a fiber. Literature search reveals that although a circular inclusion shape is most common, other shapes like elliptical and square have also been considered with various geometric and loading configurations.

Analytical Approaches

As the literature search below reveals, the conventional analytical treatment of the crack-fiber interaction problem has been mostly two-dimensional in nature in that the fiber cross-section lies in crack-plane (plane of crack propagation). Typically, an isotropic fiber is considered in an infinite isotropic matrix. The exact elasticity treatment of a more complex three-dimensional problem where the orientations are arbitrary is very complicated and hence not much has been reported on the same [29]. As we review the literature, we come across four prominently used approaches, which are the singular integral equation method, the weight function method, the boundary element method, and the finite element method [30].

Singular integral equation methods have been widely used to analyze crack-fiber interaction problems. The basic approach involves modeling crack as a distribution of dislocations. Using solutions for the dislocations as Green's functions a system of singular integral equations is then obtained [30]. The singularity is then extracted and the resulting nonsingular integral equations can be solved easily. This approach yields excellent solutions, however it requires an extensive analytic formulation that is different for each new problem. For three-dimensional problems, the derivation of integral equations can be cumbersome. Details of the method can be found in [31].

The weight function method employs weight functions, which are first order tensors that depend only on the geometry of the cracked body. Given the weight function for a particular configuration, it is possible to compute stress intensity factors for any boundary conditions. A weight function can be interpreted as the stress intensity resulting from a unit force applied to the crack face [23].

The boundary element formulation is based on Betti's theorem. In this approach, the boundary element method (BEM), the boundary of the domain of interest is discretized using elements, which are interconnected at discrete points called nodes. For three-dimensional problem, the mesh is two-dimensional and for two-dimensional problems, the mesh is one-dimensional. The boundary element method is particularly attractive for the reason that only

the boundaries in the given configuration need to be discretized. It is a quickly convergent and very robust method for the solutions of elasticity problems involving cracks. It is often computationally superior to the finite element method for two-dimensional problems. For three-dimensional problems, boundary element method is computationally expensive as the resulting linear system of equations is dense, unbanded, and often unsymmetrical. Details of the boundary element method can be found in [32]

Recently, finite element method has become a natural choice for crack problems as it can handle a wide variety of crack geometries involved, not to mention the complex loadings [33]. The finite element method (FEM) is perhaps most versatile of the approaches discussed herein. The formulation of the finite element method is based on a variational representation of governing equations. Although whole domain is discretized, unlike the boundary element method the resulting system of algebraic equations is relatively banded and symmetric for most problems. Indeed, computation of two-dimensional stress intensity factors for linear elastic fracture mechanics (LEFM) is now commonplace in commercial finite element software. Even for nonlinear fracture problems finite element method is now widely employed [34]. The drawback of the finite element method is need for remeshing, which can be time consuming in case of a crack-propagation analysis.

Research Efforts to Date

Various configurations of crack-inclusion interaction have been considered after the initial works of Tamate and Erdogan: a crack near an inclusion; a crack terminating on the inclusion-matrix interface; and a crack partially penetrating or inside an inclusion, are some of the commonly analyzed configurations. Although, majority of work reported so far deals with a single inclusion and a crack case, multiple inclusions interacting with a single or multiple cracks have also been investigated. In terms of inclusion geometry, circular, and elliptical inclusion shapes are most common, although other shapes have also been considered.

As mentioned earlier Tamate [28] and Erdogan [29] were the first ones to consider crack-inclusion interaction problem. Tamate used complex stress potentials to investigate the effect of a circular elastic inclusion on an external radial crack. For the case of uniaxial loading, a Laurent series expansion was determined for the complex stress potentials required for solving the resulting dual Hilbert problem. It was shown that a relatively rigid inclusion decreases the stress intensity factor of the crack whereas a more compliant inclusion increases it.

Erdogan et al. [29] considered an arbitrarily oriented straight crack interacting with a circular elastic inclusion embedded into an elastic matrix. The solution was obtained by superposition of two solutions for plane strain or generalized plane stress conditions. The first one was the problem of a circular elastic inclusion inserted into a matrix without the crack. The second one was the stress disturbance due to the existence of the crack. The first problem was solved using the existing solutions for the edge dislocations as Green's functions. The integral equations for the second problem involving a line crack were obtained as a system of singular integral equations with simple Cauchy kernels. Various crack orientations were considered and corresponding stress intensity factors given. For the material properties that roughly corresponded to a metallic inclusion embedded into an epoxy type matrix, results indicated that as the crack tip approaches, the inclusion-matrix interface stress intensity factor goes to zero. Also, the model predicted that for an inclusion softer than the matrix the crack would propagate toward the interface and for an inclusion stiffer than the matrix the crack would deviate away from it.

Cheeseman et al. [35] considered a curved matrix crack interacting with a circular elastic inclusion. The problem was formulated using the Kolosov-Muskhelishvili complex stress potential technique where the crack was represented by unknown distributions of dislocations. The resulting singular integral equations were solved by the Lobatto-Chebyshev quadrature technique. Results indicated that for a parabolic crack interacting with an inclusion, the inclusions stiffness and the crack's curvature were competing influences. Unlike

the case of a straight crack, there exist geometries and loadings where a stiff inclusion does not shield the crack, but could actually enhance the stress intensity factor depending on the crack's curvature.

Helsing et al. [36] considered the same problems as in [29] and [35] and computed the results using an algorithm based on a pair of integral equations for the crack and inclusion problem. More recently Wang et al. [37] solved the same problems as mentioned above using Galerkin boundary integral (GIB) method and a complex variable boundary element method. Both these methods are based on a complex hypersingular integral equation written in terms of the tractions on the boundary of the inclusion and the displacement discontinuities along the crack.

Helsing [38] considered elastostatic problem involving a crack close to and in front of an inclusion interface and presented a stable algorithm based on integral equations of Fredholm's second kind. Using this algorithm stress intensity factors were computed and compared with those of cracks close to straight infinite bimaterial interface. Muller [39] applied the techniques in [33] in his investigation of external radial cracks in fiber-reinforced composites under thermal and mechanical loadings. Patton et al. [40] considered the problem of a crack interacting with an elliptical inclusion. Using Kolosov-Muskhelishvili complex potential approach to formulate the dislocation problem with care taken to include the effect of the elliptical inclusion's rigid body rotation, the resulting singular equations were numerically solved.

Among the works on a crack terminating at the inclusion-matrix interface are those by Atkinson [41], Erdogan et al. [42], and Romeo et al. [43]. Another class of problems is the one involving cracks inside or partially penetrating an inclusion. Selvadurai [44] considered the problem of penny-shaped crack which is formed by the development of a crack in both the fiber and the matrix in composite containing an isolated elastic fiber in an infinite matrix. He used two integral-equation based approaches for the analysis. The first approach considered formulation of complete integral equations governing the associated elasticity problem for a

two-material region. The second approach considered the boundary integral equation formulation of the problem. Numerical solutions were obtained from both methods and stress intensity factors computed. The stress intensity values obtained were greater when fiber was present as opposed to when the crack was in matrix without fiber being present.

Mao et al. [45] solved the problem of crack penetrating into or deflecting at the fiber-matrix interface using boundary element method. The possible penetration into the fiber or deflection of the crack along the interface was predicted using the ratio of energy release rate along the two directions. Steif et al. [46] considered a crack partially penetrating an inclusion. The influence of moduli difference on the reduction of stress intensity factors was evaluated by using the complex potential approach. Qin et al. [47] considered the problem of interactions between an inclusion and multiple cracks in a thermopiezoelectric solid using boundary element method. Stress intensity factors were computed using the least-squares method incorporating the boundary element method. The stress intensity factors agreed well with those from other numerical methods.

Li et al. [48] developed expression for stress intensity factors for a crack that partially penetrates an inclusion of arbitrary shape. The closed form solution is valid for the case when the inclusion size is small compared with the length of the crack and other dimensions of the cracked body. Finite element analyses were performed to verify the accuracy of the formula developed. Results from the analyses matched those predicted by the model.

Li et al. [49, 50] modeled the process zone that contains an array of defects as an elastic inclusion in order to consider the interaction between a crack and an array of defects in the process zone. The crack was modeled as penetrating the inclusion and finite element method was used as the computational tool. Crack propagation towards the inclusion was simulated by placing the crack tip at different positions. Energy release rates were computed for various inclusion shapes. It was found that a soft inclusion results in amplification effect on energy release rate, whereas a rigid inclusion results in crack shielding as it approaches the

inclusion. It was also observed that both amplification and shielding effects of the inclusion decrease as the ratio of inclusion and matrix elastic moduli approaches one.

There have also been research efforts that take in to account the effects of an interphase region between a fiber and matrix in conjunction with the crack-fiber interaction problems. Knight et al. [51] performed a parametric study of the interaction between a propagating edge- crack and an embedded elastic fiber using the boundary element technique. Both uncoated and coated fibers were considered and energy release rates computed for uniaxial loading conditions in plane strain. Elastic moduli, Poisson's ratios, and crack-offset distance from the inclusion centerline were the parameters. It was observed that as the Poisson's ratios for the matrix and the fiber phases became more incompressible ($\nu_l = \nu_m \rightarrow 0.5$) the crack sensed the presence of inclusion much less and hence experienced reduced shielding. Also, by including coating as a third phase with different elastic properties distinct changes in crack-tip energetics were observed. For a thin coating the solutions approached those of two-phase model with E_f/E_m dominating the behavior, whereas with increasing coating thickness E_c/E_m influenced the solutions more.

Xiao et al. [52] considered the interaction between a coated fiber and a line crack. The two-dimensional problem was solved for far field tensile and shear loading conditions. The crack was modeled as a continuous distribution of edge dislocations so that the problem could be formulated using Green's function approach that yields singular integral equations. The results indicated that the thickness and the elastic properties of the coating had a considerable effect on the stress intensity factor. Also, it was observed that as the thickness of the coating decreased the stress intensity factor values approached those for the two-phase (inclusion and fiber) system.

Cheeseman et al. [53] considered the problem of a radial or circumferential matrix crack interacting with a circular inclusion surrounded by an interphase region. The problem was formulated using Kolosov-Muskhelishvili complex potentials where the crack was modeled as a distribution of dislocations. The influence of interphase stiffness and thickness on a radial or

circumferential matrix crack was studied for a glass fiber-epoxy composite. The results indicated that compliant interphases increased the mode I stress intensity factors for radial cracks where as stiff interphases provided a shielding effect.

Most crack-fiber interaction studies reported to date assume a perfect fiber-matrix interface. But the interface can be imperfect for various reasons like debonding. Such features render interface imperfect and can significantly affect the crack-fiber interaction as the crack approaches interface. Liu et al. [54] used series method (which uses analytic continuation) to model an imperfect interface under various remote loading conditions. The model assumed continuous tractions and discontinuous displacements across the interface. Two non-negative and constant interface parameters were introduced in the formulation to model interface as perfect or imperfect. Infinite values of the interface parameters implied vanishing displacements across the interface where as finite values meant displacement jump across the interface and hence an imperfect interface. Results obtained showed that even when a stiff inclusion is present the stress intensity factors at the tip of radial matrix crack increased instead of decreasing as in the case of perfect interface. In fact it was observed that there was a critical value of interface parameters below which a radial matrix crack will grow toward a stiff inclusion instead of deviating as in case of a perfect interface.

Literature review of the crack-fiber interaction problem shows that there has not been much reported on fiber-matrix tractions which determine the probability of a secondary failure mechanism. Among the very few works is the effort by Bush [55] who studied the crack trajectory and energetics when a crack interacts with a single particle or a cluster of particles. The numerical approach used in the two-dimensional analyses was based on dual boundary integral method coupled with maximum energy release rate criteria to determine the direction of crack propagation. Interface tractions were monitored and it was observed that the interface tractions and stresses at the center of the particle were significantly amplified as the crack approached the inclusion. The elastic properties used were that of an Aluminum matrix with Silicon Carbide discontinuous reinforcement. Results showed that although the crack

senses the presence of the particle several particle diameters away it does not actually deflect until it is within one particle radius away from the inclusion. Also, it was observed that a cluster consisting of a large number of particles behaves qualitatively like a pair of particles. The energy release rate decreases as the crack approaches the cluster, implying increased fracture toughness.

The analysis of crack-fiber interaction has been predominantly considered for mode I conditions and there is relatively small body of work with regards to mode II crack energetics or mixed mode conditions. Yang et al. [56] analyzed the crack-inclusion interaction for a mode-II crack using Eshelby equivalent inclusion method. The solution technique was based on the transformation toughening theory. The closed form solutions to predict the variations in stress intensity factors were developed both for the cases when the crack tip was in the matrix and in the inclusion. Note that Eshelby equivalent inclusion theory is more accurate for an ellipsoidal inclusion in an infinite matrix. The other limitation to the solutions developed was that the inclusion size had to be small compared with the length of the crack and other dimensions of the cracked body.

In one of rare works of its kind, Shen An et al. [57] considered a plane problem of vertical contact between line crack and rigid line inclusion in an infinite matrix. Stresses and stress intensity factors near the crack tip were obtained using singular integral equation approach. Lam et al. [58] combined what were two different problems analyzed to date, which were crack-inclusion interaction and a branched crack in a matrix. They considered a symmetrically branched crack in front of a circular inclusion in an elastic infinite medium. They used the singular integral equation approach in which the branched crack was modeled as three straight cracks and each one of the intersecting cracks was treated as an unknown continuous distribution of edge dislocations. Mode-I and mode-II stress intensity factors were obtained at the branch tips for various crack-inclusion configurations. The results showed that an inclusion has an enhancement effect if it is softer than the matrix and shielding effect if it is harder.

Besides the circular or cylindrical inclusions, other inclusion shapes have also been considered. Chen [59] analyzed the interaction between an elliptical inclusion and a crack by body force method. The effect of inclusion shapes on the crack tip stress intensity factor was investigated. Noda [60] et al. considered a square array of inclusions under longitudinal tension. Generalized stress intensity factors at the corners of inclusions were computed with varying shape and spacing of a square array of square and rectangular inclusions.

The above literature review summarizes two-dimensional studies of various crack-fiber (inclusion) interactions. In many cases, two-dimensional studies may provide an upper bound on the shielding effect of a fiber on a crack in a matrix. A three-dimensional study may provide a more conservative analysis of the problem since arbitrary fiber or crack orientations can be considered and the influence can also be studied along the crack front, which in many cases is not possible through a two-dimensional analysis. At the same time a three-dimensional crack analysis becomes much more complex. An approach like J-integral is relatively easy to utilize in two-dimensions. However, in three dimensions, the contour integral becomes a surface integral and is extremely difficult to evaluate numerically [23]. Thus, perhaps not surprisingly there is comparatively much smaller body of work published on three-dimensional crack-inclusion interaction. A summary is presented below.

Dong et al. [61] used singular integral equation method to examine various crack-inclusion problems in three-dimensional infinite elastic domain. The inclusion and matrix were considered isotropic with the inclusion matrix modular ratio being approximately equal to two. Numerical implementation of the formulation consisted of using finite elements to discretize the crack and inclusion into isoparametric quadratic elements. Stress intensity factors and stresses at the interface in the inclusion and the matrix were computed. Computations showed that stress intensity factors, as the crack approached the inclusion, depended on whether the inclusion was soft or hard. The interface stresses at a given point were higher in the inclusion for a hard inclusion and lower when the inclusion was soft.

Larson [62] considered small-scale interaction of a three-dimensional matrix crack with a fiber. The experiments with a model brittle matrix and brittle fiber system recorded the three-dimensional crack growth history of an initial penny-shaped fracture that quasistatically propagated toward a cylindrical inclusion. The experimentally determined crack patterns supported the micromechanical computational simulations which were conducted using a three-dimensional surface integral method. Li [63] considered interaction between three-dimensional crack and near hard piezoelectric fiber. Finite element method was used to investigate the behavior under various combinations of electric and mechanical loadings.

Summary

Nanofibers are relatively novel materials with a promise of being a reinforcement material for composites. Nanofibers have a hollow cylindrical geometry with variable diameter and wall thickness values. Their elastic properties are difficult to measure and are likely to show a significant variation. The fracture characterization of nanofiber reinforced composite needs to take into account the hollow nanofiber geometry and variable elastic properties. Also, due to the nanoscale nature of the problem, an interphase region between a nanofiber and the matrix will be an important factor influencing the fracture behavior. However, the fracture characterization work to date remains empirical in nature. The literature review reveals a lack of analytical fracture models for a material system like nanofiber-reinforced composites.

Investigating the interaction between a stiff or compliant second phase like an inclusion or a fiber and a crack is an established way of understanding the fracture behavior of a material system. The literature search reveals that, although various configurations of an inclusion-crack interaction have been investigated, the problem is not considered in conjunction with a material like nanofibers. Thus, the influence of hollow fiber geometry on crack energetics remains to be investigated.

The literature search discussed in this chapter comprises a discussion on vapor grown carbon nanofibers and its potential influence on the fracture toughness of nanocomposite.

The lack of analytical models that describe the influence of such nanoscale material on fracture parameters and possible inadequacy of existing crack-inclusion interaction problem for the same make a strong case for an investigation to study the interaction between a hollow nanofiber and a crack.

CHAPTER III

ANALYTICAL APPROACH

The characterization of the influence of reinforcing nanofibers on the fracture behavior of a polymer matrix is investigated by considering the nanofiber – crack interaction. A crack is considered propagating self-similarly towards a nanofiber in an infinite matrix phase under uniaxial loading conditions. Energy release rate is computed for the propagating crack to evaluate the influence of the configuration being considered. For selected configurations, two-dimensional analysis results are corroborated by a three-dimensional analysis. To study secondary failure mechanisms like debonding, maximum values of interface normal and shear tractions are computed in the case of two-dimensional analyses. Also, the locations of these maximum traction components are observed as the crack propagates towards the nanofiber. As discussed in the literature review, nanofibers can be considered within the framework of continuum mechanics as anisotropic homogeneous inclusions [9]. The interaction studies are performed based on fracture mechanics principles and the analytical approach adopted is described in the following sections.

Assumptions

The material behavior is assumed to be linear elastic. The nanofiber-matrix bond is assumed to be perfect both at the nanofiber sides and ends. The nanofiber is considered to be straight and fiber end effects are neglected. The nanofiber properties are transversely isotropic whereas the matrix properties are isotropic. The matrix properties used are typically those for an Epoxy matrix. The crack growth in both two-dimensional and three-dimensional analyses is assumed to be self-similar. The crack propagation is assumed to take place in plane strain conditions.

Analysis Tool

As reviewed in the last chapter, there are various analytical approaches adopted in conjunction with the crack-fiber (inclusion) interaction. In this study, various geometric configurations are considered as a part of the parametric investigation. Also, Three-dimensional studies are performed. Accordingly, finite element method is chosen as the computational tool in this study as it is the most understood and versatile method for fracture mechanics problems and seems to be the most suitable given the geometry of the problem. All analyses are performed using ANSYS [64].

Two-Dimensional Problem

The two-dimensional crack propagation analysis considers the case when the nanofiber cross-section is in the plane of the crack extension. As mentioned earlier, nanofibers are transversely isotropic in terms of their elastic properties. In the two-dimensional investigation, the plane of isotropy lies in the plane of the crack extension. Thus, the nanofiber properties that need to be considered are the nanofiber transverse modulus and the transverse Poisson's ratio.

Schematic of Two-Dimensional Problem

The two-dimensional crack propagation analysis considers the case when the nanofiber cross-section is in the plane of the crack extension. As mentioned earlier, nanofibers are orthotropic (transversely isotropic) in terms of their elastic properties. In the two-dimensional investigation, the plane of isotropy lies in the plane of the crack extension. Thus, the nanofiber properties that need to be considered are the transverse modulus and the transverse Poisson's ratio. Figure 4 shows the schematic of the crack propagation analysis. The parameters describing the crack geometry are its initial length and orientation along with the crack tip location with respect to the nanofiber. Three different crack orientation angles are considered, namely, 0, 22.5, and 45 degrees measured from the global x – coordinate as

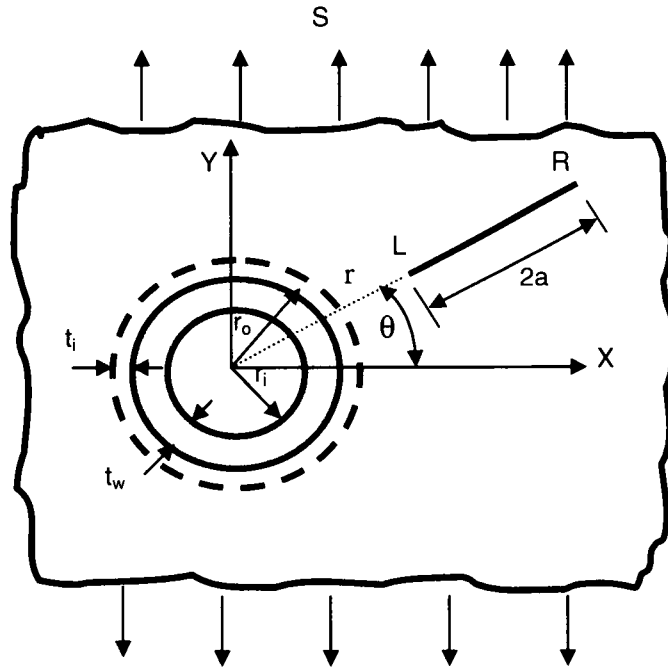


Figure 4. Schematic of the nanofiber-crack interaction problem

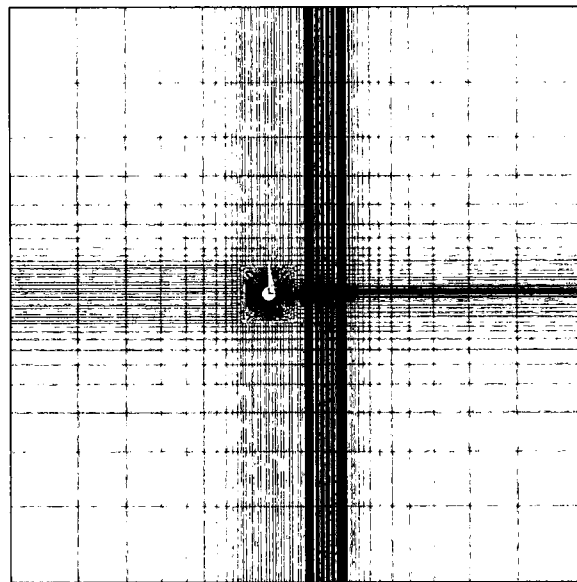


Figure 5. Two-dimensional finite element model

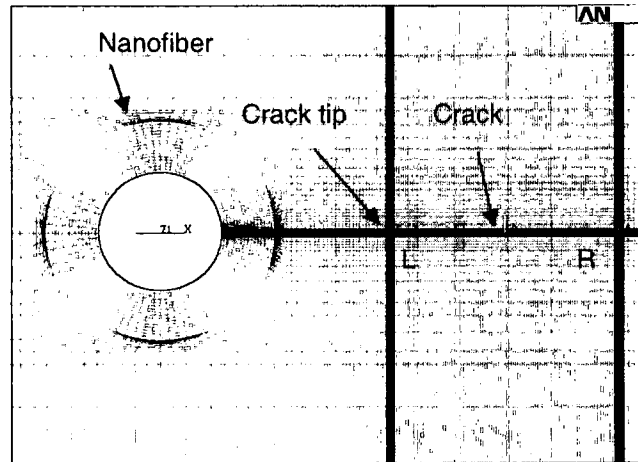


Figure 6. Details of finite element mesh showing hollow fiber and crack oriented at $\theta = 0$

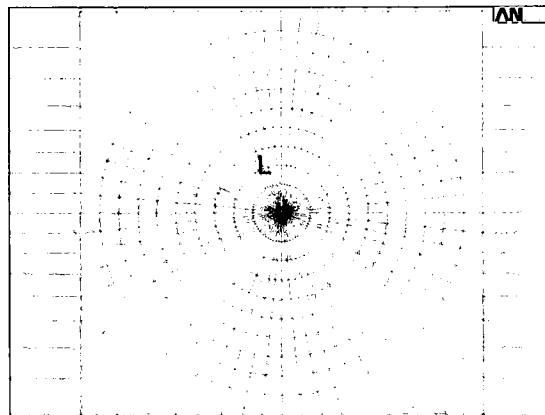


Figure 7. Mesh details near crack-tip L

shown in figure 4. For a crack orientation of 0 degrees, pure mode I conditions exist, whereas for the nonzero values of θ mixed mode conditions are created.

One technique to simulate crack propagation towards a nanofiber is to place the crack tip at various positions [19, 20]. Similar approach is adopted in the two-dimensional studies. A crack of length ($2a$) is propagated self-similarly towards the nanofiber center. The right crack tip (R) is fixed, whereas the left crack tip (L) is moved towards the nanofiber to simulate crack propagation. As figure 4 shows, at any given instant, the crack tip (L) is at a radial distance (r) from the nanofiber center. The initial crack length is assumed to be equal to the nanofiber diameter ($2r_o$). The farthest distance of the left crack tip L from the nanofiber center is four times the nanofiber outer radius (r_o), whereas the closest distance is approximately ten percent of the nanofiber outer radius from the nanofiber wall. In between, approximately 30 different crack tip positions are modeled. At each of these positions, energy release rates and maximum values of interface traction components along with their locations are computed.

Two-Dimensional Finite Element Model

The finite element modeling is performed using ANSYS® 8.1 [64]. The ANSYS Parametric Design Language (APDL) feature is used for the modeling purpose (see appendix A). Solid modeling approach is used for the two-dimensional crack propagation analysis. The model is built and solved using isoparametric eight-node PLANE82 elements. Figures 5, 6, and 7 show the details of the finite element mesh. ANSYS has the capability to automatically create singular crack-tip elements using command KSCON. But it is difficult to create multiple rings of elements surrounding the crack tip using KSCON. To increase accuracy of the computed stress intensity factors and consequently the energy release rates, each crack tip is surrounded by at least ten rings of elements. To this end, the crack tip elements are created manually. The midpoint nodes are subsequently shifted to the quarter point locations. The finite element mesh has approximately 48500 to 49000 nodes (15200 - 15500 elements) depending on the configuration. In order to capture the singular stress field at the crack-tip,

the mesh is made very fine near the crack tips (figures 5, 6). The radius of the crack tip elements is taken as $(a / 512)$ where 'a' is the half crack length. The model dimensions are taken sufficiently large compared to the crack-length and fiber diameter so that there will be no boundary effects in the area of interest.

APDL code in ANSYS

For the two-dimensional crack propagation analysis, the ANSYS Parametric Design Language (APDL) is used to write an input file. The code incorporates various parameters like crack length (a) and orientation (θ) and nanofiber diameter along with material property details. The code also contains a macro for the stress intensity factor computations using J-integral method. The macro takes the argument values in terms of the node numbers that define the particular path for the J-integral computations. The computations for mixed mode stress intensity factors are performed for a particular crack length within a DO loop. These computations are performed using at least two different approaches, namely, the nodal displacement extrapolation technique (KCALC), and the J-integral method. For selected cases, another scheme, which is virtual crack extension method, is also included to validate the computations further.

For the J-integral based computations of the stress intensity factors, at least three different contours are defined for each stress intensity factor calculation. Thus the consistency in the pattern of stress intensity factor values is monitored thought. Subsequent to the stress intensity factor computations, interface tractions are computed using the path operations feature in ANSYS. Both, the normal and shear tractions are computed. Then, the maximum values of the normal and shear tractions are identified. Further, the locations of these maximum traction values are obtained. At the end of a DO loop the crack length is incremented and next iteration is performed.

Loading

The loading on the finite element model is applied in the form of displacement boundary conditions that correspond to uniaxial applied stress in plane strain conditions. Thus,

$$\sigma_y = S$$

$$\sigma_x = 0$$

$$\sigma_{xy} = 0$$

$$\varepsilon_y = \frac{1}{E_m} [\sigma_y], \text{ thus}$$

$$u_y = \sigma_y \frac{1 - \nu_m^2}{E_m} y \quad (1)$$

$$\varepsilon_x = -\sigma_y \frac{1 - \nu_m^2}{E_m} \frac{\nu_m}{1 - \nu_m}, \text{ thus}$$

$$u_x = -\sigma_y \frac{\nu_m(1 + \nu_m)}{E_m} x$$

Where ε_x and ε_y are the strains and u_x and u_y are the corresponding displacements. The distances x and y are measured from the model center to the boundaries. Finally, E_m and ν_m are the matrix elastic modulus and Poisson's ratio respectively.

Computation of Energy Release Rate

Let K_I and K_{II} be the stress intensity factors for pure mode I and mode II conditions respectively. Then the mixed mode stress intensity factors for a crack oriented at angle θ (where, θ is the angle as shown in figure 4) are given by,

$$K_I^\theta = K_I \cos(\theta),$$

or

$$K_I^\theta = \sigma_y \sqrt{\pi a} \cos(\theta) \quad (2)$$

and

$$K_{II}^{\theta} = K_{II} \cos(\theta) \sin(\theta)$$

or

$$K_{II}^{\theta} = \sigma_y \sqrt{\pi a} \cos(\theta) \sin(\theta)$$

The K_I^{θ} and K_{II}^{θ} values are obtained using the aforementioned nodal displacement extrapolation technique (KCALC in ANSYS) after establishing the accuracy of the approach as discussed. We now compute energy release rates as,

$$\begin{aligned} G_I^{\theta} &= \frac{(1 - \nu_m^2)}{E_m} K_I^{\theta^2} \\ G_{II}^{\theta} &= \frac{(1 - \nu_m)}{G_m} K_{II}^{\theta^2} \end{aligned} \tag{3}$$

The above energy release rate values are normalized with those for a similar crack propagating in an infinite matrix in the absence of the fiber, namely, G_{I0} and G_{II0} respectively.

Accuracy of Energy Release Rate Computations

The energy release rates are obtained from the stress intensity factors computed using nodal displacement extrapolation (NDE) technique (using KCALC in ANSYS). This technique relies on the displacements computed very close to the crack tip, and thus on details of mesh near the crack tip. On the other hand, a global approach like J-integral method is based on the fact that, under the conditions of material homogeneity, the strength of crack-tip fields (K_I for instance) is governed by an integral computed over a path that is far removed from the crack-tip [25]. This means stress and displacements used in the computations do not have to be those in the region close to the crack tip. Another global method is the virtual crack extension method (VCE), which utilizes reduction in strain energy with crack-advance to compute energy release rate. The energy computations are not dependent on the details

near the crack tip and hence can give accurate fracture parameter values with relatively course mesh.

In the context of the above discussion, energy release rates are computed using all of the above techniques for a selected set of models in the present study. Comparison shows (see table 1) that energy release rates from the NDE technique are within one percent of those obtained from the J-integral and virtual crack extension methods. This suggests that the mesh is sufficiently fine near the crack-tip region. Thus, all other energy release rate computations presented below are carried

Table 1. Selected values of normalized mode I stress intensity factors at crack tip L from various approaches

($\theta = 0$, $E_f / E_m = 7.74$, $t_i = 0$, $t_w = 0$, $v_{FT} = v_m$)

r / r_0	K_I / K_{I0}			% Difference	
	NDE	J-INT	VCE	NDE, J INT	NDE, VCE
4	0.997549	0.9919488	0.994656	0.546331796	0.28957951
3.9	0.997101	0.9912156	0.994174	0.561362004	0.28998929
3.8	0.996608	0.9905598	0.993701	0.590252946	0.29352946
3.7	0.996063	0.9897107	0.993181	0.606884444	0.29165359
3.6	0.99546	0.9890384	0.992607	0.637777796	0.28936396
3.5	0.994789	0.9880977	0.99197	0.645114085	0.28663973
3.4	0.994039	0.9872283	0.991262	0.672587659	0.28329787
3.3	0.993197	0.9863157	0.99047	0.685105747	0.27932481
3.2	0.992248	0.9853223	0.989581	0.692844103	0.27453527
3.1	0.991172	0.9841459	0.988578	0.697965807	0.26872327
3	0.989945	0.9827999	0.987439	0.708821739	0.26165263

Three-dimensional Problem

Figures 8 through 12 schematically show the details of the three-dimensional study. In the three-dimensional study, the crack-nanofiber interaction is modeled for a penny shaped crack interacting with a pair of symmetrically placed nanofibers in an infinite matrix medium (figure 8). The crack is assumed to be near two symmetrically placed fibers such that, taking advantage of symmetry, only half of the penny-shaped crack and a single nanofiber are modeled as shown in the figure 9. Unlike the two-dimensional study, the three-dimensional study focuses mainly on mode-I crack propagation conditions. As such, mode-I energy release rate is the only fracture parameter computed in the majority of the configurations considered.

As expected, three-dimensional investigation results in new geometric variables like the angles (θ) and (ϕ) as shown in figures 10 and 11. Angle (θ) defines the locations along the crack front where the stress intensity factor and subsequently the energy release rate computations are performed. (ϕ) is the angle by which the nanofiber longitudinal axis deviates from the original positions (which is that of nanofiber longitudinal axis being perpendicular to the plane containing the crack front). Similar to the two-dimensional study, crack propagation is simulated in the three-dimensional study by incrementing the crack size ($2a$) after each analysis. Figure 12 shows this process schematically. At any given instance, the point on the crack front closest to the nanofiber is at distance (r) from the nanofiber center.

Another nanofiber geometric parameter that is introduced in the three-dimensional studies is the nanofiber length. As discussed in the literature survey, the nanofibers considered in this study have a large aspect ratio. The effective aspect ratio may be smaller because the nanofibers may not be straight [7]. In the three-dimensional studies, the nanofiber length is modeled as being infinite with respect to the crack dimension. To this end, the crack is assumed to be propagating far away from the fiber ends so that the fiber end effects do not influence the crack energetics.

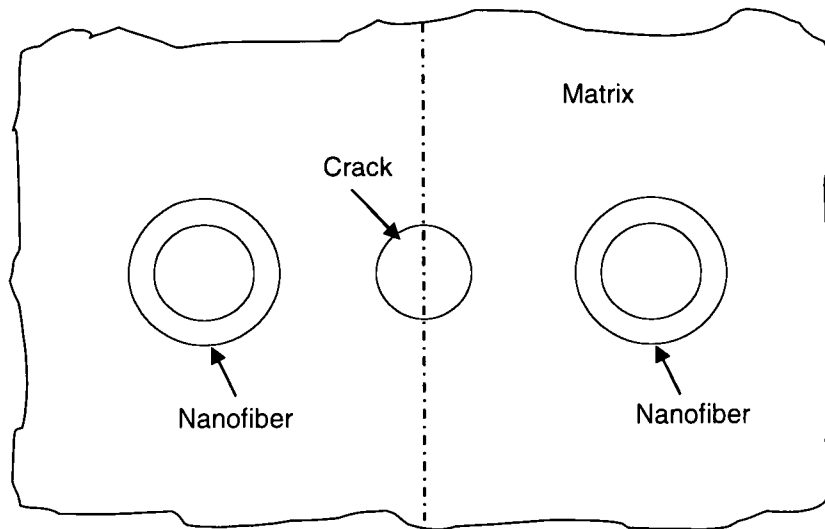


Figure 8. Schematic of the three-dimensional problem

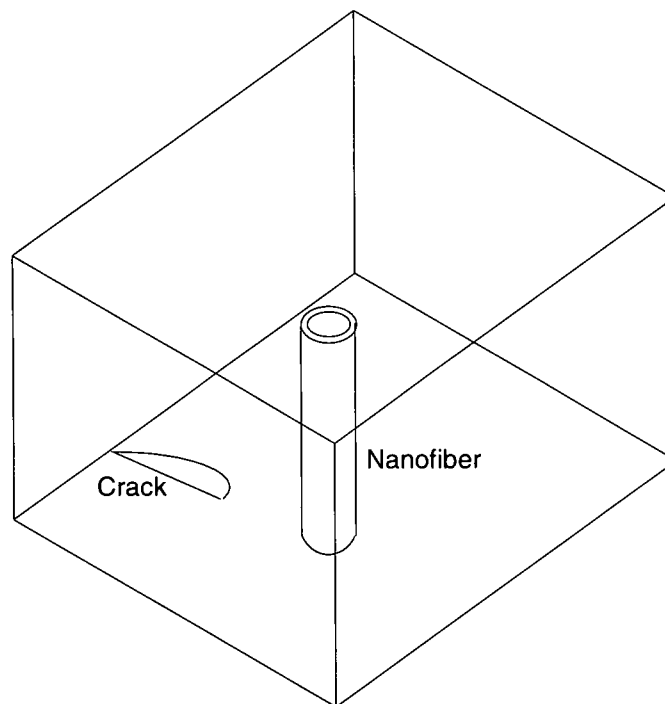


Figure 9. Schematic of the portion to be modeled

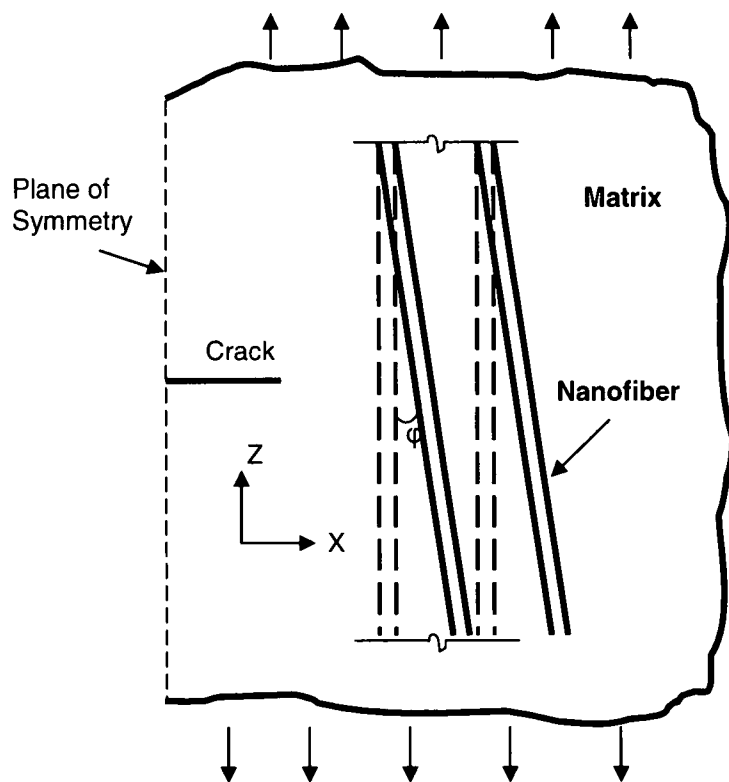


Figure 10. Schematic showing nanofiber longitudinal section

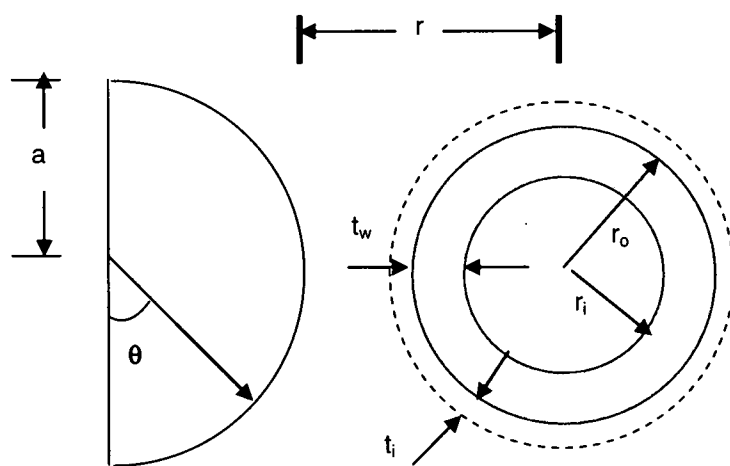


Figure 11. Geometric parameters in three-dimensional study

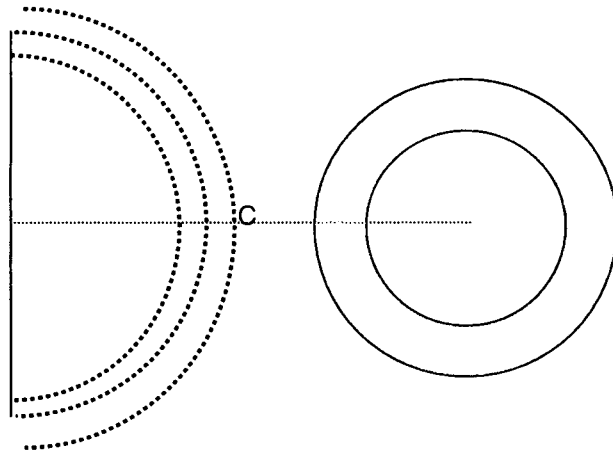


Figure 12. Successive crack positions

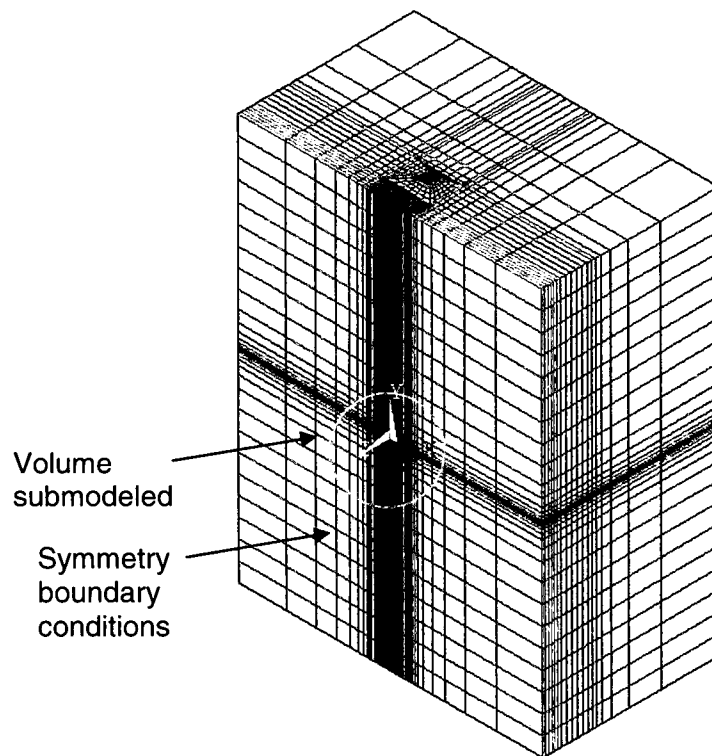


Figure 13. Coarse Model

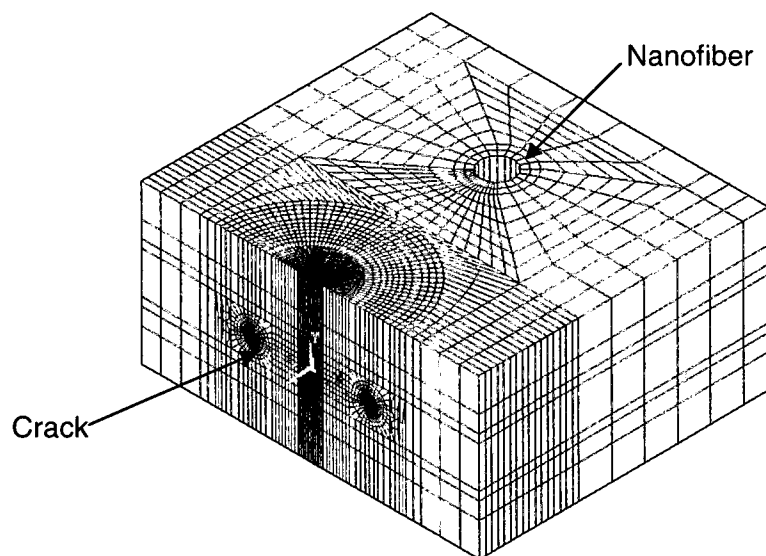


Figure 14. Submodel

Finite Element Model

Compared to two-dimensional analysis, the three-dimensional modeling is considerably more complex. ANSYS does not automatically generate the quarter point singular elements (KSCON not available) for a three-dimensional fracture problem, thus one needs to shift the midside nodes to quarter point positions manually. Also, applying J-integral approach for energy release rate computations is a challenging task in a three-dimensional fracture mechanics problem [23].

The element type selected for the three-dimensional modeling is SOLID95, a twenty-node solid element. The element is collapsed in to a wedge around the crack tip and the midpoint nodes are moved to quarter point locations to model the crack tip singularity. The accuracy of stress intensity factors computed depends on the size and number of the crack tip elements. With a three-dimensional model, having a reasonably fine mesh near a crack tip requires considerably large number of nodes in the crack front region. Therefore a submodeling approach is suitable here and is adopted for the three-dimensional finite element analysis.

Submodeling is a technique using which a finite element analysis is performed in two steps. The approach is based on the Saint Venant's principle, which states that if the actual loading on a system is replaced by a statically equivalent system of loads, the solution is altered only near the boundary where the statically equivalent loading is prescribed. Thus, at far away places in the model the solution will remain unaltered. In submodeling approach, a relatively coarse model is first solved. The mesh in the region of interest need not be very fine for this analysis. After this first step, a region of interest is cut from the whole model and is now accurately modeled and finely meshed. In this case, this is the region containing the crack front. This model is called the submodel. The submodel should be large enough that the region of interest is far enough from the model boundaries. The loads applied on the submodel are computed from the previously solved coarse model (CBDOF operation in ANSYS).

The submodeling approach explained above is used in the current three-dimensional finite element study. In the first step, a relatively coarse model is created without using singular crack tip elements and a fine mesh near the crack front. This model is created using SOLID95 elements and is shown in the figure 13. The coarse model contains approximately 90000 nodes. The coarse model is large enough so that the distance of the outer boundaries from the crack is approximately ten times the final crack length. The nanofiber length is fixed and is approximately ten times the final crack size (a_f).

A typical submodel cut from the coarse model is shown in the figure 14. As shown in the figure, the submodel contains the whole crack front for a better accuracy. Also, whole nanofiber cross-section is included in the submodel. The submodel has approximately 121000 nodes and contains singular crack front elements with the midside nodes shifted to the quarter point locations. The radius of the crack front elements surrounding the crack front is $(a / 80)$ where 'a' is the current crack radius. Thus, although the model and the nanofiber dimensions for a coarse model remain constant, the submodel dimensions vary with the varying crack length. At the same time, the submodel dimensions are taken large enough so that the crack front region is sufficiently away from the boundaries.

Similar to the two-dimensional finite element studies, the crack propagation is simulated by solving the finite element model for varying (increasing) crack radius. The crack size increment is fixed and is ten percent of the initial crack radius. Thus, for a given crack length, the analysis is performed in two steps using the submodeling approach. Then the crack radius is increased and a new two-step analysis is performed. The initial distance of the crack front from the nanofiber center is approximately 3.5 times the nanofiber outer radius r_o . after the final crack size increment, this distance is reduced to approximately 1.5 times the fiber radius. A distance closer than this is not possible because of the presence of a transition region in the submodel, which helps reduce the geometric complexity away from the crack front region so that modeling the other geometric features like the fiber becomes easier.

Loading

As in the case of the two-dimensional analysis, the infinite matrix domain that contains the crack and the pair of nanofibers is assumed to be at the center of a very large region in the state of uniform strain. Displacement boundary conditions corresponding to the uniaxial stress $\sigma_z = S$ are applied on the model. Thus, with respect to the global coordinates shown in the figure 10,

$$\sigma_z = S$$

$$\sigma_x = 0$$

$$\sigma_y = 0$$

Now, the displacement boundary conditions to be applied on the finite element model corresponding to uniaxial loading conditions are obtained as follows,

$$\varepsilon_z = \frac{1}{E_m} [\sigma_z], \text{ thus}$$

$$u_z = \frac{\sigma_z}{E_m} z \tag{4}$$

$$\varepsilon_x = -\nu_m \frac{\sigma_z}{E_m}, \text{ thus}$$

$$u_x = -\nu_m \frac{\sigma_z}{E_m} x$$

Similarly,

$$\varepsilon_y = -\nu_m \frac{\sigma_z}{E_m}, \text{ thus}$$

$$u_y = -\nu_m \frac{\sigma_z}{E_m} y$$

The displacement values u_z , u_x , and u_y thus obtained are applied to the coarse model. Of course, the boundary conditions that are applied on the submodel are obtained from the nodal results of the coarse model.

Validation of the Mesh Size Near Crack

Unlike in the case of the two-dimensional crack analysis presented in the earlier chapters, the stress intensity factors are obtained using only one scheme, which is the nodal displacement extrapolation technique (KCALC). To ascertain that the stress intensity values computed are accurate, modification is done to the finite element model. A typical finite element model has three regions, the crack region, the fiber region, and the surrounding infinite medium. The model is modified by replacing the nanofiber region with a solid with the properties of the surrounding matrix medium. With this modification, the model essentially converts to a case of a penny shaped crack in an infinite domain, under the action of uniaxial stress. The closed form solution for the mode I stress intensity factor for this case exists and is given by

$$K_I = \frac{2}{\pi} \sigma \sqrt{\pi a} \quad (5)$$

Where 'a' is the crack radius and σ is the applied uniaxial stress. Now this case becomes the reference case to establish the validity of the finite element solution.

With the above knowledge, finite element analyses are performed for all crack sizes and stress intensity values computed. It is observed that the mode I stress intensity factor values for all crack sizes as obtained from the finite element analyses are within 0.5 to 0.6 percent of the exact values. These values are obtained with the crack front element size of $(a / 80)$, where 'a' is the crack radius. This validates the fineness of the mesh in the crack region.

Computation of Energy Release Rate

The mode I stress intensity factors obtained from the finite element analysis are converted in to energy release rates using the relation

$$G_I = \frac{K_I^2(1 - \nu_m^2)}{E_m} \quad (6)$$

Where G_I is the mode I energy release rate, ν_m is the matrix Poisson's ratio, K_I is the mode I stress intensity factor, and E_m is the matrix Young's modulus. Note that the above expression is valid for plane strain conditions. The energy release rate obtained is normalized with respect to the corresponding energy release rate (G_{I0}) of a propagating crack with respect in an infinite matrix phase in the absence of another phase like a fiber.

The energy release rates computed are analyzed in two ways, the variation along the crack front (for various values of θ as shown in figure 11) for each crack position and also the variation in the direction of crack propagation. This variation along the direction of the crack propagation is evaluated by comparing the values of the energy release rates computed at the center point (c) of each crack position. This is shown by the figure 12.

CHAPTER IV

CHARACTERIZATION OF THE INFLUENCE OF NANOFIBER MODULI AND POISSON'S RATIO

As discussed in the literature review, the determination of the elastic properties of nanofibers is a tough task due to the nanoscale dimensions of nanofibers that render the experimental evaluation extremely difficult. At the same time, the properties are expected to be transversely isotropic with the longitudinal modulus approaching a value up to 600 GPa. The properties of nanofibers are a function of the orientation of the graphitic planes (figure 3). Various geometries and possibly elastic properties result when this orientation varies. With the lack of adequate controllability on the geometry and subsequently elastic properties of nanofibers, there is likely to be significant variation in the elastic properties of nanofibers. These elastic properties include the nanofiber moduli and Poisson's ratio. The influence of these elastic properties and their variation on crack energetics is characterized as explained in the following sections.

Characterization of the influence of Nanofiber Moduli

For this study, the nanofiber longitudinal modulus is fixed with a value of 600 GPa. On the other hand, not much is known or reported about the transverse modulus. In conventional carbon fiber reinforced composites, the fiber transverse modulus is typically reported as 20 GPa, which is 1/10 of the longitudinal value of about 200 GPa. In the absence of any other information, three different nanofiber transverse modulus values are considered such that,

$$\frac{E_{fl}}{E_{ft}} = 10, 25, 50, \text{ where } E_{fl} = 600 \text{ nN/nm}^2 (600 \text{ GPa}) \text{ and } E_{ft} \text{ is fiber transverse modulus.}$$

The epoxy matrix is considered to be isotropic with an elastic modulus of 3.1 GPa. Correspondingly, the modular ratios between the nanofiber (transverse) and the matrix moduli are,

$$\frac{E_{ft}}{E_m} = 19.35, 7.74, 3.87$$

The nanofiber transverse Poisson's ratios are,

$$\nu_{ft} = 0.25$$

$$\nu_{ft} = 0.38$$

The matrix Poisson's ratio is assumed to be equal to the nanofiber transverse Poisson's ratio.

Influence of variation in Transverse Modulus

The understanding of the influence of a nanofiber on the fracture behavior is developed by computing the energy release rate as the crack propagates towards the nanofiber. The variation of the energy release rate as a matrix crack propagates towards a second phase may look as shown in the figure 15. When the nanofiber provides a toughening effect, the energy release rate (G) curve will show a convex up show with decreasing G values. On the other hand, if the nanofiber causes the crack to be attracted towards it, the energy release rate values will show an increase as the crack approaches the nanofiber.

Figures 16 to 19 show the results of the study conducted to characterize the influence of the variation in the transverse modulus of the nanofiber. As described above, three different nanofiber transverse modulus values are considered. Figures 16 to 19 show the normalized mode I energy release rates G_I/G_{I0} for various nanofiber transverse modulus values and for each of the crack orientations considered. The normalizing factor G_I here is the energy release rate for an identical crack propagating in an infinite matrix in the absence of a nanofiber. For the given nanofiber wall thickness, a larger E_{ft} results in a smaller G_I/G_{I0} as the crack approaches the fiber, indicating a greater resistance to the crack propagation. Even

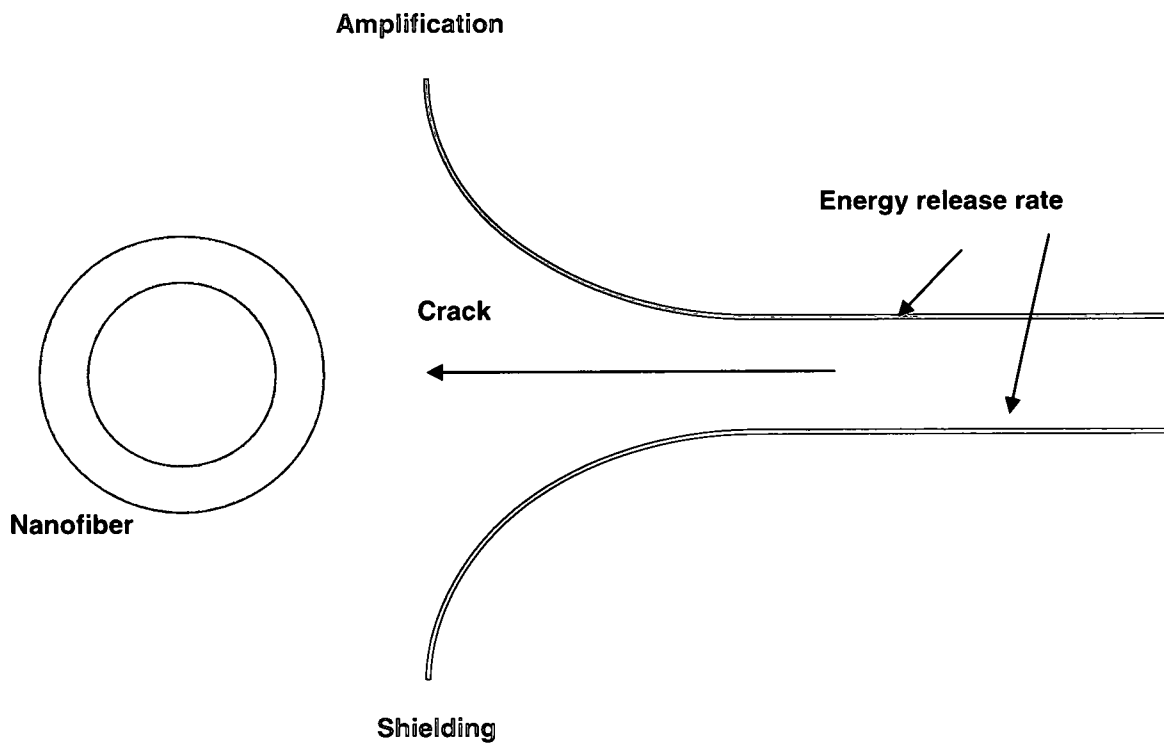


Figure 15. Variation of energy release rate for a propagating crack

with the smallest E_f considered, the mode I crack driving force decreases as the crack approaches the fiber. A comparison among different crack orientations reveals that a change in the crack orientation (θ) does not significantly influence the nature of variation of G_I/G_{I0} with E_f/E_m . This is an important result as it shows that when considering the controllability aspect of the nanofibers from the perspective of the fracture behavior, one may not have to include the crack orientation with respect to the nanofiber as a factor.

Figures 20 to 22 show the results for the normalized mode II energy release rates. As the figures show, the mode II energy release rate is more sensitive to the variation in the nanofiber transverse modulus as compared to mode I. G_{II}/G_{II0} shows a steep gradient as the crack gets within one and a half fiber radiuses, whereas G_{II} / G_{II0} shows such gradient for comparatively fewer and smaller nanofiber-crack distances, and instead shows a relatively smooth gradient for almost all the way up to the nanofiber. Thus, for a given value of the nanofiber transverse modulus, there is less toughening in mode II than in mode I as the crack approaches the nanofiber. At the same time, at the farthest crack positions there is more toughening effect of the nanofiber as compared to the corresponding case in mode I. Figures 20 to 22 also show that like mode I, the mode II behavior is not sensitive to the variation in the crack orientation (θ).

For the case of nanofiber wall thickness $t_w = 20$ nm, the influence of the nanofiber modulus variation on the behavior of G_{II}/G_{II0} seems to be opposite to that of G_I/G_{I0} for the same nanofiber wall thickness. There is an amplification effect on mode II energy release rate for lower values of E_f/E_m . Even for the highest E_f/E_m , the G_{II}/G_{II0} shows relative decrease only when the crack is at its closest positions near the fiber. Note that for the same set of conditions, mode I energy release rate decreases as the crack approaches the fiber for all values of E_f/E_m .

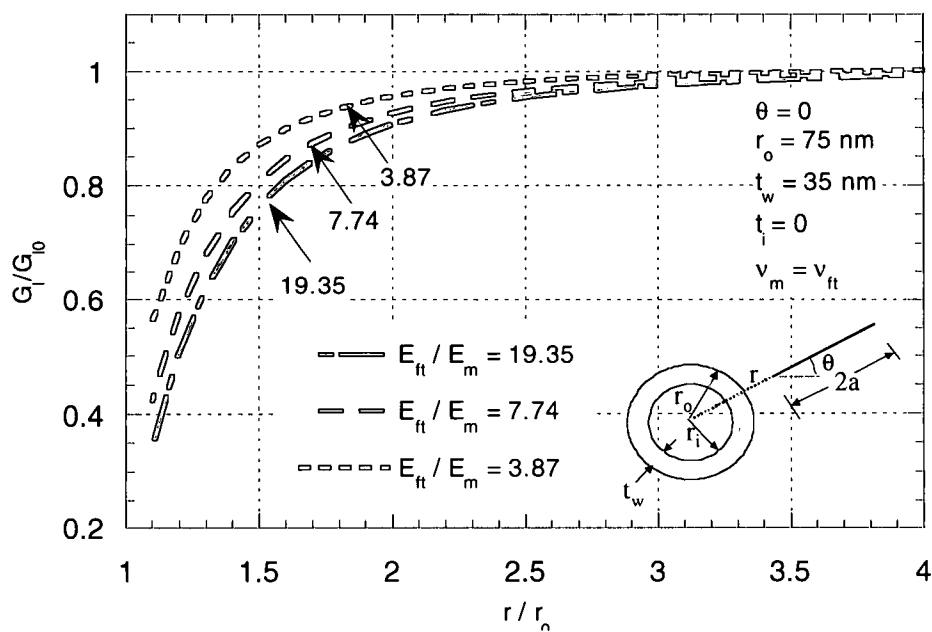


Figure 16. Influence of E_{ft} on G_l/G_{l0} , $\theta = 0$

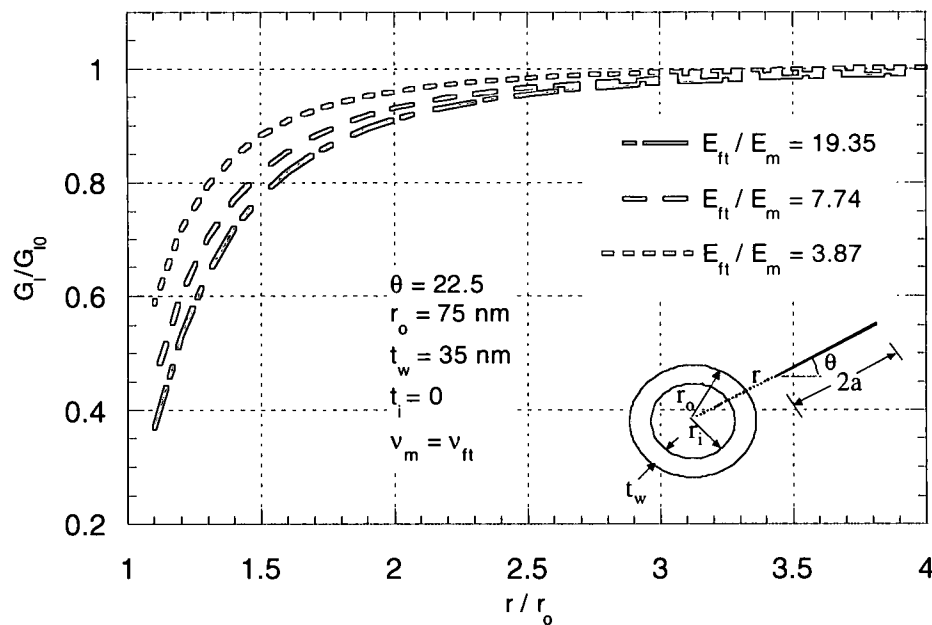


Figure 17. Influence of E_{ft} on G_l/G_{l0} , $\theta = 22.5$

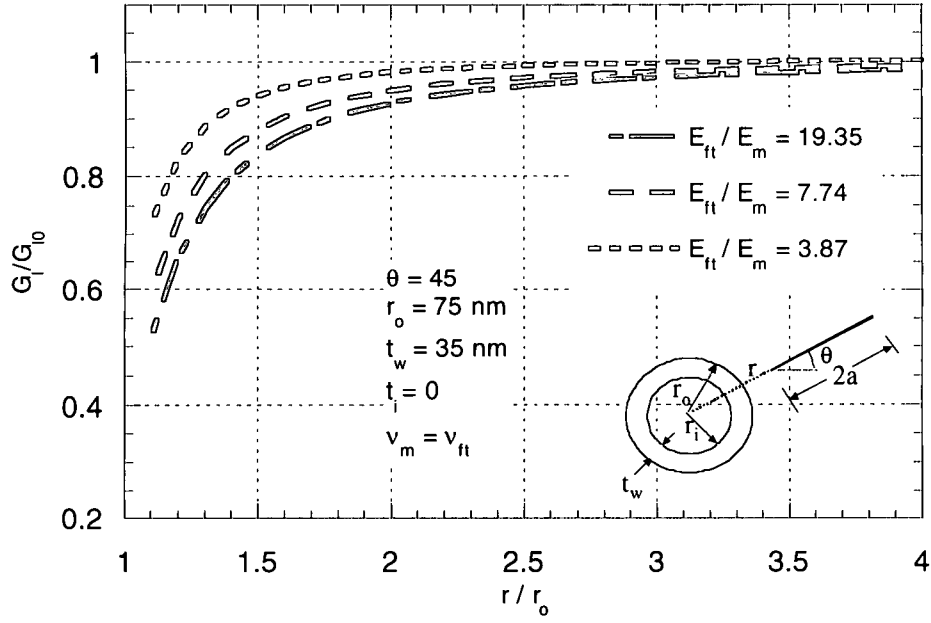


Figure 18. Influence of E_{ft} on G_l/G_{l0} , $\theta = 45$

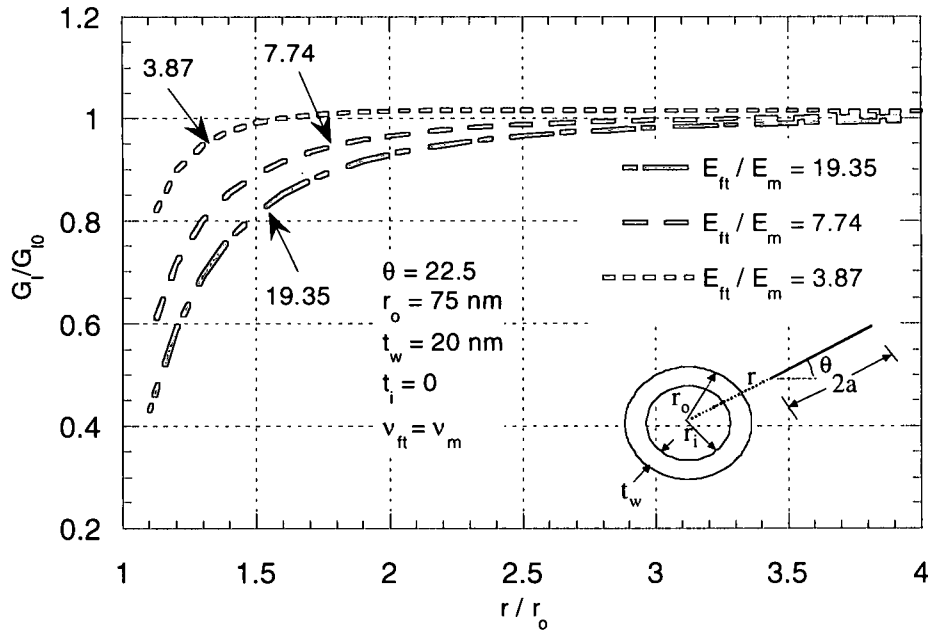


Figure 19. Influence of E_{ft} on G_l/G_{l0} , $\theta = 45$ and $t_w = 20$ nm

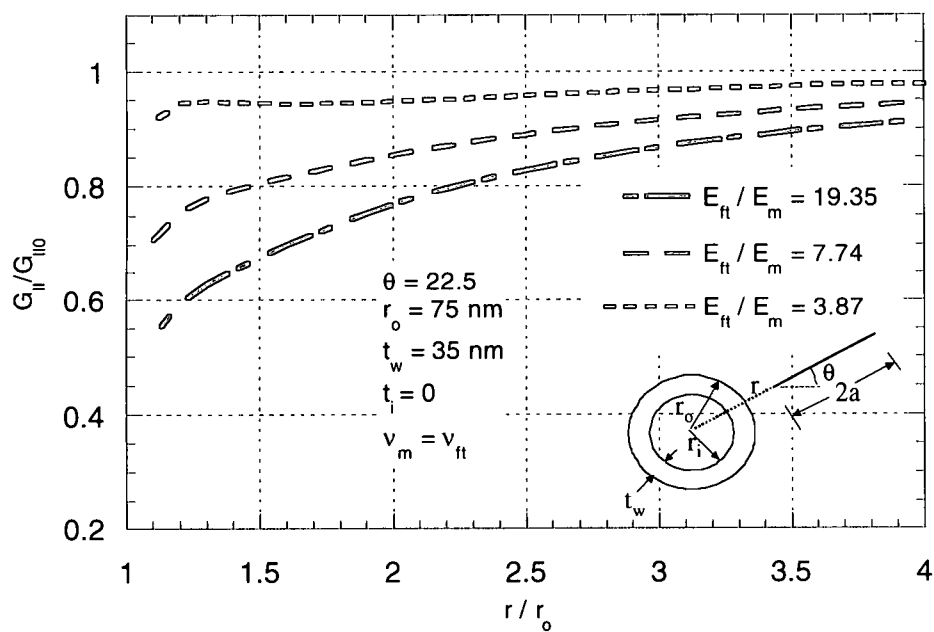


Figure 20. Influence of E_{ft} on $G_{||}/G_{||0}$, $\theta = 22.5$

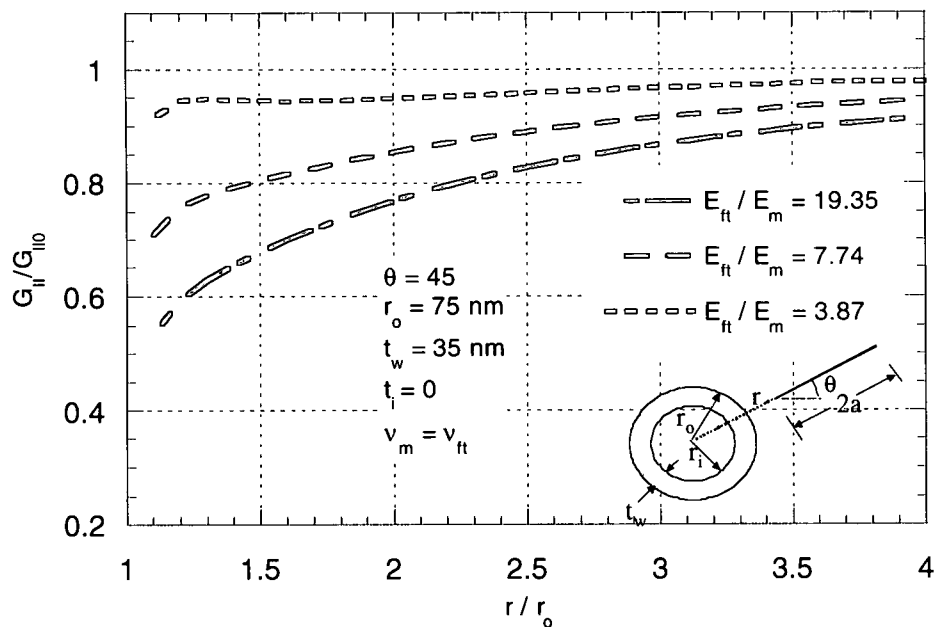


Figure 21. Influence of E_{ft}/E_m on $G_{||}/G_{||0}$, $\theta = 45$

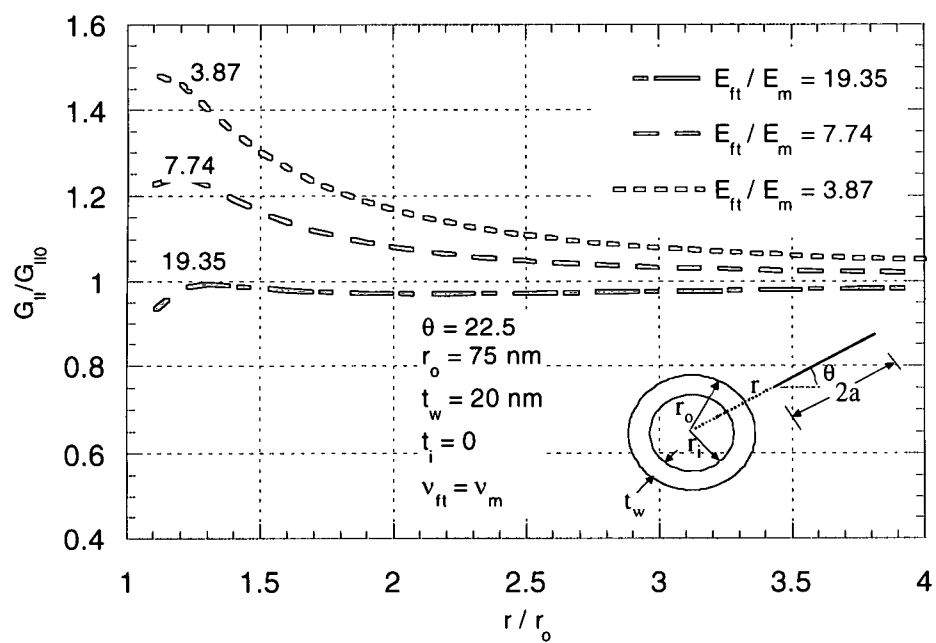


Figure 22. Influence of E_{ft}/E_m on $G_{||}/G_{||0}$, $\theta = 22.5$ and $t_w = 20\text{nm}$

Influence of Nanofiber Longitudinal Modulus

The influence of the nanofiber longitudinal modulus on the crack energetics is evaluated using the three-dimensional study and as such the energy release rates computed are analyzed in two ways, the variation along the crack front (for various values of θ as shown in figure 10) for each crack position and also the variation in the direction of crack propagation (figure 11). This variation along the direction of the crack propagation is evaluated by comparing the values of the energy release rates computed at the center point (c) of each crack position.

Figures 23 to 26 show the influence of a large nanofiber longitudinal modulus on the crack energetics. The modular ratio between the nanofiber longitudinal modulus and the matrix modulus is approximately 193, and its effect on the energy release rate is significantly large even at the farthest crack position. The normalized energy release rate (G_I/G_{I0}) is significantly small and suggests the strong influence of the large nanofiber elastic modulus on the crack energetics. Note that the normalizing factor here is the energy release rate for the crack of the same size in an infinite matrix phase for which closed form solution is known. Figure 23 schematically shows the trend of variation in mode I energy release rate G_I as the crack propagates towards the nanofiber in a three-dimensional configuration. In the middle region of the crack front, which is closer to the nanofiber, there is a continuous decrease in the G_I values. On the other hand, towards the end regions of the crack, G_I gradually increases. This is shown again in figure 24. The x coordinate here is the angle θ measured as shown in the figure 10. As shown in the figure, the shielding effect of the nanofiber is sensed in the middle region of the crack spanning approximately 100 degrees. As the crack approaches the nanofiber, the sag in the curves for the successive crack positions increases. This indicates the toughening effect of the stiff nanofiber. On the other hand, for the remaining portion of the crack front that approximately spans the remaining 40 degrees towards each end of the crack front, the normalized mode I energy release rate increases as the crack propagates towards the nanofiber.

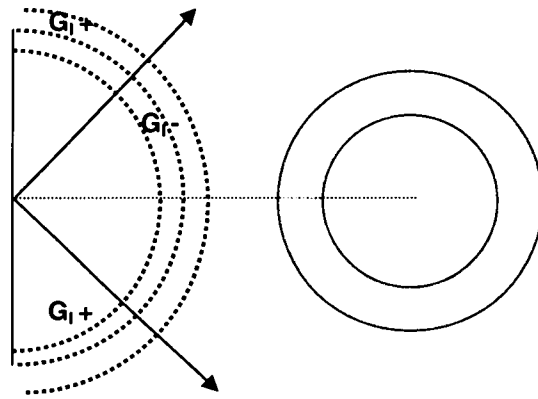


Figure 23. Energy release rate along the crack front

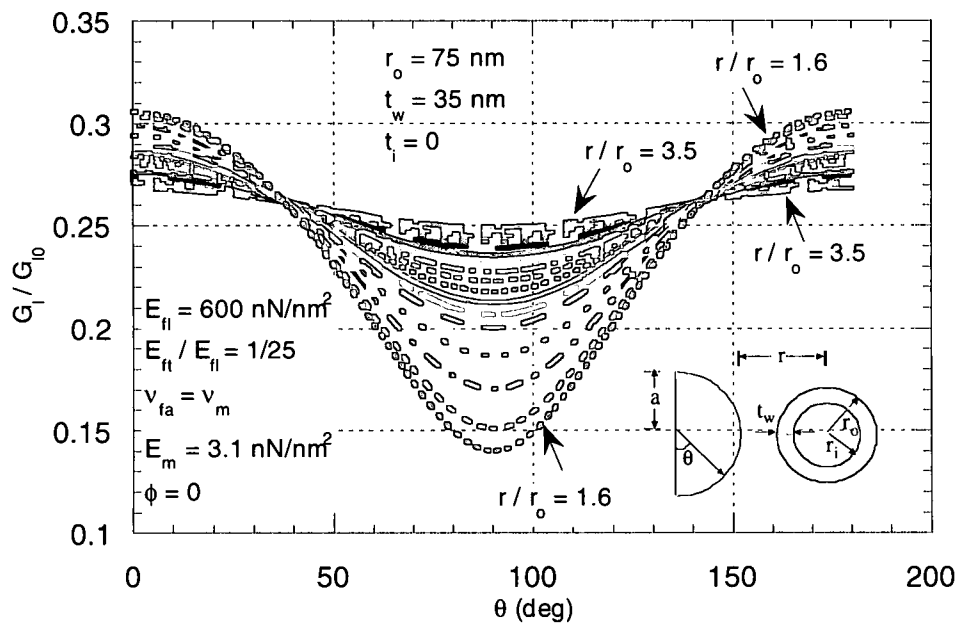


Figure 24. Energy release rate along all crack fronts

Figure 25 shows the variation of G_I/G_{I0} at the center point of the crack front ($\theta = 90^\circ$) and at the endpoint ($\theta = 0^\circ$) for the successive crack positions. The energy release rate here is plotted against the normalized distance r/r_0 between the crack front and nanofiber. As shown in the figure, the G_I/G_{I0} shows a smooth reduction in the value as the crack advances. Due to the dominance of the large nanofiber longitudinal modulus, the normalized mode I energy release rate is significantly small even for the farthest crack position. This is different from the typical crack energetics observed in the two-dimensional crack propagation study, wherein the nanofiber transverse modulus is dominant. In that case the mode I energy release rate shows a steep gradient within approximately two nanofiber radii. On the other hand, for ($\theta = 0^\circ$), the G_I/G_{I0} shows a continuous increase as the crack propagates. The increase in the G_I/G_{I0} is almost linear as shown by the corresponding curve. However, even for the largest crack size, the G_I/G_{I0} values are significantly small.

Figures 26 to 28 show the influence of the nanofiber longitudinal modulus when the nanofiber is slightly misaligned with respect to the direction normal to the crack plane. This misalignment is represented by angle (ϕ) in figure 9. Three different orientations are considered, namely, 0, 5, and 10 degrees. As figure 23 shows, the mode I energy release rate is influenced by the variation in (ϕ). A smaller ϕ results in a smaller G_I/G_{I0} . As figures 27 and 28 show, the nanofiber orientation influences the crack energetics for both the farthest and the closest crack position. Although the change in the nanofiber orientation seems to be resulting in a significant change in the mode I energy release rate, the energy release rate values are still reasonably small. Thus, for a nanofiber-crack system with the nanofiber longitudinal axis approximately perpendicular to the crack plane, a large nanofiber longitudinal modulus provides a significant toughening effect. Even with slightly misaligned nanofibers, an effective crack shielding can be achieved as a result of the nanofiber longitudinal modulus being as large as 600 GPa.

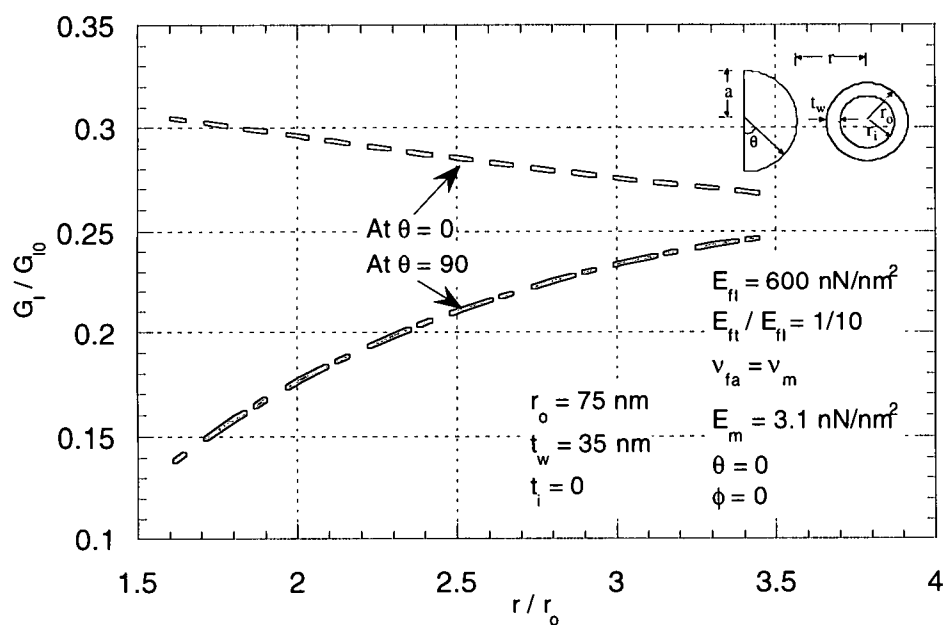


Figure 25. Variation of G_I at closest and farthest points on the crack front

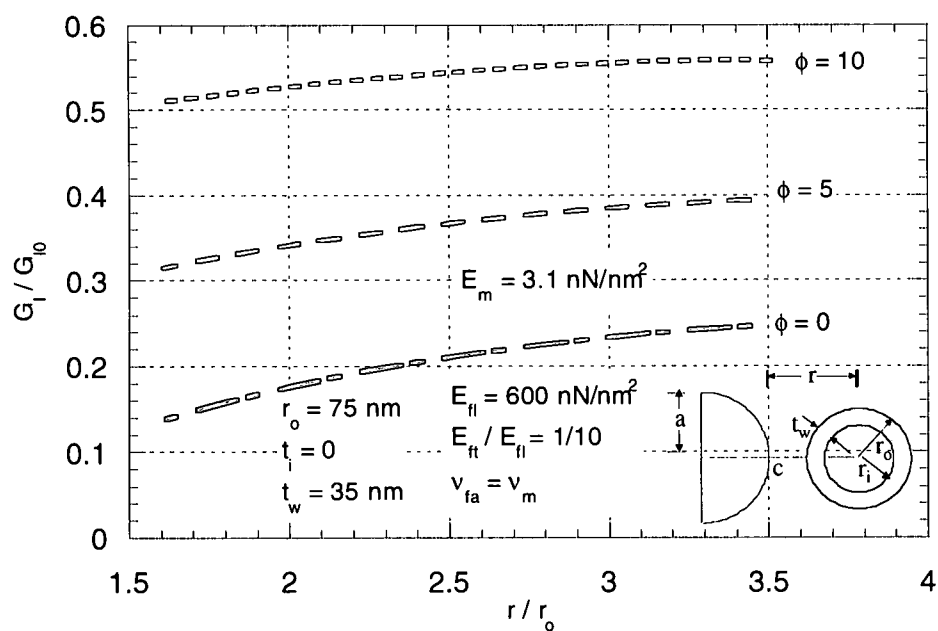


Figure 26. Mode I energy release rate at $\theta = 90$ (point c) at successive crack positions for various fiber orientations

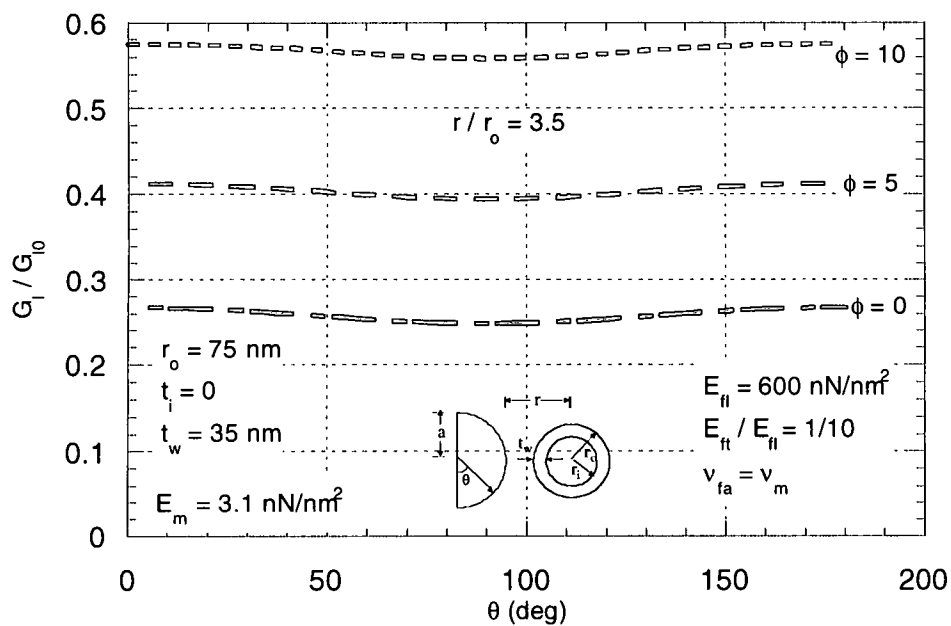


Figure 27. Mode I energy release rate along the farthest crack front position for various nanofiber orientations

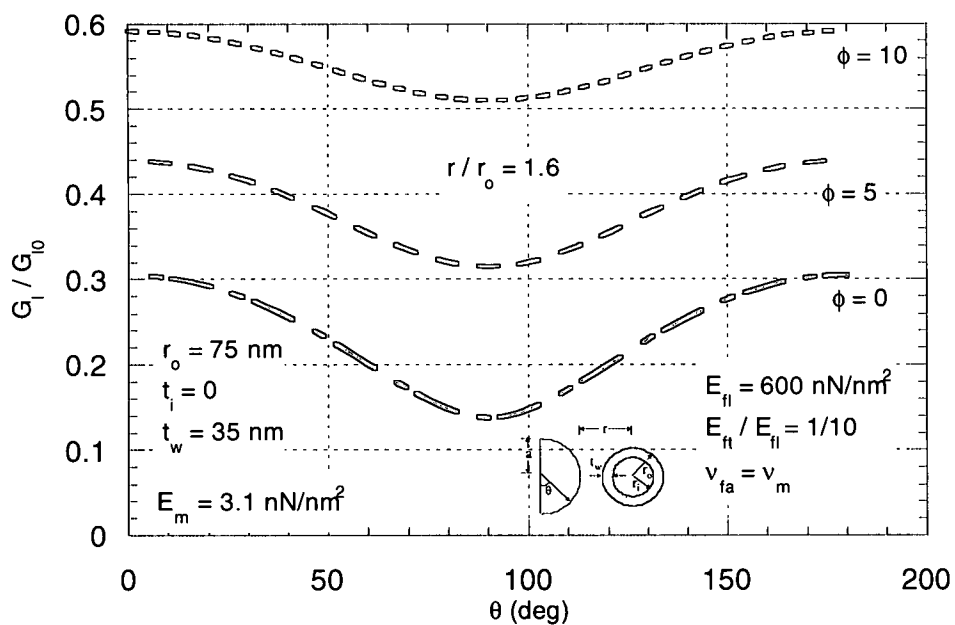


Figure 28. Mode I energy release rate along the closest crack front position for various nanofiber orientations

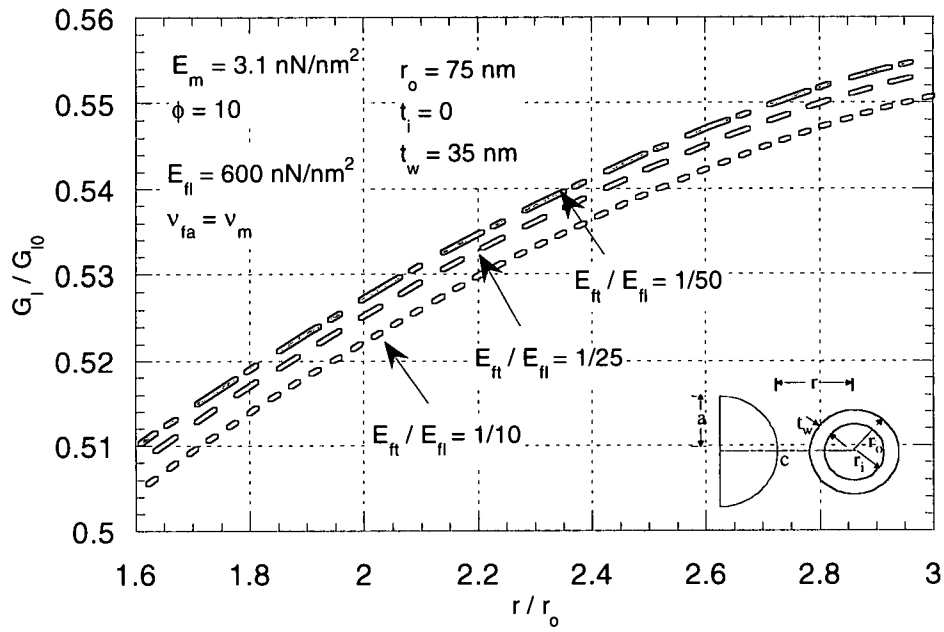


Figure 29. Mode I energy release rate for various nanofiber anisotropy ratios

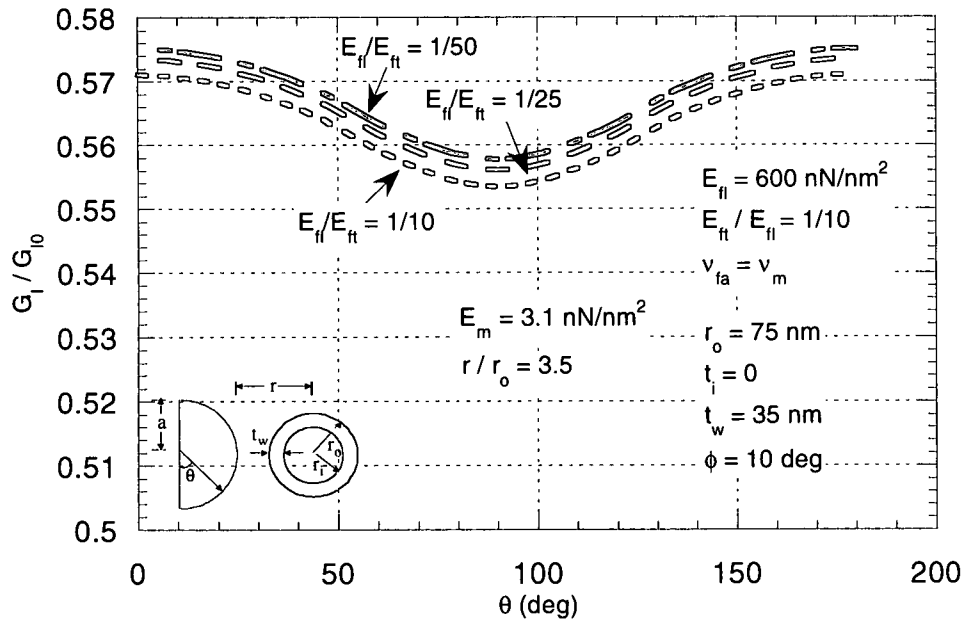


Figure 30. Mode I energy release rate for various nanofiber anisotropy ratios

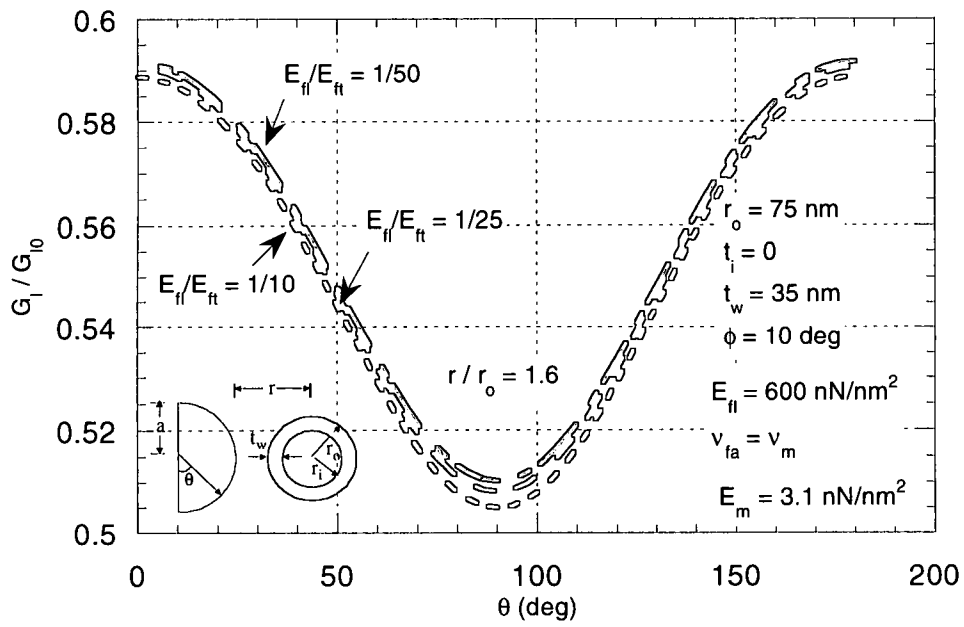


Figure 31. Mode I energy release rate for various nanofiber anisotropy ratios

Figures 29 to 31 show another instance of the influence of nanofiber longitudinal modulus. In this case, various nanofiber anisotropy ratios considered are incorporated in the study by using the nanofiber orientation of ($\phi = 10$ deg). Again, the nanofiber longitudinal modulus causes a significant shielding against the crack propagation as shown by the energy release rates. The energy release rates for various nanofiber transverse moduli are considerably close to one another and hence don't seem to be significantly sensitive to the nanofiber anisotropy ratios.

Influence of Nanofiber Moduli on Interface Traction

Investigating interface tractions in conjunction with a crack-nanofiber interaction comprises computations of the maximum values of normal and shear traction and their corresponding locations (figures 32, 33). The location of the maximum traction value is represented by the angles α and β for the normal and shear tractions respectively, measured as shown in the figure 33. Figure 34 shows the influence of the variation in the nanofiber transverse modulus on the maximum normal traction (SR_{max}) at the fiber-matrix interface. The maximum radial traction at the interface is relatively insensitive to the changes in the stiffness values. The SR_{max} value increases as the crack tip approaches the stiff nanofiber. Also, the decay of SR_{max} value with distance away from the fiber is relatively smooth approaching a plateau value at approximately three times the fiber outer radius. To investigate the influence of the variation in the crack orientation angle θ on maximum traction values, the traction values are computed for various crack orientations considered. As figures 34 and 35 show, the behavior of maximum normal traction is not sensitive to the change in the crack orientation angle θ , in that the traction values still show a relative insensitivity to the variation in the nanofiber elastic modulus, especially when the crack is close to the nanofiber.

In contrast to the SR_{max} behavior, the maximum shear traction (SRT_{max}), as shown in the figures 36 and 37 has a behavior dependent on the crack orientation. For $\theta = 22.5$ deg, it shows a steep gradient approaching a plateau value as the crack tip is within one and a half

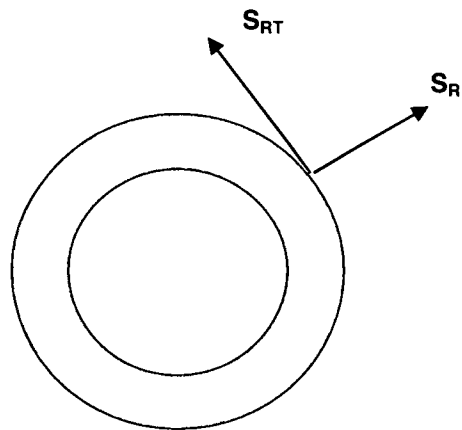


Figure 32. Normal and shear components of interface traction

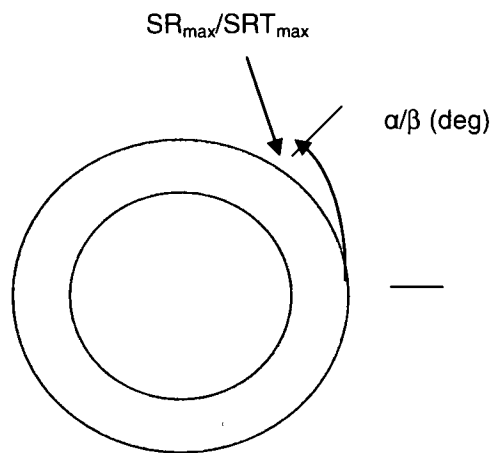


Figure 33. Measurement of location of maximum normal and shear tractions at the nanofiber-matrix interface

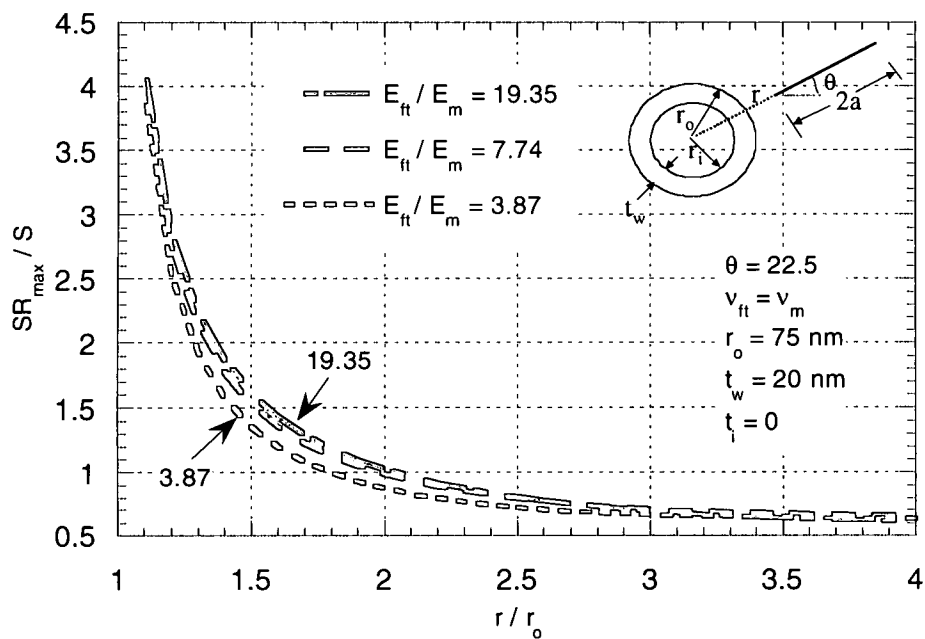


Figure 34. Influence of E_{ft}/E_m on maximum interface normal traction

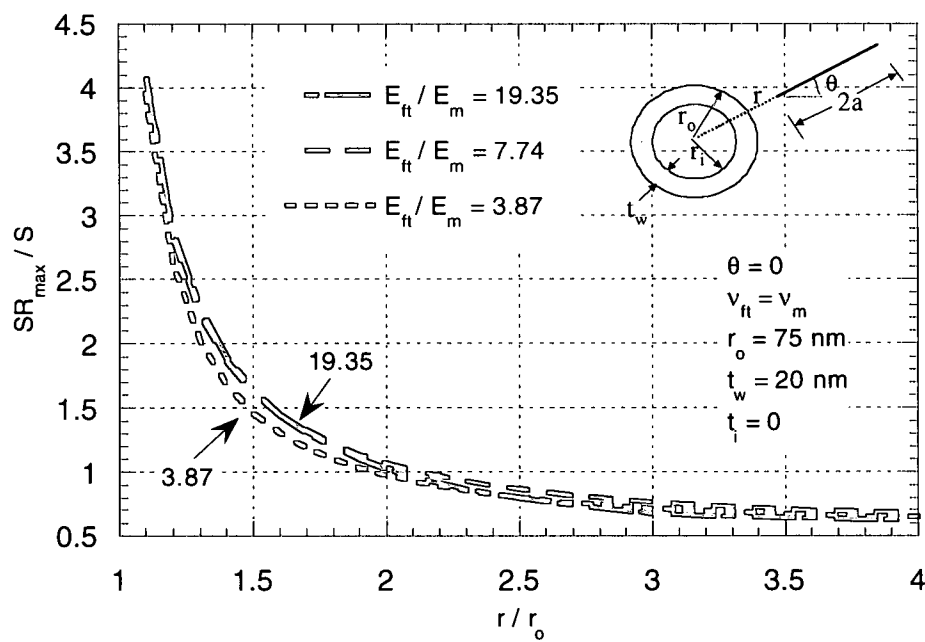


Figure 35. Influence of E_{ft}/E_m on maximum interface normal traction

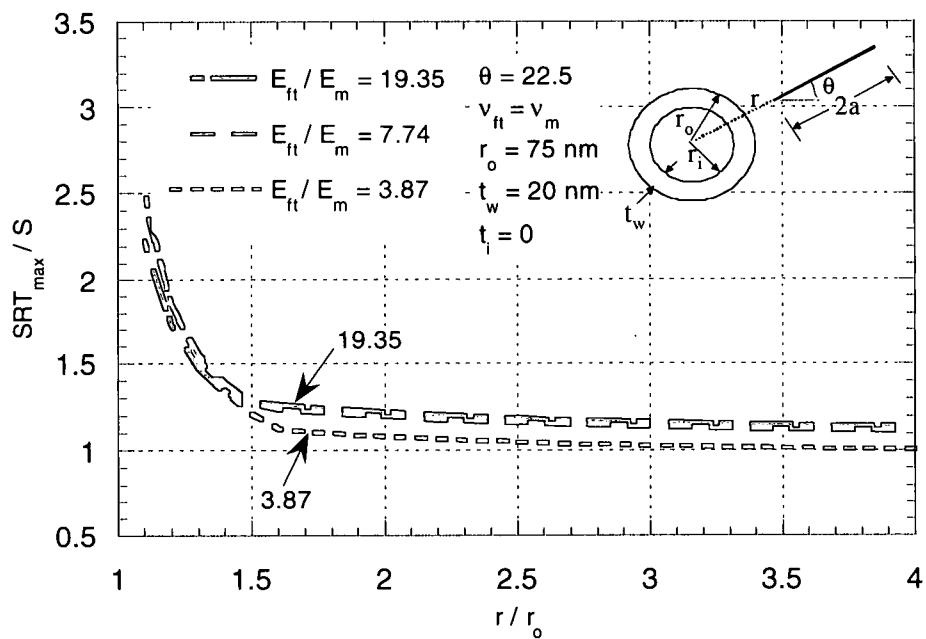


Figure 36. Influence of E_{ft}/E_m on maximum interface shear traction

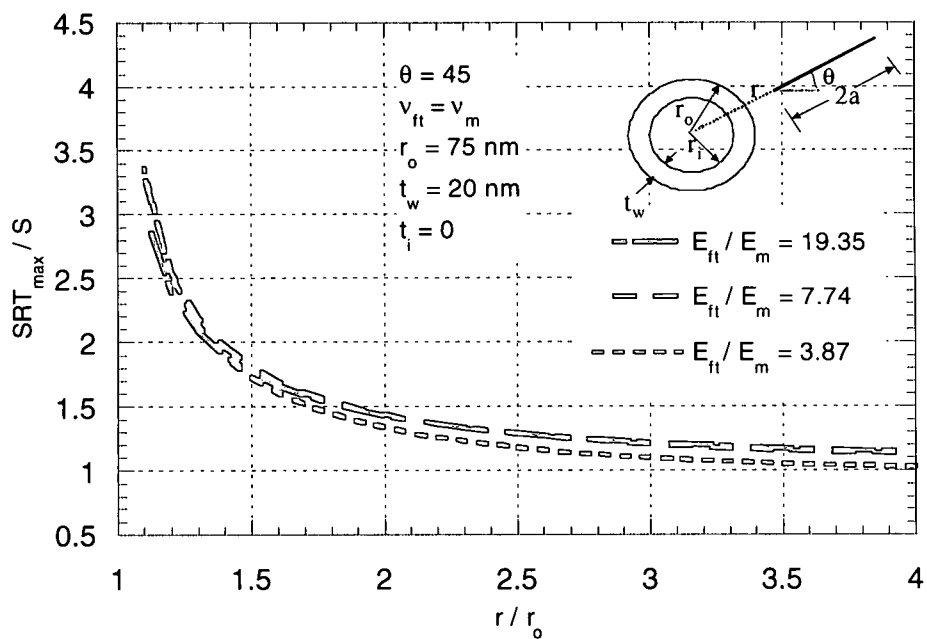


Figure 37. Influence of E_{ft}/E_m on maximum interface shear traction

radii away from the fiber center, and hence decays faster away from the fiber. When the crack orientation is changed to 45 deg, this gradient seems to be smoothened.

The study of interface tractions shows that both SR_{max} and SRT_{max} do not show a significant sensitivity to the variation in the nanofiber transverse modulus, especially when the crack is relatively close to the nanofiber. At the same time, both SR_{max} and SRT_{max} show an increase in the magnitude as the crack propagates towards the nanofiber. However, the maximum normal traction shows a greater increase over the course of crack propagation as compared to the maximum shear traction, suggesting that a secondary failure mechanism dominated by the SR_{max} like debonding is a more likely result of the crack propagation towards the nanofiber.

An important parameter in the investigation on the maximum values of interface traction is the location of the maximum traction and its variation as the crack propagates towards the fiber. Figure 38 shows the location (α) for various fiber-matrix modular ratios for a crack oriented at $\theta = 0$. At larger crack tip distances, the maximum radial stress occurs at the pole of the nanofiber, i. e., at $\alpha = 90$. As the crack approaches the fiber, there is an abrupt change in α . For all modular ratios, $\alpha = 0$ when the crack is closest to the fiber, indicating that as the crack approaches the fiber the location of the maximum normal interface stress shifts towards the point where the crack will intersect the fiber surface. This can be observed for all modular ratios considered, the only difference being that for the lower E_f/E_m this transition occurs when the crack is slightly farther from the fiber. Figure 39 shows the behavior for $\theta = 22.5$. Again, as seen with $\theta = 0$, as the crack approaches the nanofiber the location of SR_{max} shifts to the approximate location where the crack is projected to intersect the interface. This trend is again evident from the figure 40, which shows the variation of α for different crack orientations. Note that as the crack approaches the fiber, $\alpha \approx \theta$ for all cases.

Figures 41 through 43 show the variation of location (β) of the maximum shear traction at the nanofiber-matrix interface for various nanofiber-matrix modular ratios and crack orientations. For a given crack orientation (θ), the curves are on top of each other indicating

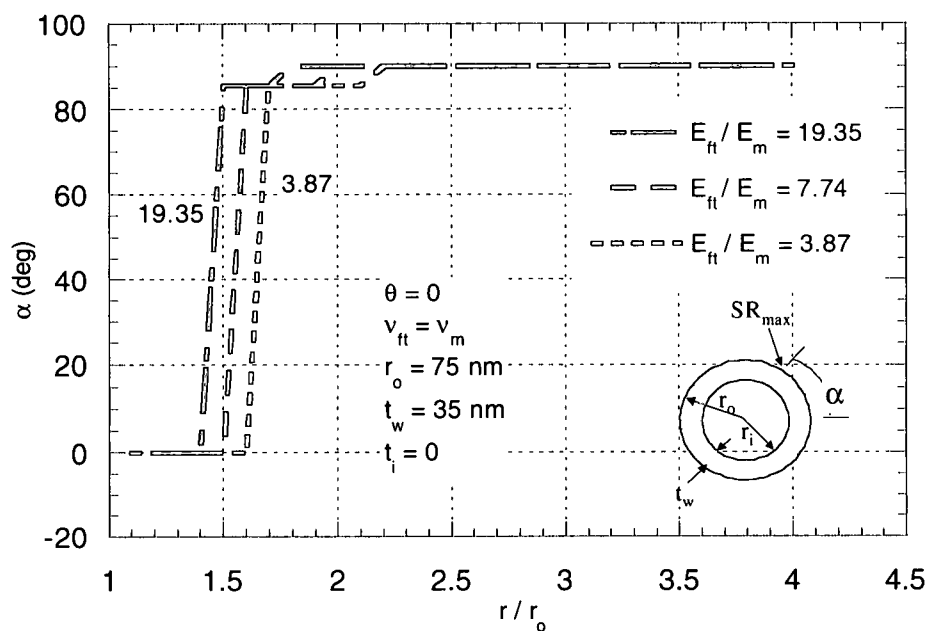


Figure 38. Location of maximum normal traction as a function of the nanofiber transverse modulus

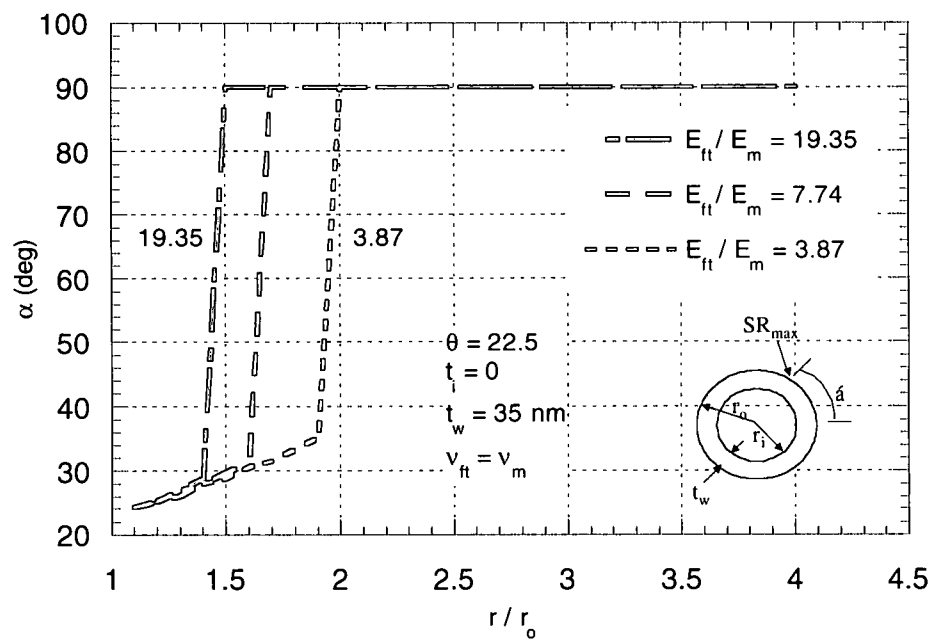


Figure 39. Location of maximum normal traction as a function of the nanofiber transverse modulus

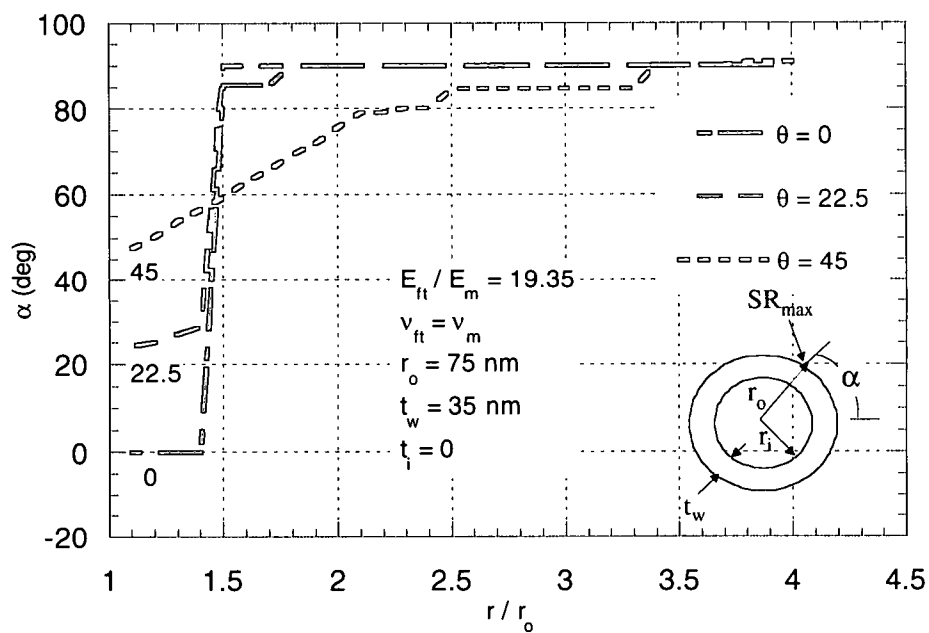


Figure 40. Location of maximum normal traction as a function of the crack orientation

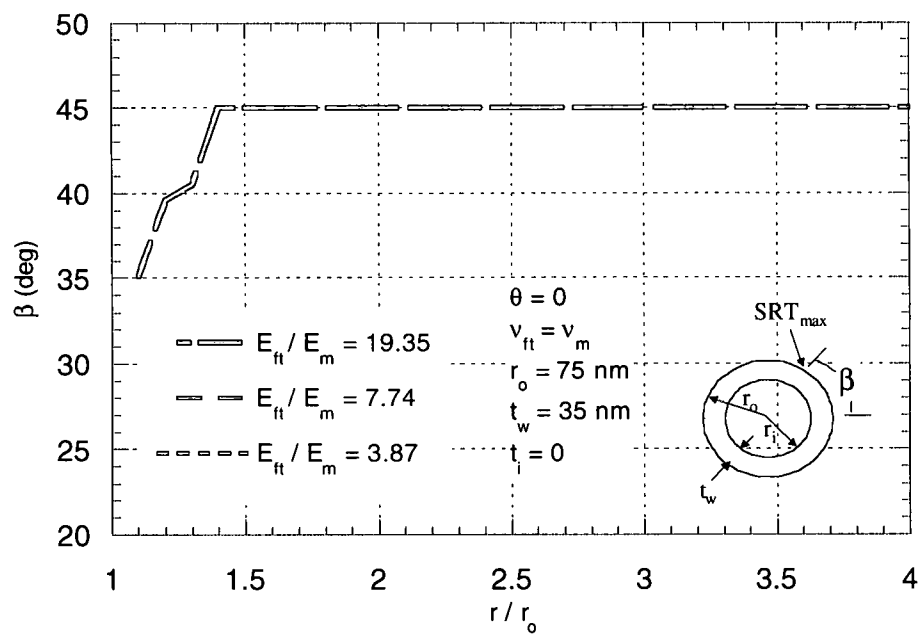


Figure 41. Location of maximum shear traction as a function of the nanofiber modulus

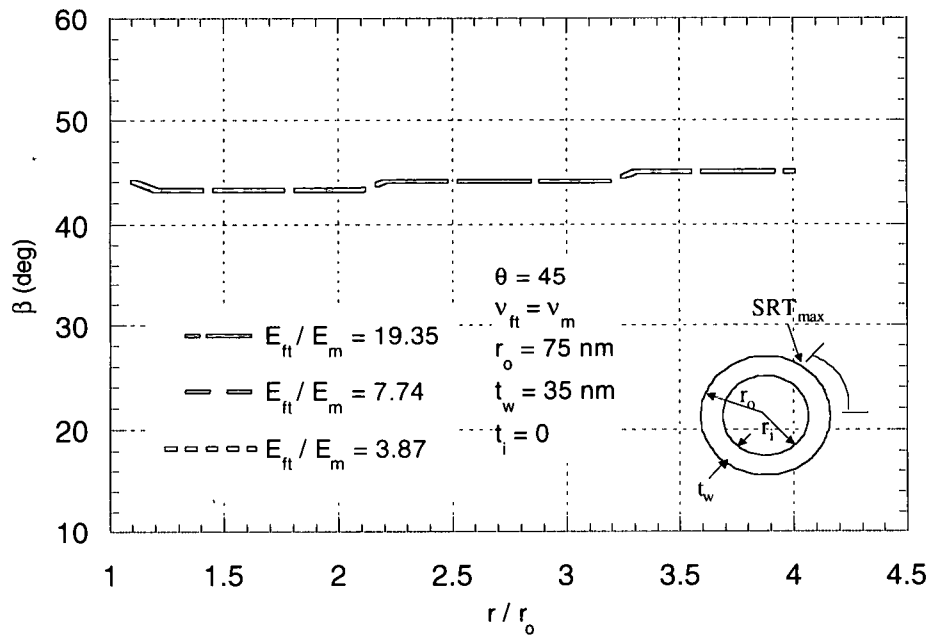


Figure 42. Location of maximum shear traction as a function of the nanofiber modulus

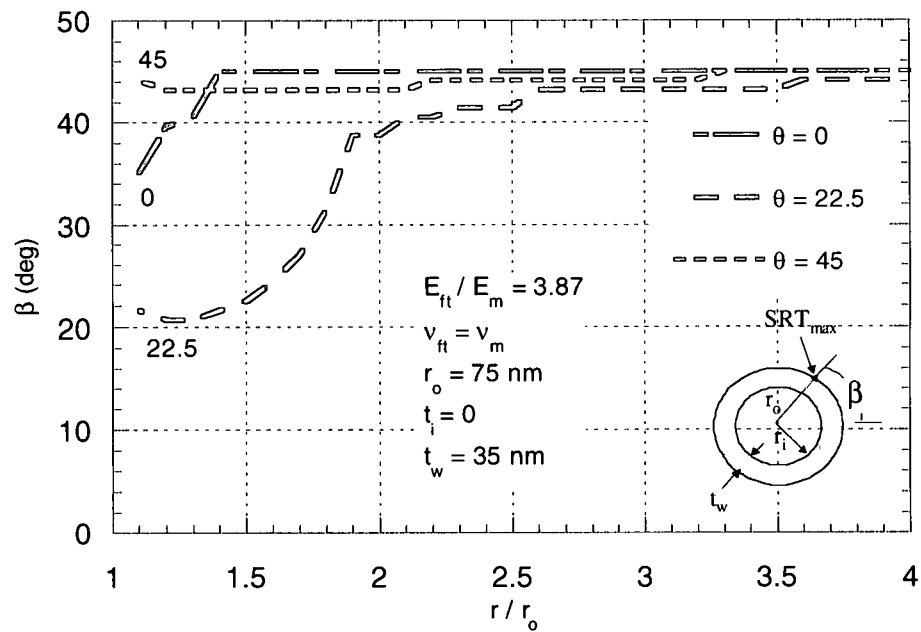


Figure 43. Location of maximum shear traction as a function of the crack orientation

negligible influence of the modular ratio on β . At relatively larger crack-nanofiber distances (r/r_0) the location of the maximum shear traction is at $\beta \approx 45$ as expected. When the crack is within a nanofiber radius distance, the location angle β changes and seems to be approaching the approximate location where the crack will intersect with the interface. Thus, for the crack orientation $\theta = 45$, the curves representing the variation of β (figure 42) remain almost flat as the starting value of β is the same value the crack is projected to intersect the nanofiber- matrix interface. Figure 43 shows the influence of crack orientation on β . Again, the β value seems to vary such that when the crack is very close to the fiber we have $\beta \approx \theta$.

Thus an investigation of the location of maximum interfacial tractions indicates that as the crack propagates towards the fiber the location of the maximum interface tractions moves towards the point where the crack is projected to intersect the fiber surface. Note that as the crack approaches the fiber the interface normal traction and shear traction values (maximum) increase. One may conclude that angles α and β , when the crack is very close to the fiber, represent the point on the interface region where possible interface failure (like debonding) can occur.

Characterization of the Influence of the Nanofiber Poisson's Ratio

As discussed in the literature review, the lack of controllability with regard to the structure of nanofibers may result in a significant variation of nanofiber elastic properties including Poisson's ratio. To evaluate the influence of Poisson's ratio on the crack energetics, a two-dimensional investigation is carried out wherein the nanofiber transverse Poisson's ratio is varied and its influence on crack energetics studied. Three different values of ν_f are considered such that

$$\nu_f/\nu_m < 1$$

$$\nu_f/\nu_m = 1$$

$$\nu_f/\nu_m > 1$$

Further, to isolate the effect of the Poisson's ratio, the nanofiber transverse modulus and the matrix modulus are assumed to be equal. Figures 44 to 48 show the results obtained for various studies in conjunction with the Poisson's ratio mismatch between the nanofiber and matrix.

As the figures show, the mode I energy release rate G_I becomes more and more sensitive to the change in the nanofiber Poisson's ratio with the increasing nanofiber wall thickness. However, perhaps a more interesting observation from the results for the mode I energy release rate is that for smaller values of the nanofiber wall thickness, the mode I energy release rate amplifies as the crack approaches the nanofiber regardless of the nanofiber Poisson's ratio value. This is indicated by figures 38 to 40, which show the amplification of the mode I energy release rate G_I/G_{I0} for all values of ν_f/ν_m as the crack tip approaches the nanofiber (at $\theta = 0$). Also, for the smallest nanofiber wall thickness, the curves for the different ν_f/ν_m are relatively close to each other. As the wall thickness is increased, the curves show a larger separation from each other. At the same time, the G_I/G_{I0} continues to show amplification in its value as the crack approaches the nanofiber (figures 38 to 40). It is only for the nanofiber wall thickness of 50 nm (figure 41), that there is a reversal in the trend for one of the Poisson's ratio mismatch values, i. e, $\nu_f/\nu_m=1.3$. Figure 42 shows the G_I/G_{I0} behavior for a different orientation of the crack. Comparing with the figure 40, it is clear that the change in the crack orientation angle θ (from $\theta = 0$ to $\theta = 45$) does not change the trend observed for a particular nanofiber wall thickness.

For each of the figures, it is observed that the higher the ν_f/ν_m , the less is the amplification effect, as shown by the lower values of G_I/G_{I0} for the highest ν_f/ν_m . Conversely, the lower value of ν_f/ν_m seems to result in a higher amplification effect on the crack driving force. Thus, for relatively small ν_f/ν_m , the crack will experience an amplification effect as it approaches the nanofiber irrespective of the nanofiber wall thickness. On the other hand, for higher values of G_I/G_{I0} there will be an amplification effect for lower values of nanofiber wall thickness (t_w) and a shielding effect for the higher values.

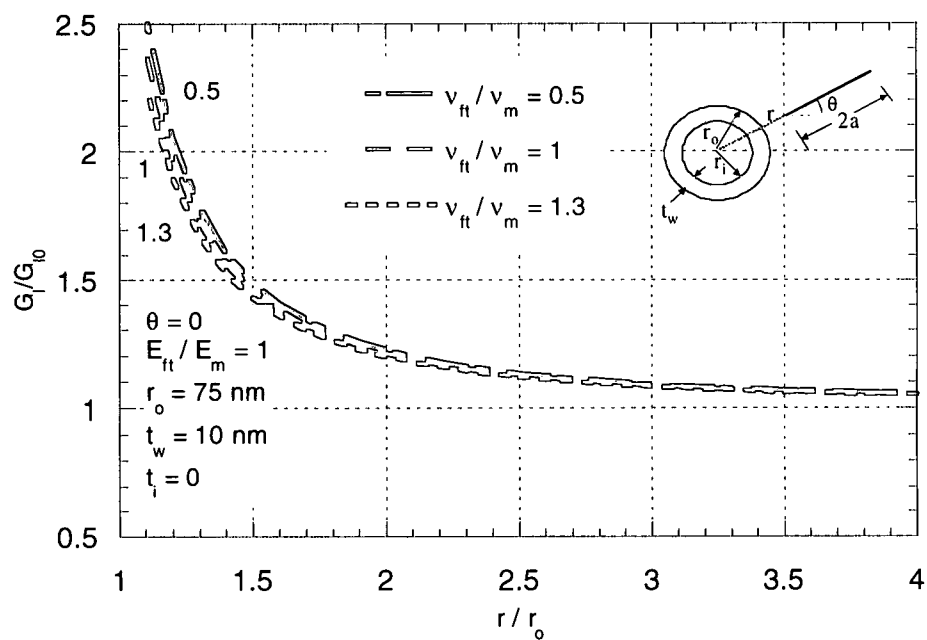


Figure 44. Influence of Poisson's ratio mismatch of nanofiber and matrix on G/G_0 , $t_w = 10 \text{ nm}$

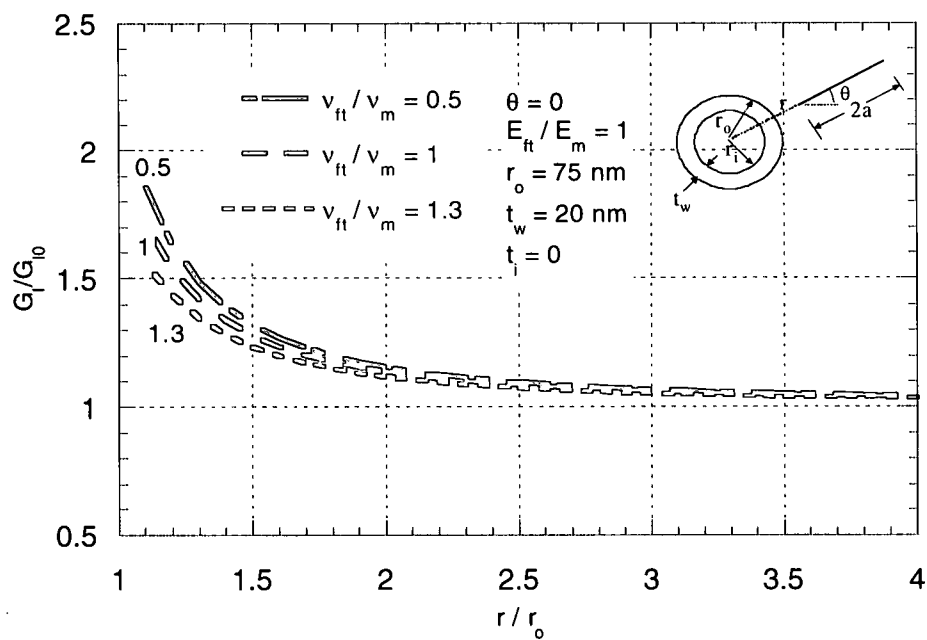


Figure 45. Influence of Poisson's ratio mismatch of nanofiber and matrix on G/G_0 , $t_w = 20 \text{ nm}$

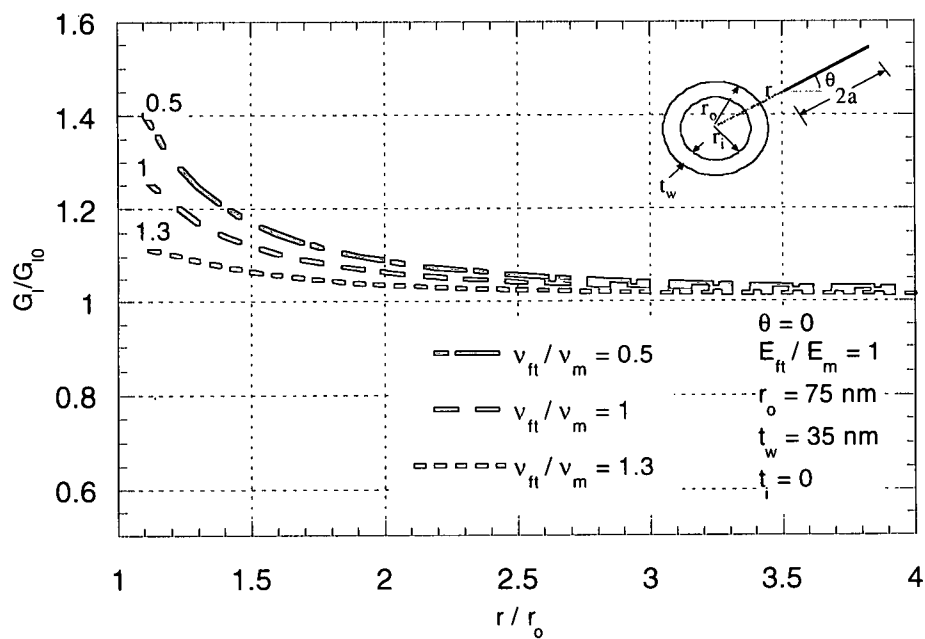


Figure 46. Influence of Poisson's ratio mismatch of nanofiber and matrix on G/G_{I0} , $t_w = 35$ nm

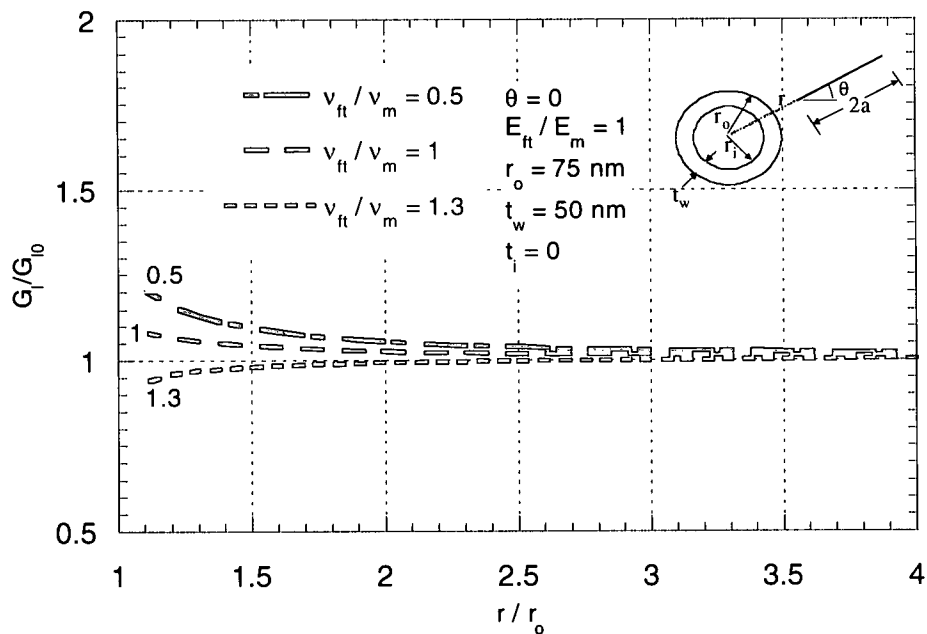


Figure 47. Influence of Poisson's ratio mismatch of nanofiber and matrix on G/G_{I0} , $t_w = 50$ nm

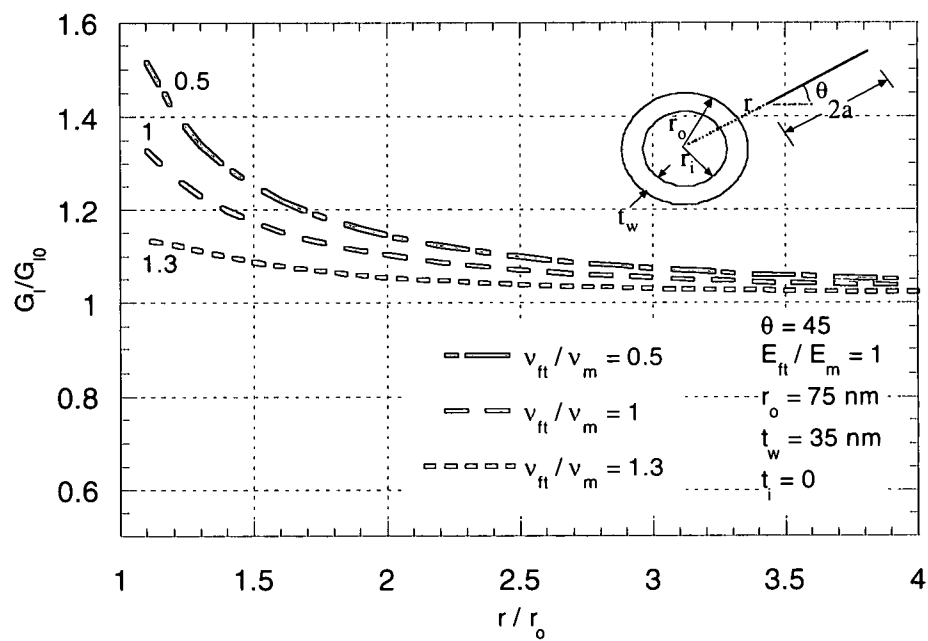


Figure 48. Influence of Poisson's ratio mismatch of nanofiber and matrix on G/G_{10} , $\theta = 45$

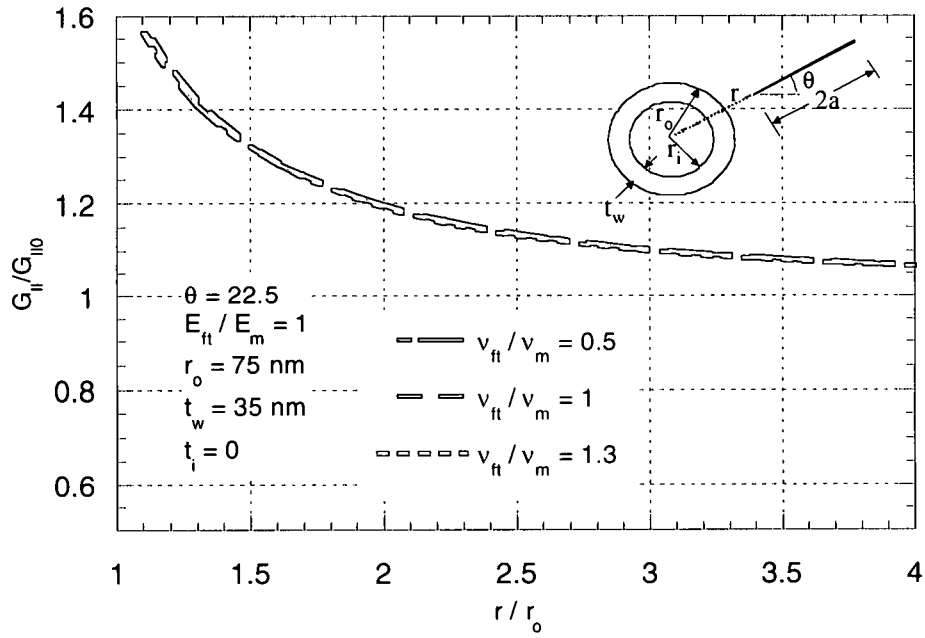


Figure 49. Influence of Poisson's ratio mismatch of nanofiber and matrix on G_{II}/G_{II0} , $\theta = 22.5$

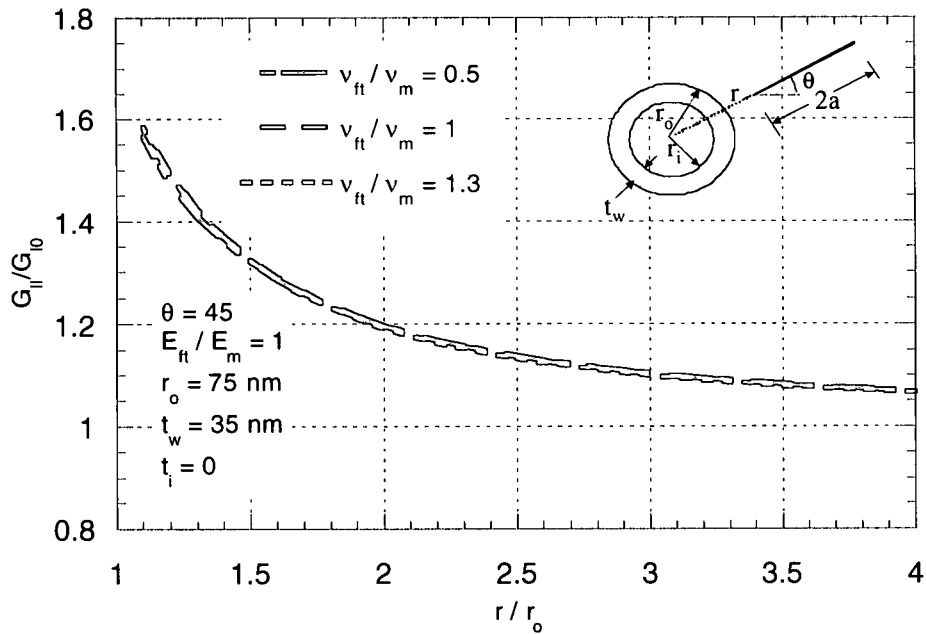


Figure 50. Influence of Poisson's ratio mismatch of nanofiber and matrix on G_{II}/G_{II0} , $\theta = 45$

Figures 43 and 44 show the influence of the mismatch in the Poisson's ratios of the nanofiber and matrix on the normalized mode II energy release rate. For all ν_f/ν_m values, the G_{II}/G_{II0} amplifies as the crack tip approaches the nanofiber. Also, all curves are almost on top of each other indicating that mode II energy release rate is not very sensitive to changes in the nanofiber Poisson's ratio. In contrast, as figures 38 through 42 indicated, G_I / G_{I0} shows more sensitivity to changes in ν_f / ν_m . On the other hand, similar to the trend for mode I behavior, mode II energy release rate shows a trend that is not sensitive to the variation in the crack orientation θ .

Figures 51 through 56 show the influence of the Poisson's ratio mismatch on the maximum normal and shear tractions at the nanofiber-matrix interface. It seems that SR_{max} is sensitive to the change in ν_f/ν_m for all crack-nanofiber distances. On the other hand, SRT_{max} seems to be sensitive to a change in ν_f / ν_m only when the crack is within one and a half fiber radii of the fiber center. Also, note that it is the highest ν_f / ν_m that gives the highest SR_{max} values, whereas in the case of shear traction at the interface, it is the lowest ν_f/ν_m that gives the highest SRT_{max} . Also, SR_{max} values seem to be converging towards each other as the crack approaches the fiber, whereas the SRT_{max} values seem to be deviating from each other as the crack approaches the fiber. The shear tractions also seem to be more sensitive to the change in the orientation (θ). For $\theta=0$, the curves for different ν_f/ν_m show more separation from each other compared to the other orientations. On the other hand for the other orientations, the curves are almost on top of each other for $\theta=22.5$ and $\theta=45$ until the crack is within one and a half nanofiber radii from the nanofiber center. Within this distance all three cases of orientations show a separation of the curves representing the various ν_f/ν_m values.

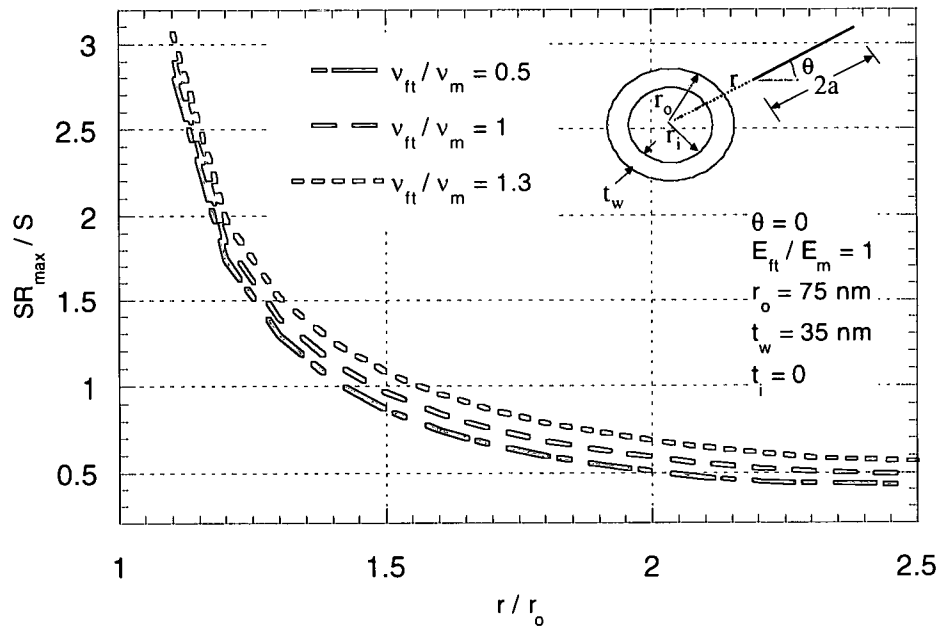


Figure 51. Influence of Poisson's ratio mismatch of nanofiber and matrix on maximum interfacial normal traction, $\theta = 0$

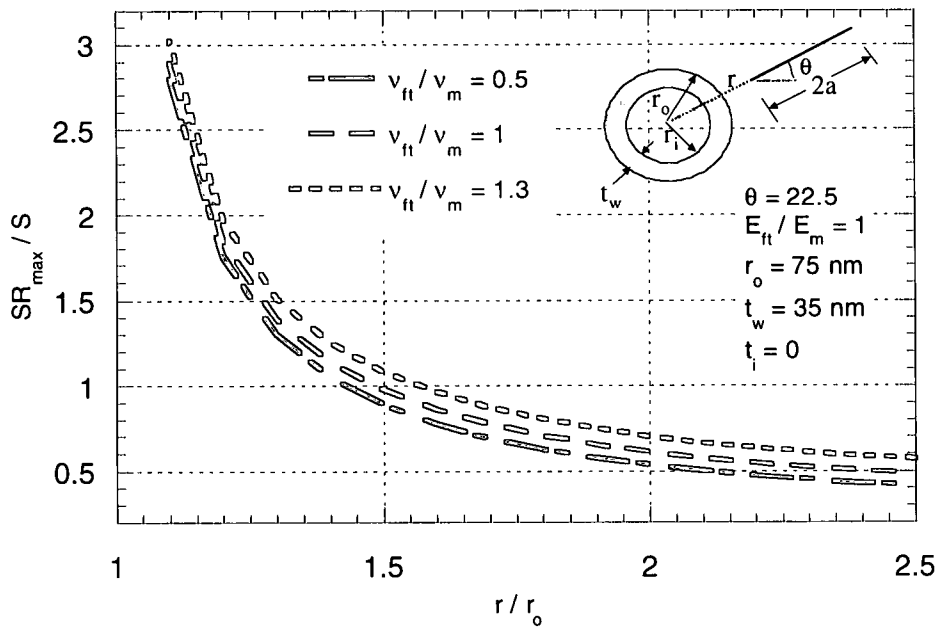


Figure 52. Influence of Poisson's ratio mismatch of nanofiber and matrix on maximum interfacial normal traction, $\theta = 22.5$

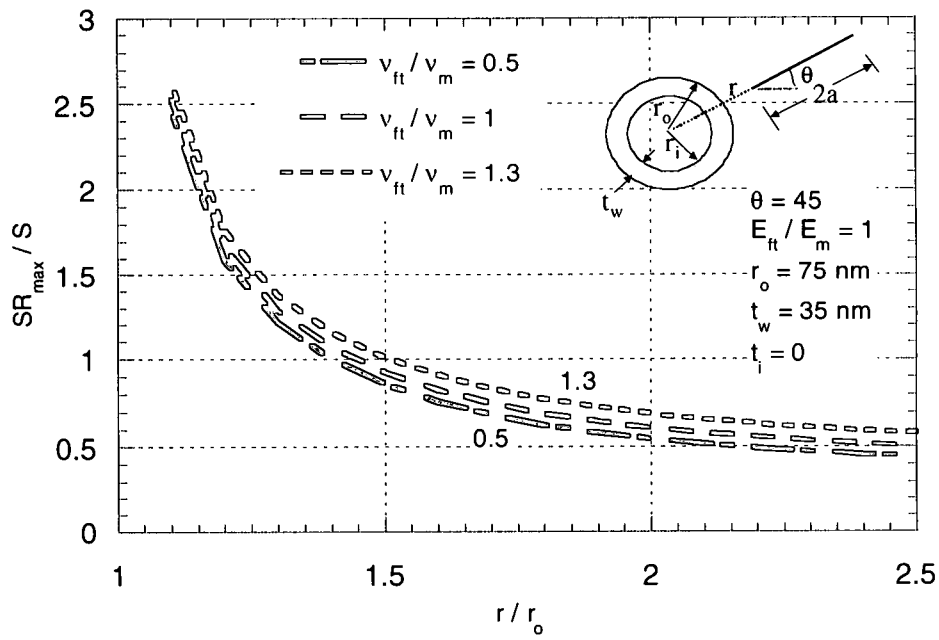


Figure 53. Influence of Poisson's ratio mismatch of nanofiber and matrix on maximum interfacial normal traction, $\theta = 45$

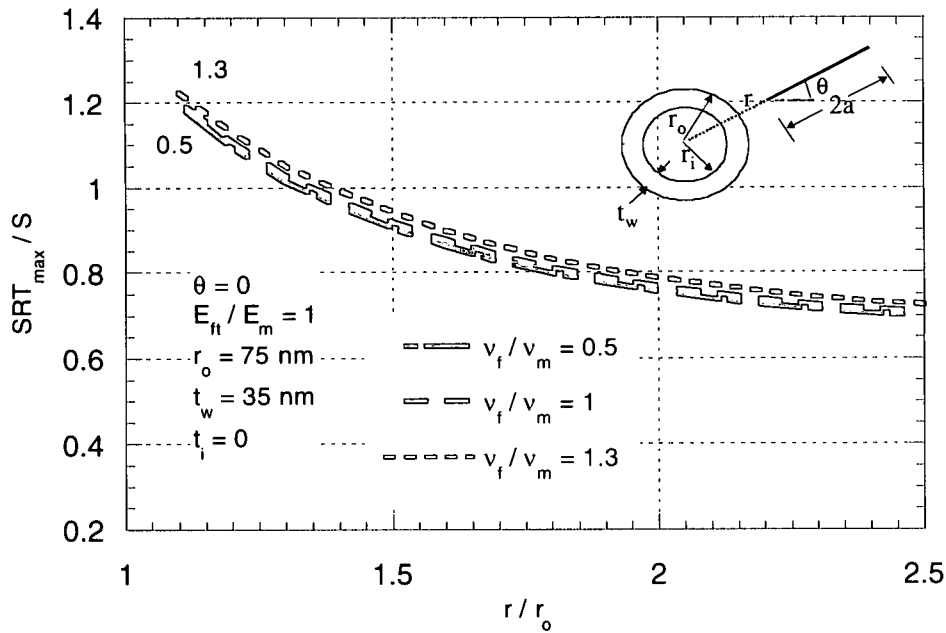


Figure 54. Influence of Poisson's ratio mismatch of nanofiber and matrix on maximum interfacial shear traction, $\theta = 0$

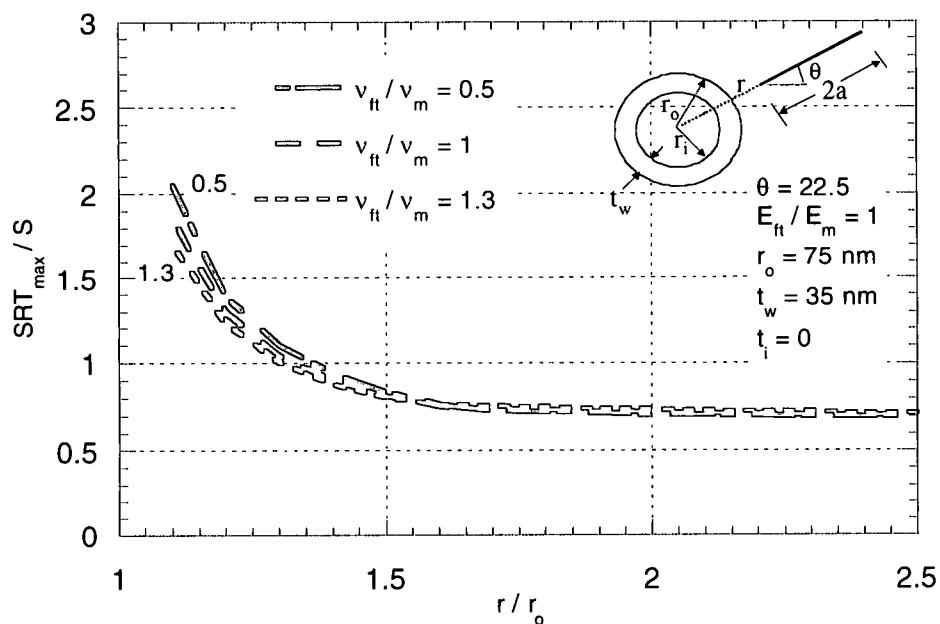


Figure 55. Influence of Poisson's ratio mismatch of nanofiber and matrix on maximum interfacial shear traction, $\theta = 22.5$

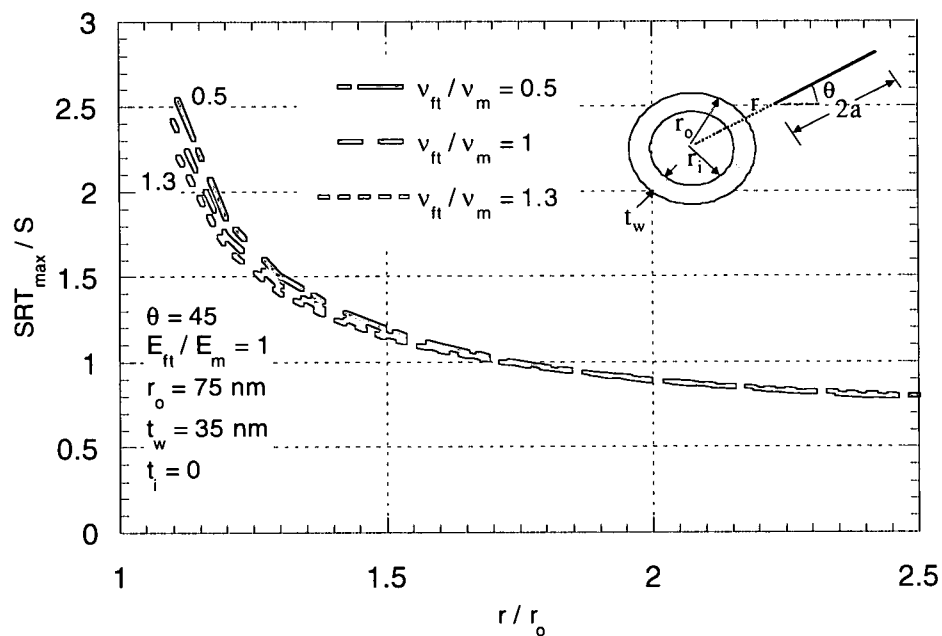


Figure 56. Influence of Poisson's ratio mismatch of nanofiber and matrix on maximum interfacial shear traction, $\theta = 45$

CHAPTER V

CHARACTERIZATION OF THE INFLUENCE OF NANOFIBER WALL THICKNESS

Nanofibers are different from the conventional fibers used as composite reinforcement in that they have a hollow cylindrical geometry. As described in the literature review, as of today the nanofiber wall thickness seems to be a quality control issue. With the lack of controllability on the nanofiber structure, nanofiber wall thickness shows a significant variation with the wall thickness being as large as up to 90 percent of the outer radius. Thus, question arises as to how the wall thickness and its variation are likely to influence the crack driving force of a crack propagating towards a nanofiber. Also, it will be interesting to investigate the influence of nanofiber wall thickness on interface tractions and their locations.

Characterization Approach

The characterization of the influence of nanofiber wall thickness on nanofiber toughening and interface tractions is done by considering the following wall thickness values,

$$t_w = 10, 20, 30, 35, 40, 50 \text{ nm}$$

For all the analyses conducted, the nanofiber outer radius is fixed and is equal to,

$$r_o = 75 \text{ nm}$$

First, two-dimensional study is performed with the above wall thickness values. In the two-dimensional investigation, interface tractions and their locations are computed besides the energy release rates. By incorporating mixed mode conditions, both mode I and mode II behaviors are investigated in the two-dimensional study. Then, three-dimensional study is performed to corroborate the trends observed for crack energetics in the two-dimensional study. In the three-dimensional study, only mode I behavior is investigated.

Influence of Nanofiber Wall Thickness on mode I behavior

Figures 57 through 82 present various results obtained in conjunction with the influence of the nanofiber wall thickness on the crack energetics and the nanofiber-matrix interface tractions. The results presented in these figures clearly show that the nanofiber wall thickness has a significant influence on the crack energetics.

Figure 57 schematically shows the effect of the increase in the nanofiber wall thickness on the energy release rate of a propagating crack. With the increasing wall thickness, the variation in the energy release rate becomes smaller and smaller. Thus, there seems to be a threshold value of the (t_w) beyond which any further increase in the nanofiber wall thickness may not result in a significant change in the crack energetics. This is true for both mode I and mode II crack propagation. Figures 58 to 63 show this behavior for mode I crack driving force. As shown in the figures, the curves representing various wall thicknesses seem to be getting closer and closer to one another as the wall thickness is increased.

The mode I energy release rate is sensitive to the nanofiber wall thickness, with the smaller wall thickness yielding a larger G_I/G_{I0} . The curves for different wall thicknesses are more closely placed for a higher E_f/E_m . Thus, there is a greater sensitivity of G_I/G_{I0} to the variation in the wall thickness (t_w) when the nanofiber transverse modulus is relatively small. Also, the figures clearly show that for a greater wall thickness the crack senses the presence of the nanofiber earlier. As figures 58 through 63 show, the trend observed for mode I energy release rate, as a function of various wall thicknesses does not change when the crack orientation is varied. There is a sharp gradient observed for all curves as the crack approaches the nanofiber, with even the smallest wall thickness providing a shielding effect as the crack nears the nanofiber.

The two-dimensional crack propagation analysis showed that the nanofiber wall thickness has a significant influence on the toughening effect of a stiff nanofiber on a propagating crack. A similar study is performed in three-dimensions and results presented in figures 64 to 67. As shown by these figures, the three-dimensional study yields the results similar to those

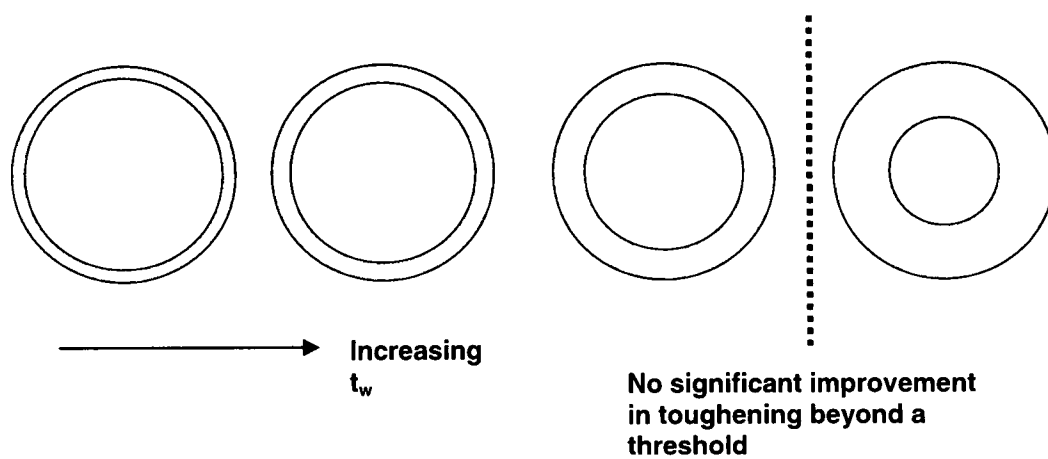


Figure 57. Influence of the nanofiber wall thickness on G_I/G_{I0}

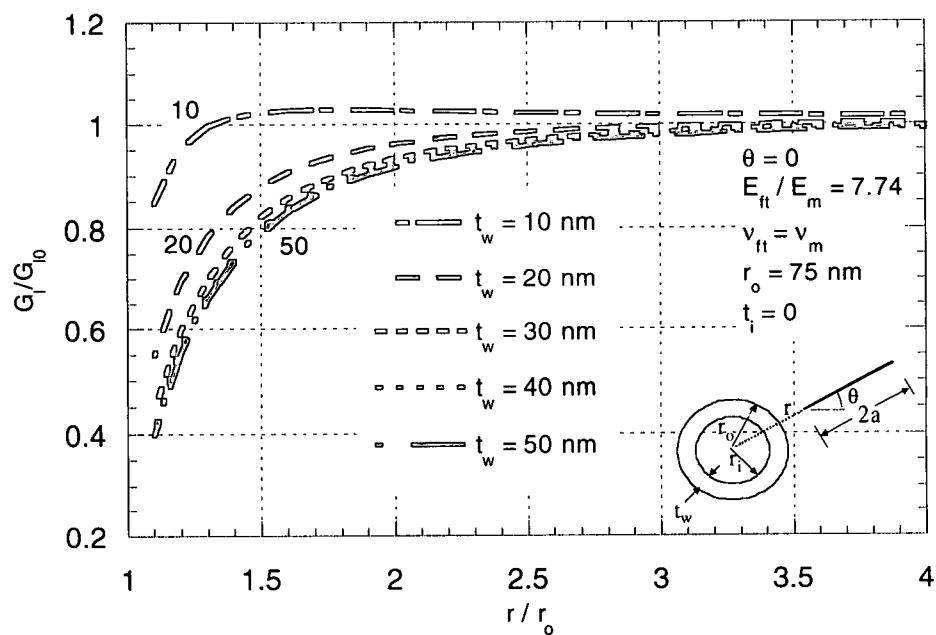


Figure 58. Influence of the nanofiber wall thickness on G/G_0

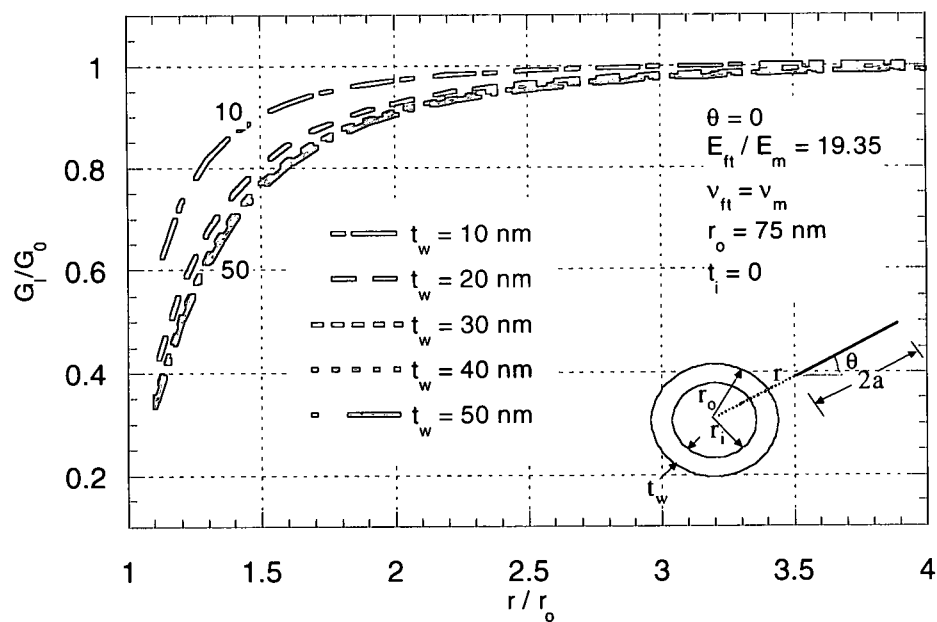


Figure 59. Influence of the nanofiber wall thickness on G/G_0

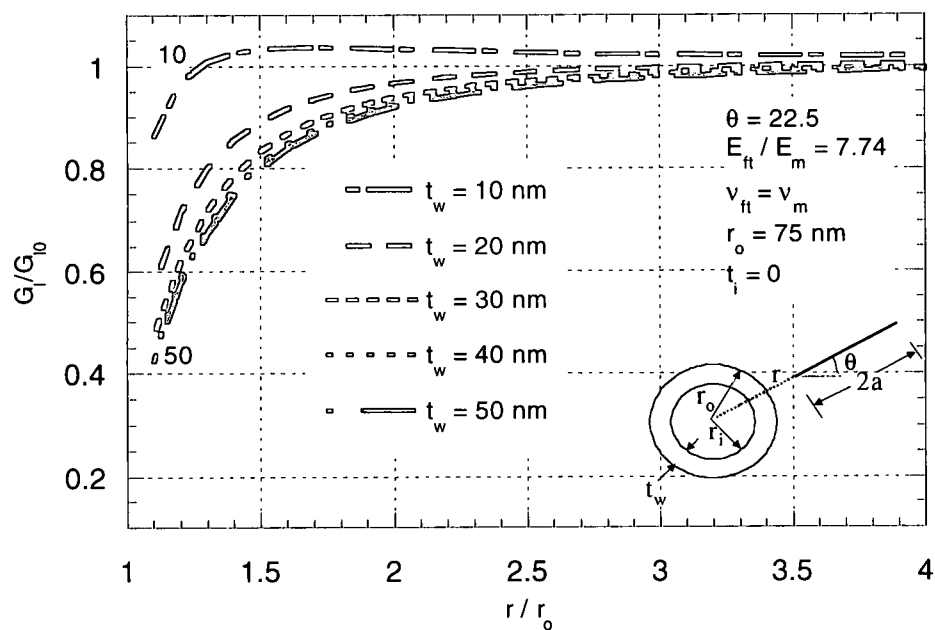


Figure 60. Influence of the nanofiber wall thickness on G/G_0

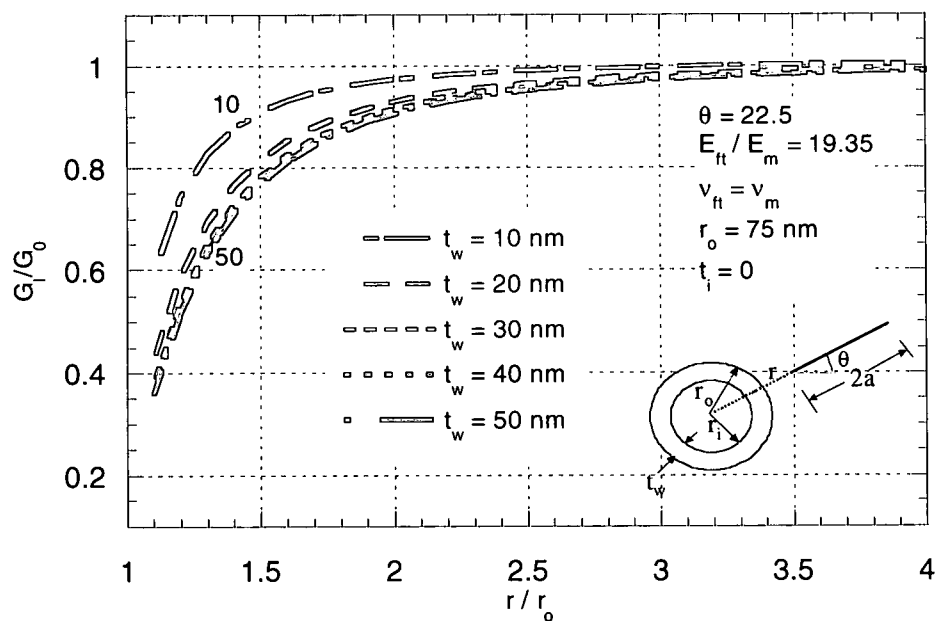


Figure 61. Influence of the nanofiber wall thickness on G/G_0

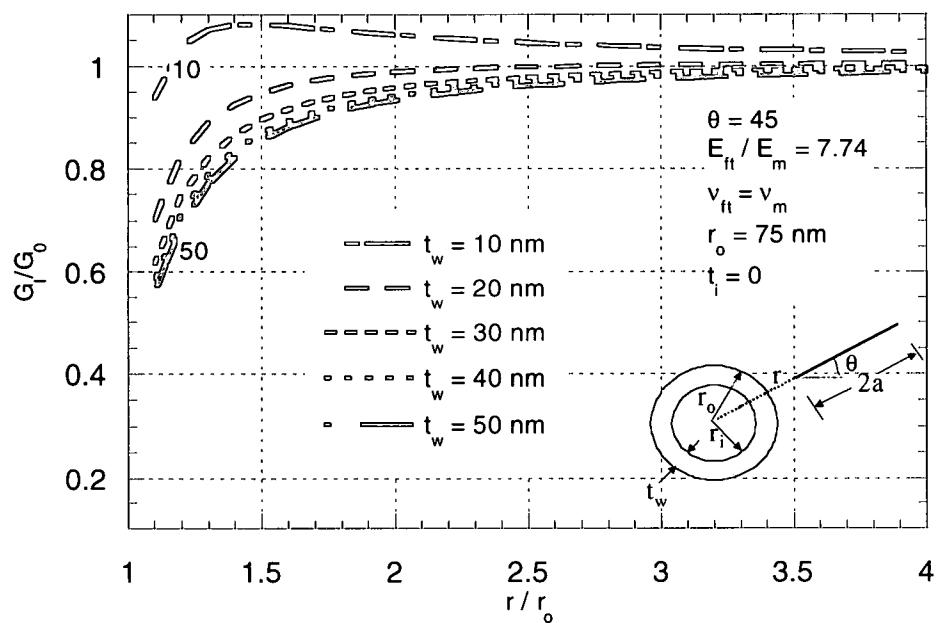


Figure 62. Influence of the nanofiber wall thickness on G/G_0

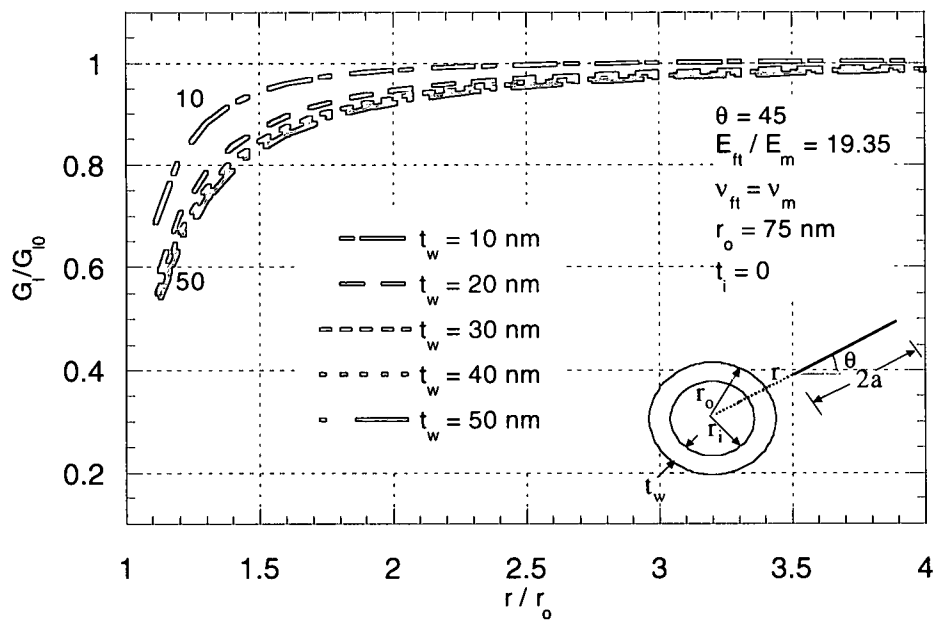


Figure 63. Influence of the nanofiber wall thickness on G/G_0

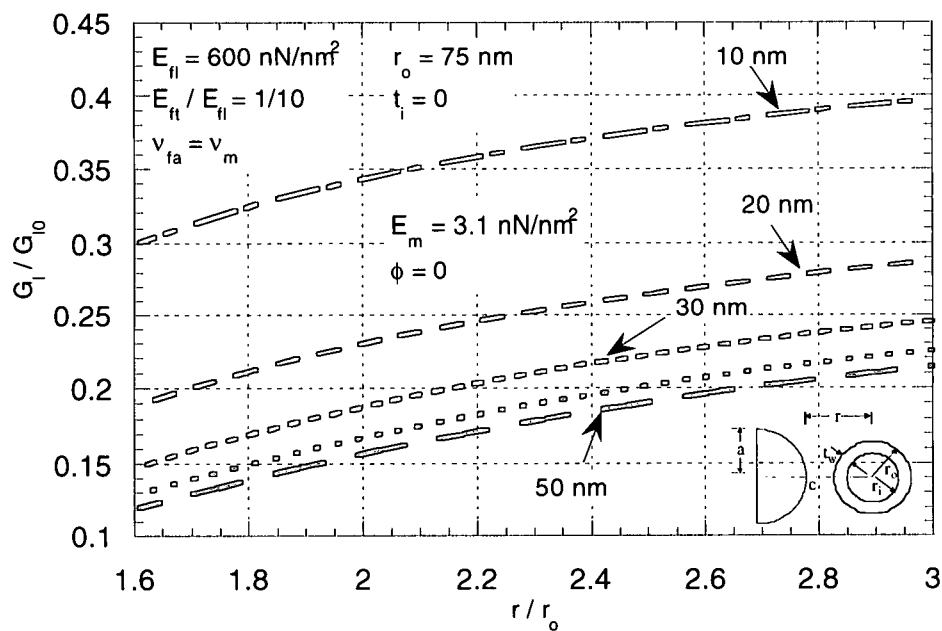


Figure 64. Mode I energy release rate at point 'c' ($\theta=90$) for successive crack front positions

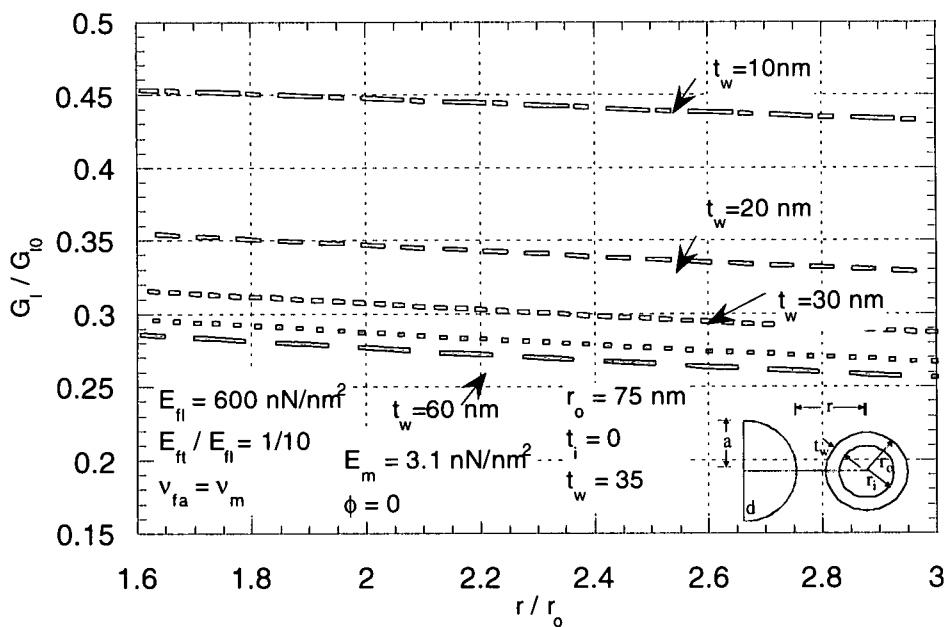


Figure 65. Mode I energy release rate at point 'c' ($\theta=90$) for successive crack front positions

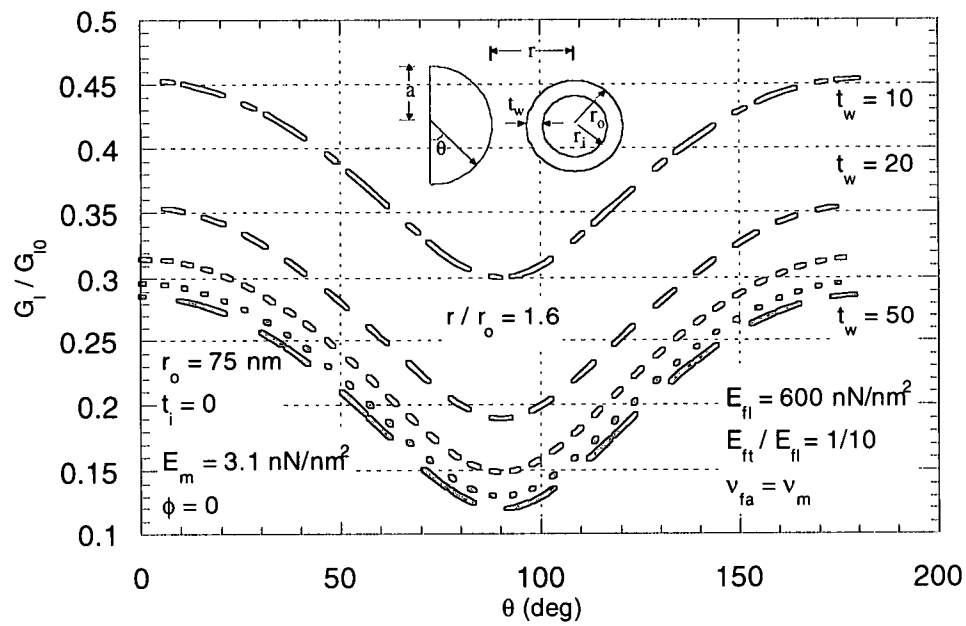


Figure 66. Influence of nanofiber wall thickness on Mode I energy release rate along the crack front

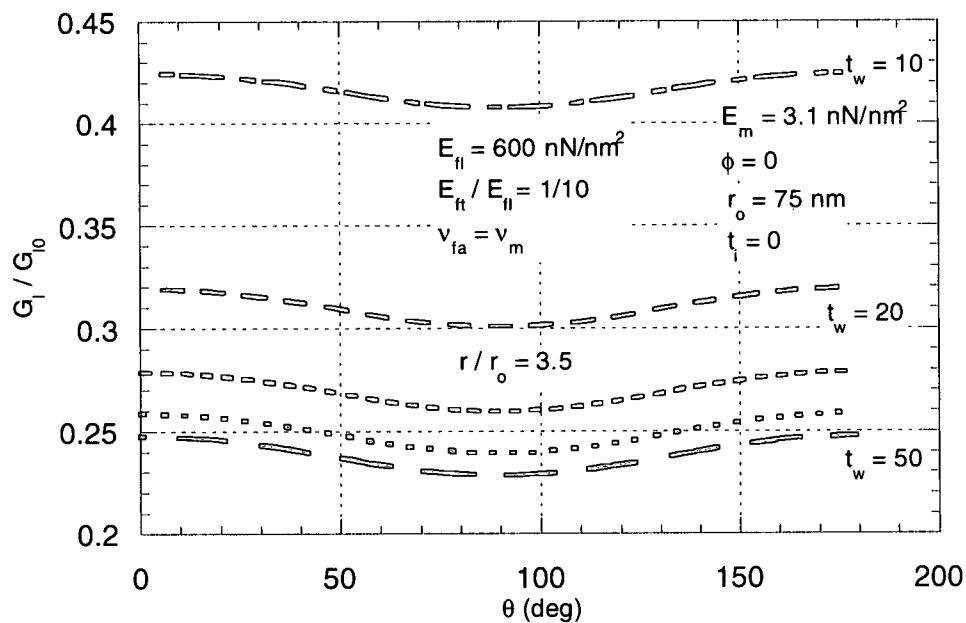


Figure 67. Influence of nanofiber wall thickness on Mode I energy release rate along the crack front

obtained in the two-dimensional crack propagation studies. As figure 64 shows, a smaller nanofiber wall thickness results in a larger crack driving force G_I/G_{I0} . This effect is observed for the portion of the crack front facing the nanofiber (figure 64). On the other hand, for the point at $\theta = 0$ (point d, figure 65), the effect of a particular nanofiber wall thickness remains the same with respect to the other wall thicknesses although the crack front experiences an increase in the G_I/G_{I0} .

Figures 66 and 67 show the influence of the nanofiber wall thickness evaluated along the crack fronts for various values of t_w . The farthest and the closest crack front positions considered show a similar influence of the wall thickness. Thus, the smallest nanofiber wall thickness results in the largest G_I/G_{I0} and vice versa. Also, a careful study of the figures 66 and 67 shows that the curves for the various t_w values are farther from each other for the farthest crack position and become closer to each other as the crack front approaches the nanofiber.

The three-dimensional study corroborates the trend observed in the two-dimensional analysis, which is that with the increasing wall thickness, the variation in the energy release rate becomes smaller and smaller. As such, the difference in the energy release rates corresponding to the wall thicknesses 10 nm and 20 nm is much greater than that in the energy release rates corresponding to the wall thicknesses 40 nm and 50 nm. Thus, there seems to be a wall thickness value beyond which any further increase in the wall thickness may not result in a significant advantage in the form of the toughening by the nanofiber.

Influence of Nanofiber Wall Thickness on mode II behavior

Mode II crack energetics shows a greater sensitivity to the variation in the nanofiber wall thickness than mode I. This is indicated by figures 66 to 71. There is not only a significant variation in energy release rate with the change in the fiber wall thickness, but also for some of the smaller values of the fiber wall thickness there is an amplification effect on G_{II}/G_{II0} . For example, with a wall thickness of 10 nm, the nanofiber provides a shielding effect for a crack

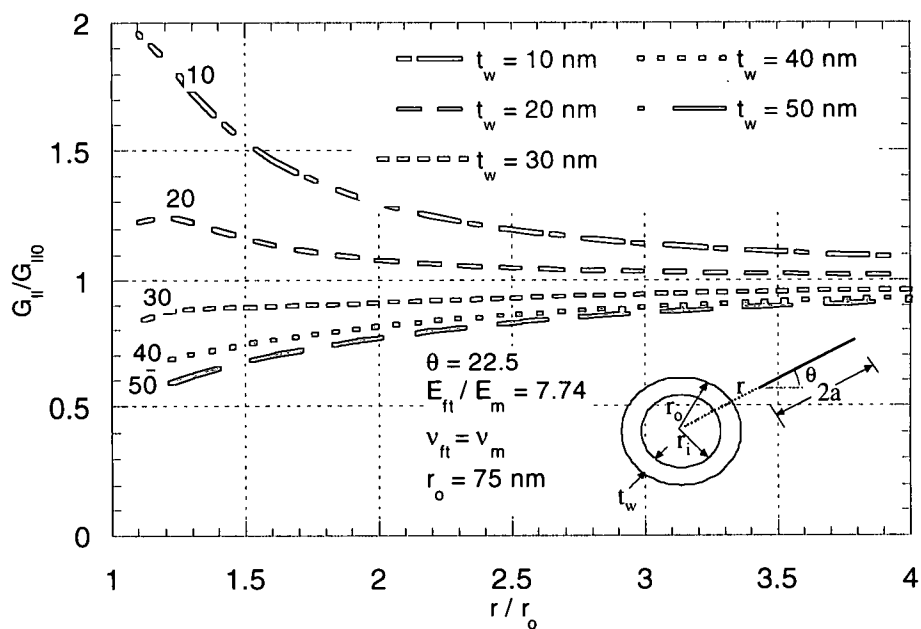


Figure 68. Influence of the nanofiber wall thickness on G_{II}/G_{II0}

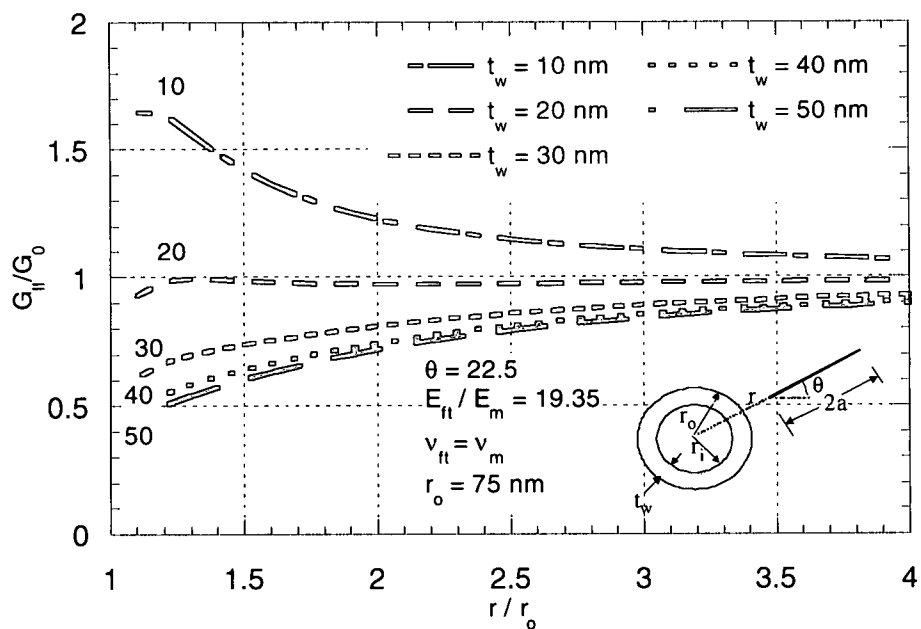


Figure 69. Influence of the nanofiber wall thickness on G_{II}/G_{II0}

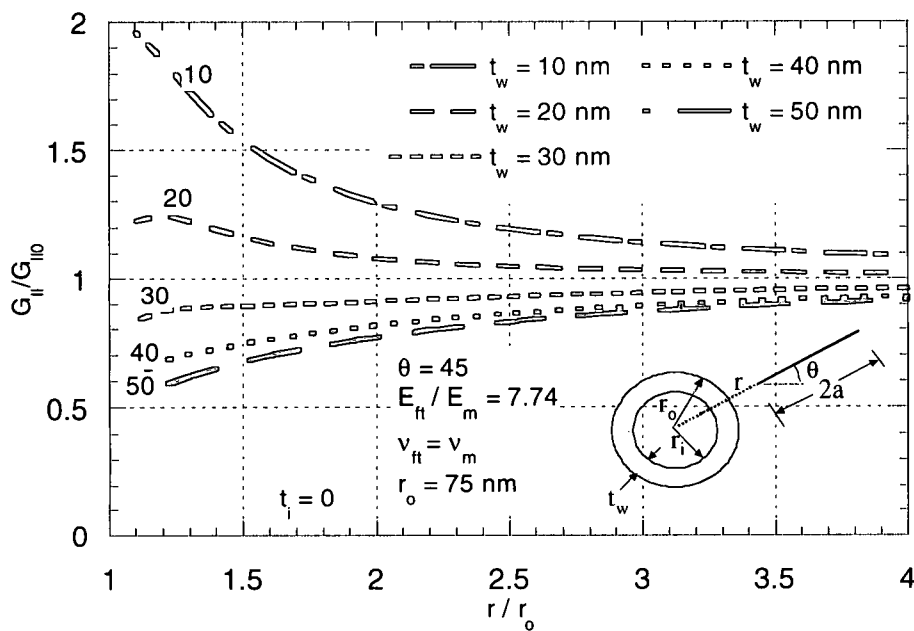


Figure 70. Influence of the nanofiber wall thickness on G_{II}/G_{II0}

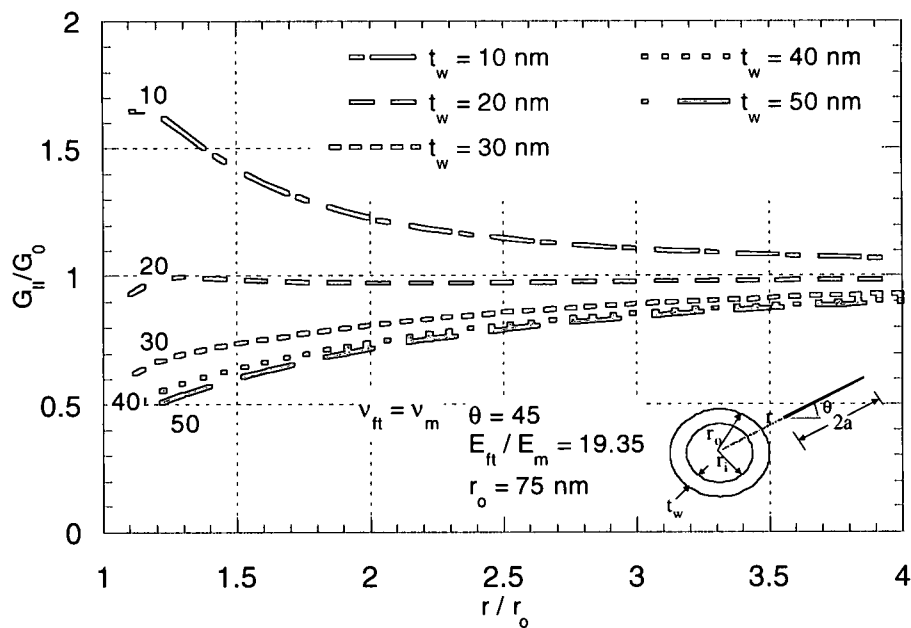


Figure 71. Influence of the nanofiber wall thickness on G_{II}/G_{II0}

propagating in mode I conditions, whereas the effect in mode II with the same wall thickness is to amplify the energy release rate and thus attract the crack. The sensitivity of the mode II behavior to the variation in the nanofiber wall thickness increases slightly with the decreasing nanofiber modulus value as shown by the figures 68 to 71. By comparison, it seems that mode I behavior is relatively more sensitive to the variation in the nanofiber modulus with respect to the influence of the nanofiber wall thickness.

The trend observed for mode I propagation wherein the variation in the crack driving force seems to decay with the increasing wall thickness, is also observed for the case of mode II crack propagation. Also, a comparison of the results for the two crack orientations that produce mode II conditions shows that variation in the crack orientation does not result in a significant change in the behavior of the propagating crack in terms of its response to the nanofiber wall thickness and its variation.

Influence of Nanofiber Wall Thickness on Interface Traction

The investigation of the dependence of the nanofiber-matrix interface tractions on the nanofiber wall thickness reveals that the maximum interface traction values are influenced significantly by the variation in the nanofiber wall thickness. Figures 72 and 73 schematically show the results of the investigation. As figure 72 shows, the maximum normal traction SR_{max} seems to experience a reversal in the trend as the crack approaches the fiber. Initially, when the crack is relatively away from the fiber the SR_{max} values are larger for the larger fiber wall thickness. However, when the crack is within one and a half fiber radii, the smaller wall thickness yields a larger SR_{max} . The SR_{max} values seem to converge towards each other once the crack is within one and half fiber radii and approaches the nanofiber. Figures 74 and 75 show the variation of maximum normal traction at the interface for various nanofiber wall thicknesses for two different crack orientations. Comparing these figures, it seems that changing the crack orientation does not change the trend observed for the variation of the SR_{max} significantly. The figures also show that for all wall thicknesses considered the

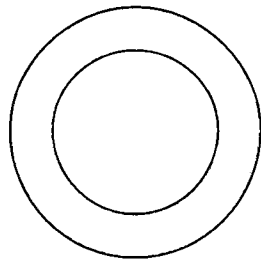
maximum normal traction value increases as the crack propagates towards the nanofiber, and especially experiences a relatively sharp increase when the crack is approximately within one and a half nanofiber radii from the nanofiber center.

Figure 73 schematically demonstrates the behavior of maximum shear traction. Unlike, the normal traction, the maximum shear traction does not show a reversal of trend in that a smaller wall thickness yields a larger SRT_{max} for a propagating crack irrespective of the distance of the crack from the nanofiber. Thus, the behaviors of SR_{max} and SRT_{max} are opposite of one another when the crack is relatively far from the nanofiber, and similar to one another when the crack is close to the nanofiber. Figures 76 to 78 show the trends obtained for the maximum shear traction with respect to its dependence on the nanofiber wall thickness. Unlike the maximum normal traction, the maximum shear traction curves corresponding to various t_w values seem to be deviating from each other as the crack approaches the nanofiber. Thus, if the closest crack positions are considered, the SR_{max} values corresponding to various nanofiber wall thicknesses are much closer to each other whereas the corresponding SRT_{max} values for various wall thicknesses show a relatively greater variation. The other difference between the maximum normal and shear traction trends is the sensitivity to the crack orientation θ . As the figures 76 to 78 indicate, the maximum shear traction SRT_{max} shows sensitivity to the change in the crack orientation. As the crack orientation is increased from 0 to 45 degrees, the maximum shear traction values for the closest crack-nanofiber distances increase.

Influence of Nanofiber Wall Thickness on the Locations of maximum tractions

Figures 79 to 81 show the influence of the nanofiber wall thickness on the locations (α) of the maximum normal tractions. The results show that the influence of the nanofiber wall thickness on the location of the maximum normal traction is there only when the crack is relatively far from the nanofiber. Figure 79 schematically shows the variation in the location of the maximum normal traction as a crack propagates towards the nanofiber at $\theta = 0$ deg.

Smaller $t_w \rightarrow$ Greater SR_{max}



Greater $t_w \rightarrow$ Greater SR_{max}



Figure 72. Influence of the nanofiber wall thickness on the behavior of maximum interface normal traction

Smaller $t_w \rightarrow$ Greater SRT_{max}

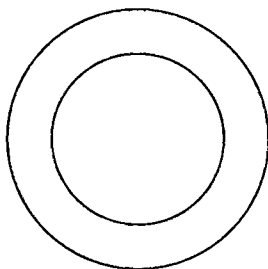


Figure 73. Influence of the nanofiber wall thickness on the behavior of maximum interface shear traction

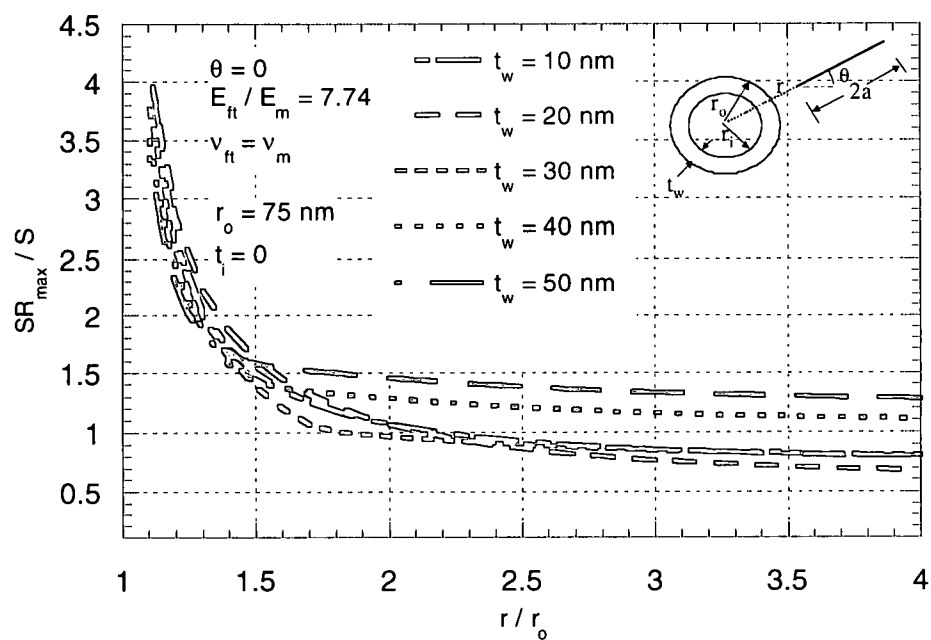


Figure 74. Influence of the nanofiber wall thickness on maximum interface normal traction

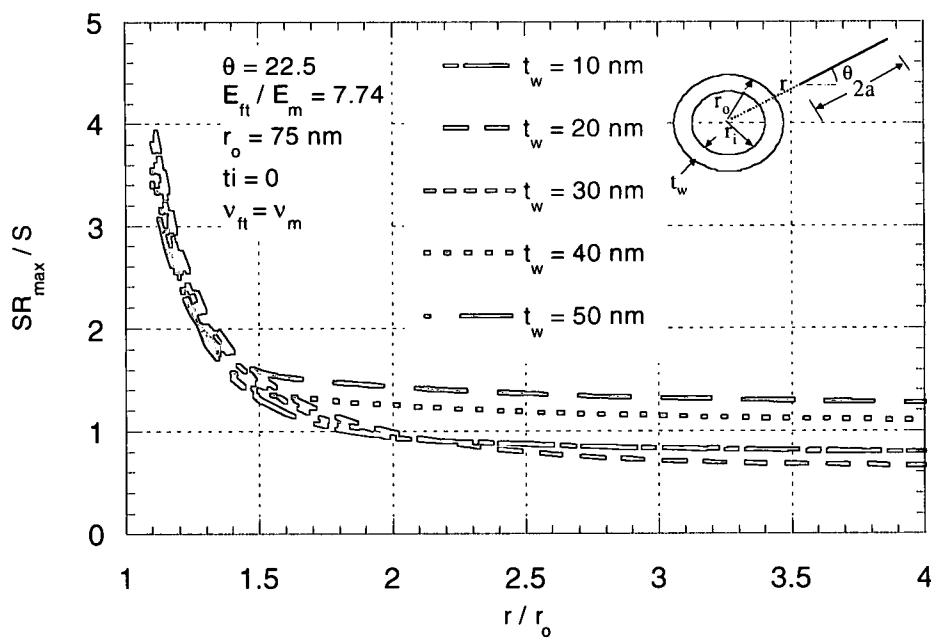


Figure 75. Influence of the nanofiber wall thickness on maximum interface normal traction

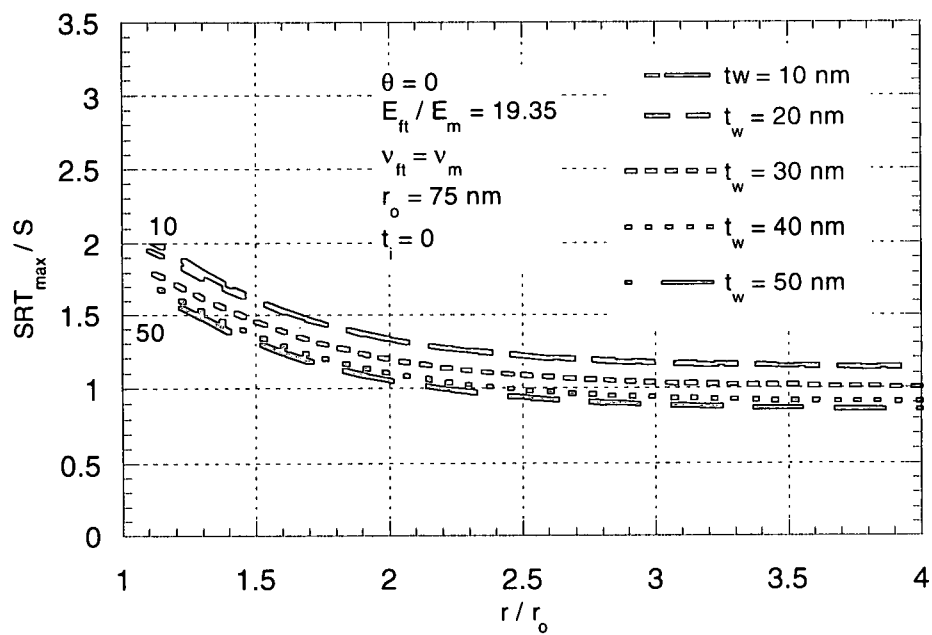


Figure 76. Influence of the nanofiber wall thickness on maximum interface shear traction

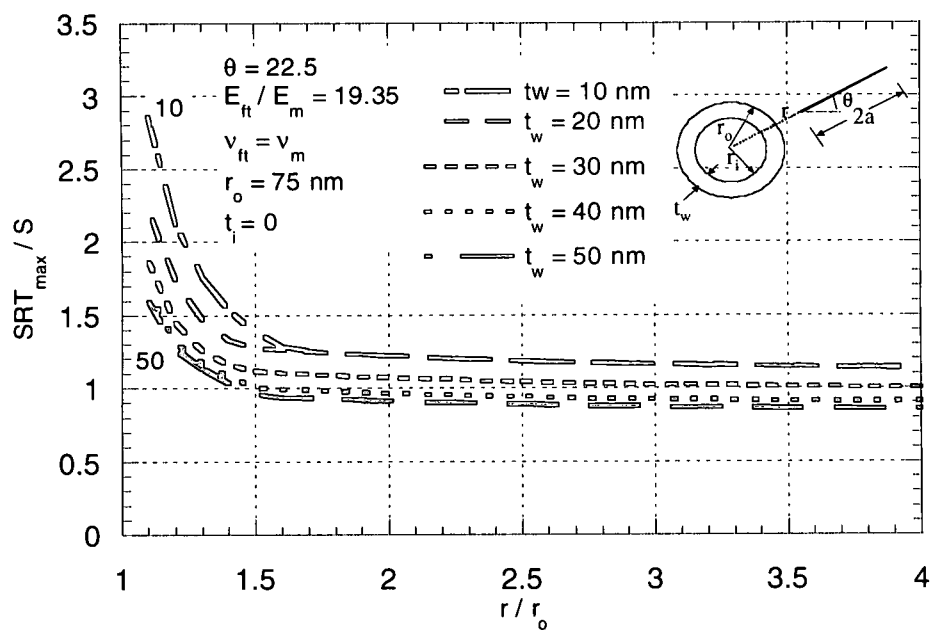


Figure 77. Influence of the nanofiber wall thickness on maximum interface shear traction

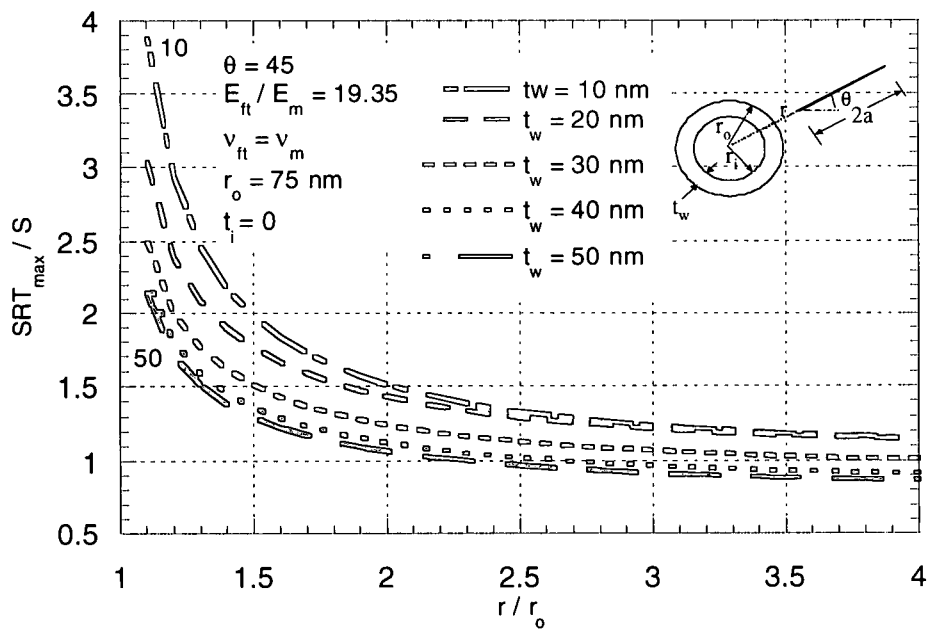


Figure 78. Influence of the nanofiber wall thickness on maximum interface shear traction

When the t_w is very small ($t_w = 10, 20$ nm), the angle (α) remains constant throughout the course of crack propagation with a value of zero. This means that the location of the maximum normal traction is at the point where the crack is projected to intersect the nanofiber-matrix interface. On the other hand, for larger values of t_w , the location of the maximum normal traction is approximately at $\alpha = 90$ when the crack is at its farthest position. However, as the crack propagates towards the nanofiber, (α) changes and approaches a value of $\alpha = 90$. Figure 80 shows these results, obtained for various wall thicknesses and a crack orientation of $\theta = 0$ deg.

The above trend is again confirmed by changing the crack orientation from $\theta = 0$ to $\theta = 45$ deg, as shown in the figure 81. Again, the location of maximum traction shifts to the point of intersection of the crack and the nanofiber-matrix interface, in this case approximately at 45 deg. This means that when the crack is at its closest position with respect to the nanofiber, the nanofiber wall thickness value has no bearing on the location of the maximum normal traction as this location shifts to the point on the nanofiber-matrix interface where the crack is projected to intersect the interface (figures 80, and 81).

Figure 82 shows the influence of nanofiber wall thickness on the location (β) of the maximum shear traction at the nanofiber-matrix interface. The influence in the case of shear traction location is perhaps not as dramatic as it is in the case of normal traction. For all t_w values considered, the location (β) starts out at approximately 45 degrees and tends to move towards the point of intersection of the crack and the nanofiber. However, unlike the case of normal traction locations, even the smallest wall thickness values show the variation of location (β) with the crack propagation that is more or less same as the locations for the larger wall thickness values.

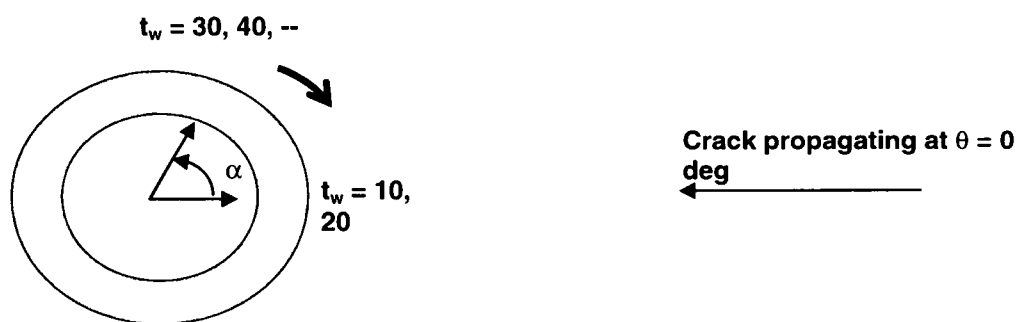


Figure 79. Influence of the nanofiber wall thickness on the location of maximum interface normal traction

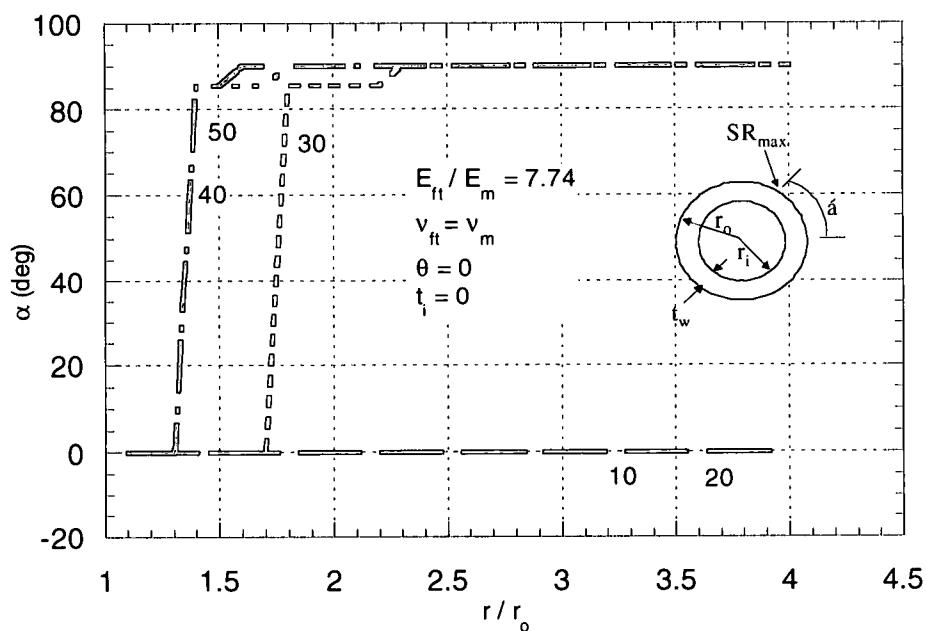


Figure 80. Location of maximum interface normal traction for various values of nanofiber wall thickness (t_w)

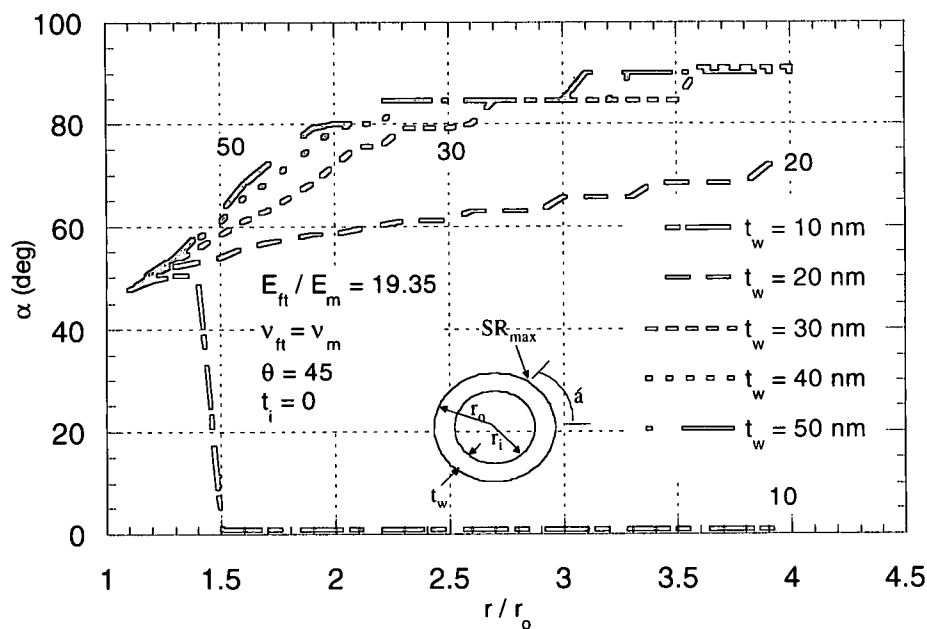


Figure 81. Location of maximum interface normal traction for various values of nanofiber wall thickness (t_w)

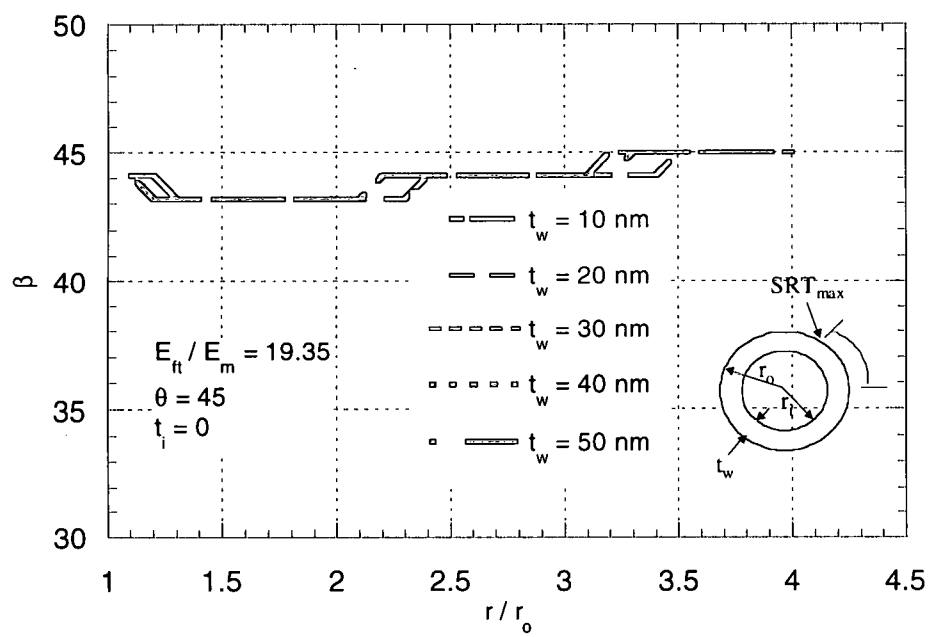


Figure 82. Location of maximum interface shear traction for various values of nanofiber wall thickness (t_w)

CHAPTER VI

CHARACTERIZATION OF THE INFLUENCE OF AN INTERPHASE BETWEEN THE NANOFIBER AND MATRIX

Nanocomposites such as nanofiber-reinforced composites are different from conventional composites in that the phenomena resulting from the nanoscale dimensions of the reinforcement material are expected to dominate the behavior of the resulting composite. One of the consequences of reinforcing a polymer matrix with a carbon nanofiber is that there is now a reinforcement material in the composite system whose dimensions are the same order of magnitude as the polymer molecule chain. As a result, there is expected to be an interphase region in a nanocomposite material system that is much more dominant than the one in conventional composite material system. However, little is known currently as to the nature of an interphase region in a nanofiber-reinforced composite or for that matter, other nanocomposite systems.

In the present work, the influence of an interphase between a nanofiber and matrix is characterized by studying the effect of its elastic properties and dimensions on crack energetics. The interphase is modeled as a region between the nanofiber and matrix with its own elastic properties. The interphase elastic properties are assumed to be constant throughout the interphase region. Since not much has been reported in the literature on the nature and the elastic properties of the interphase region, the elastic properties are assumed to be similar to those in a study by knight [51].

Influence of Interphase Elastic Modulus

To investigate the influence of the interphase elastic modulus on the energy release rate of a propagating crack, various configurations are considered as shown in tables 2 and 3. Two types of interphase, namely, a stiff and a compliant interphase are considered. A stiff

Table 2. Isolated influence of interphase

t_i	E_i / E_m	E_{ft} / E_m	Model
$0.1r_o$	0.1	1	Compliant interphase
$0.1r_o$	10	1	Stiff interphase

Table 3. Incorporation of the effect of a stiff nanofiber

t_i	E_i / E_m	E_{ft} / E_m	Model
$0.1r_o$	0.1	10	Compliant interphase Stiff nanofiber
$0.1r_o$	5	10	Stiff interphase Stiff nanofiber

Table 4. Reference cases

t_i	E_i / E_m	E_{ft} / E_m
0	0	1
0	0	10

interphase is one whose elastic modulus is greater than that of the matrix, whereas a compliant interphase is one with a modulus smaller than that of the matrix.

As table 2 shows, to isolate the effect of the interphase, the nanofiber and matrix moduli are assumed to be equal in the first step of the study ($E_f/E_m = 1$). A compliant interphase has a modulus that is ten percent of the matrix modulus ($E_i/E_m = 0.1$). On the other hand, a stiff interphase has a modulus ten times the modulus of the matrix ($E_i/E_m = 10$). The interphase thickness is assumed to be ten percent of the nanofiber radius ($0.1r_o$). The Poisson's ratios of the three constituents i.e., nanofiber, matrix, and the interphase are assumed to be the same. Table 4 shows the reference cases against which the results are compared. These are the cases with no interphase between the nanofiber and matrix.

After studying the influence of the interphase in an isolated configuration, a stiff nanofiber is considered with a compliant and then a stiff interphase. The properties used in this configuration are shown in the table 3. The interphase properties are unchanged from the ones used above. The results from these studies are compared to the reference configuration, which is the case when the interphase is absent ($t_i = 0$)

Figures 83 and 84 show the results for the effect of interphase elastic properties on mode I energy release rate of the propagating crack. From these figures, it is clear that the presence of an interphase has a profound influence on crack energetics. First of all, the influence of the interphase elastic properties is evident for the cases where the effect of the interphase is isolated ($E_f/E_m = 1$). The mode I energy release rate G_I/G_{I0} increases as the crack approaches the fiber with a compliant interphase ($E_f/E_m = 1$, $E_i/E_m = 0.1$) indicating an amplifying effect of the interphase. On the other hand, a stiff interphase ($E_f/E_m = 1$, $E_i/E_m = 10$) causes a shielding effect as shown by the decrease in the G_I/G_{I0} as the crack approaches the fiber.

The significant influence of the interface is again evident for the cases where a stiff nanofiber is considered. A compliant interphase around a stiff fiber ($E_f/E_m = 10$, $E_i/E_m = 0.1$) causes an amplifying effect on G_I/G_{I0} . As figure 84 shows, the curves belonging to all cases

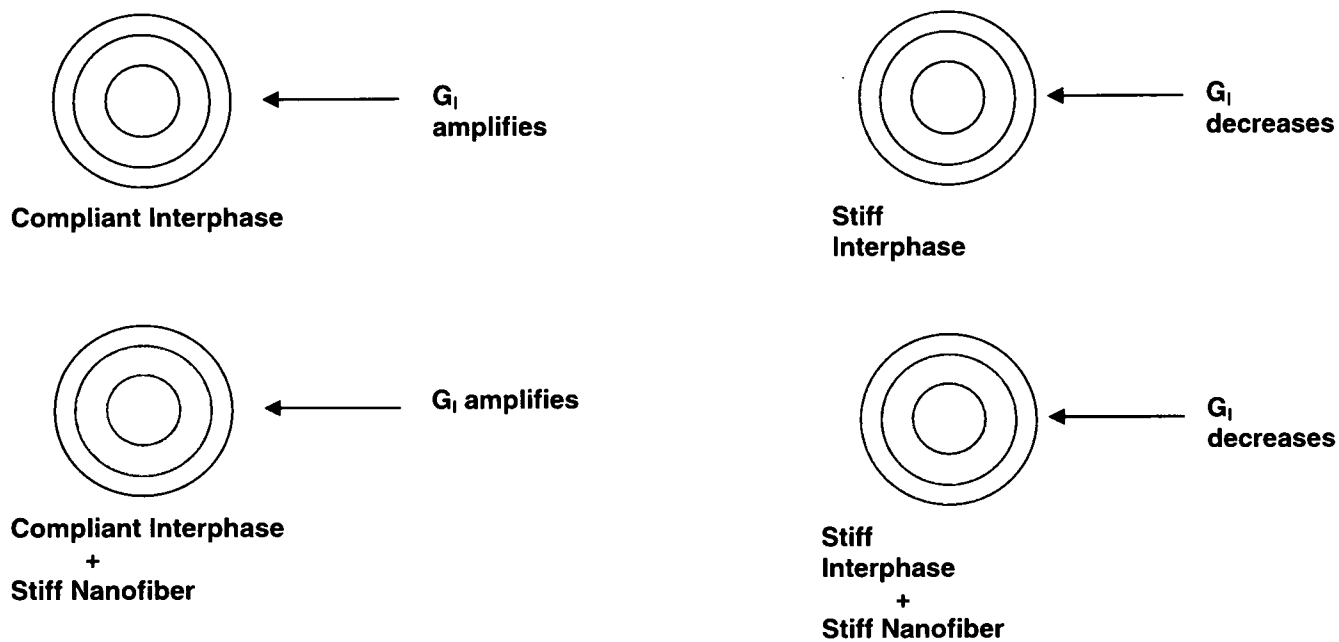


Figure 83. Influence of interphase elastic properties on mode I crack behavior

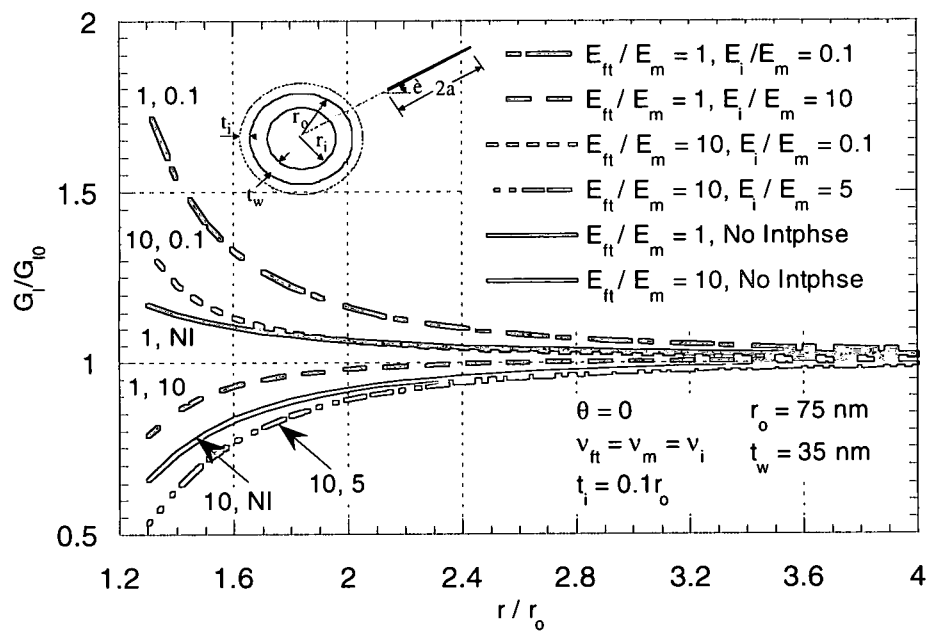


Figure 84. Influence of a stiff and a compliant interphase on G_I/G_{I0}

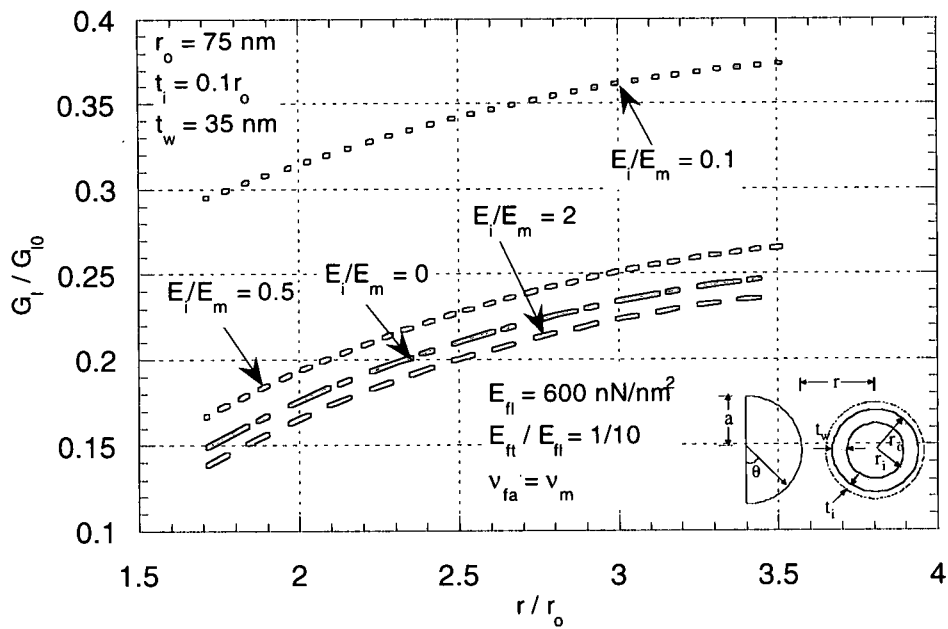


Figure 85. Influence of a stiff and compliant interphase on the mode I energy release rate

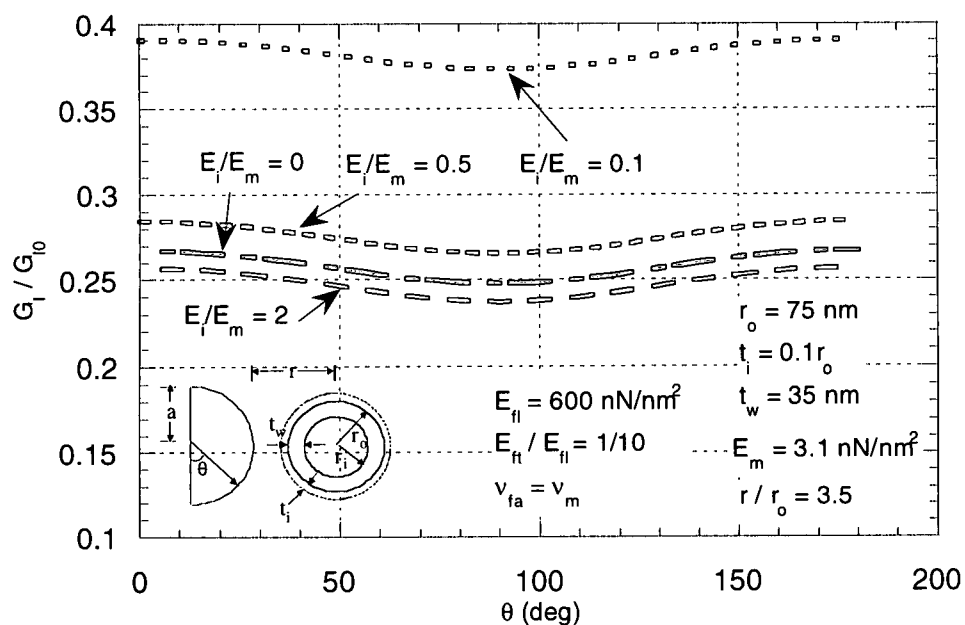


Figure 86. Influence of a stiff and compliant interphase on the mode I energy release rate at the farthest crack position

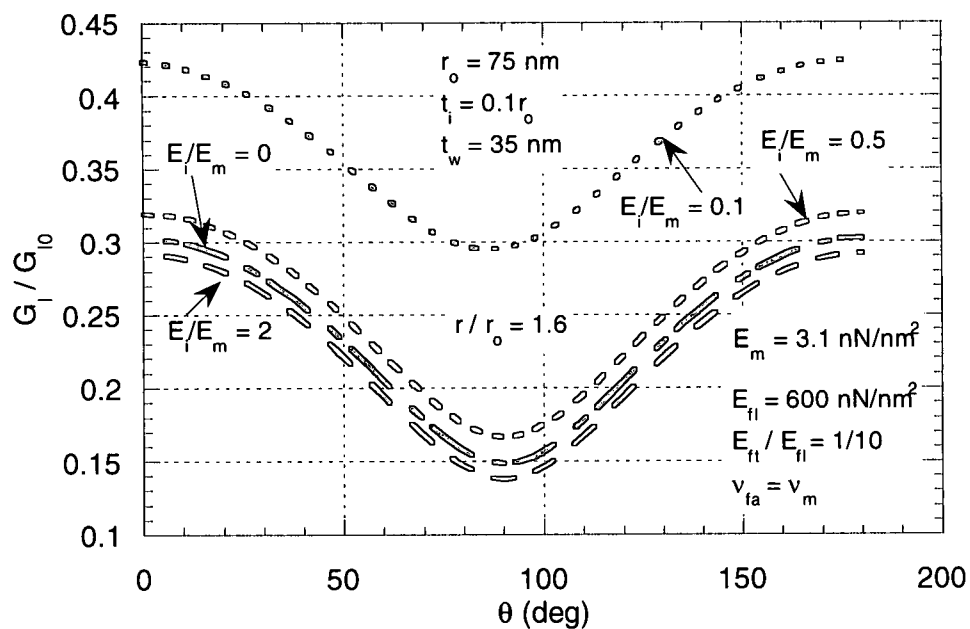


Figure 87. Influence of a stiff and compliant interphase on the mode I energy release rate at the closest crack position

when the interphase is compliant turn upward as the crack nears the nanofiber indicating an amplification effect. On the other hand, a stiff interphase in the similar configuration ($E_{if}/E_m = 10$, $E_i/E_m = 5$) provides a shielding effect, as the curve corresponding to this condition shows that the crack driving force decreases as the crack approaches the nanofiber. Now comparing the aforementioned results to the reference cases, one finds that in the absence of the interphase, a stiff fiber causes a shielding effect ($E_{if}/E_m = 10$, $E_i/E_m = 0$) whereas a fiber with the same properties as the matrix but without any interphase ($E_{if}/E_m = 1$, $E_i/E_m = 0$) causes an effect of a hole thereby amplifying G_I/G_{I0} as the crack approaches the fiber. From these results it is clear that in the presence of an interphase region between the nanofiber and crack, the behavior of a crack propagating towards the interphase is influenced more by the elastic properties of the interphase than those of the nanofiber itself.

Figures 85 to 87 show the results from the three-dimensional model. The three-dimensional model has the nanofiber longitudinal modulus incorporated. In this investigation, an interphase region is modeled with elastic properties that render the interphase stiff or compliant. The interphase modulus here is much smaller than the nanofiber longitudinal modulus. As is clear from figure 85, although the nanofiber longitudinal modulus seems to dominate the behavior, interphase properties can make a significant variation in the crack energetics. This can be seen from the curve for the most compliant interphase modulus ($E_i/E_m = 0.1$). Although there is a decrease in the energy release rate as the crack propagates towards the nanofiber, the energy release rate is approximately larger by 100 percent than the case when there is no interphase due to the presence of a very compliant interphase surrounding a very stiff nanofiber.

Figure 88 shows the influence of the interphase properties on mode II energy release rate. For the case when the matrix and nanofiber modulus values are assumed equal, a compliant interphase ($E_{if}/E_m = 1$, $E_i/E_m = 0.1$) clearly amplifies the energy release rate. A stiff interphase ($E_{if}/E_m = 1$, $E_i/E_m = 10$) also shows a different behavior as compared to the corresponding mode I case. The normalized mode II energy release rate G_{II}/G_{II0} slowly

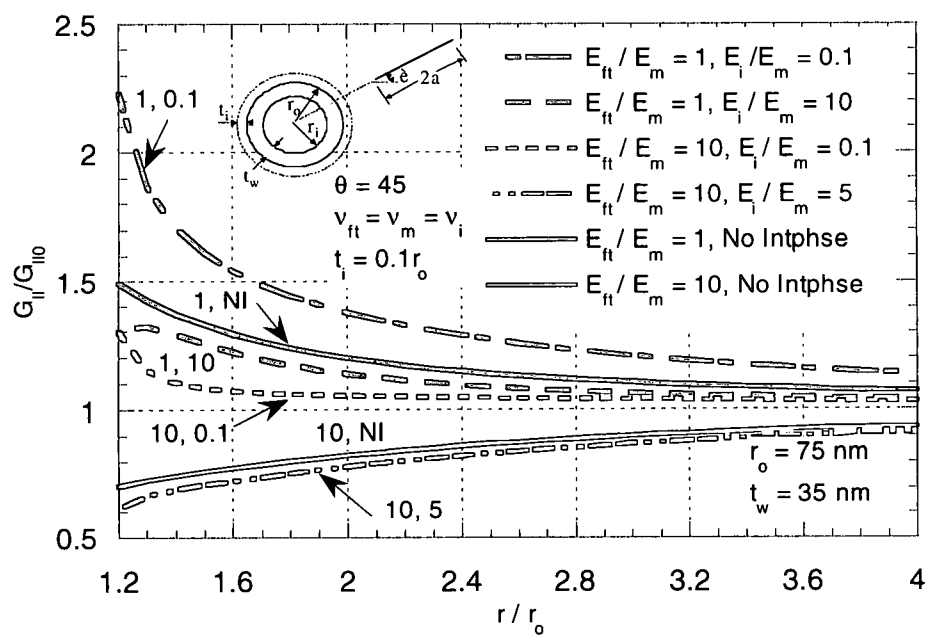


Figure 88. Influence of a stiff and a compliant interphase on G_{II}/G_{II0}

increases as the crack approaches and then seems to drop as the crack is very close to the fiber. This indicates that an interphase with a given elastic properties may have a more degrading effect on the mode II crack propagation as compared to mode I.

For the case of a stiff fiber and a compliant interphase ($E_f/E_m = 10$, $E_i/E_m = 0.1$), G_{II}/G_{II0} remains almost constant as the crack approaches the fiber. It shows the effect of a nearby weak interphase as it is within approximately one and half fiber radii away from the nanofiber center as it amplifies. For the same nanofiber-matrix modular ratio but with an interphase stiffer than the matrix ($E_f/E_m = 10$, $E_i/E_m = 5$), there is a significant change in the trend as the crack now experiences a shielding effect as shown in the figure. In comparison, there is a shielding effect in mode II with a fiber with the same stiffness as above but without any interphase being present ($E_f/E_m = 10$, $E_i/E_m = 0$) between the fiber and matrix. Thus the mode II crack propagation behavior in the presence of a stiff fiber can still be dictated by the interphase properties rather than the fiber properties.

Influence of Interphase Thickness

The other variable that is investigated besides the interphase elastic properties is the interphase thickness. Like the elastic properties, the interphase thickness for a nanofiber-matrix system is not very well known to date. To investigate the influence of interphase dimensions on the crack energetics, three different interphase thicknesses are considered as shown in the table 5. The interphase thickness values considered are 5, 10, and 20 percent of the nanofiber outer radius. Again, a compliant and a stiff interphase are modeled. The nanofiber and matrix moduli are assumed to be the same in order to isolate the effect of the interphase. Figures 7 to 9 show the results of the investigation.

As shown schematically in figure 89, the influence of an increasing interphase thickness can be advantageous or disadvantageous depending upon whether the interphase is stiff or compliant. Figure 90 shows that a compliant interphase ($E_i/E_m = 0.1$) will have a more and

Table 5. Details of the models considered to investigate the influence of the interphase thickness

t_i	E_i / E_m	E_{it} / E_m	Model
$0.05r_o, 0.1r_o, 0.2r_o$	0.1	1	Compliant interphase
$0.05r_o, 0.1r_o, 0.2r_o$	10	1	Stiff interphase

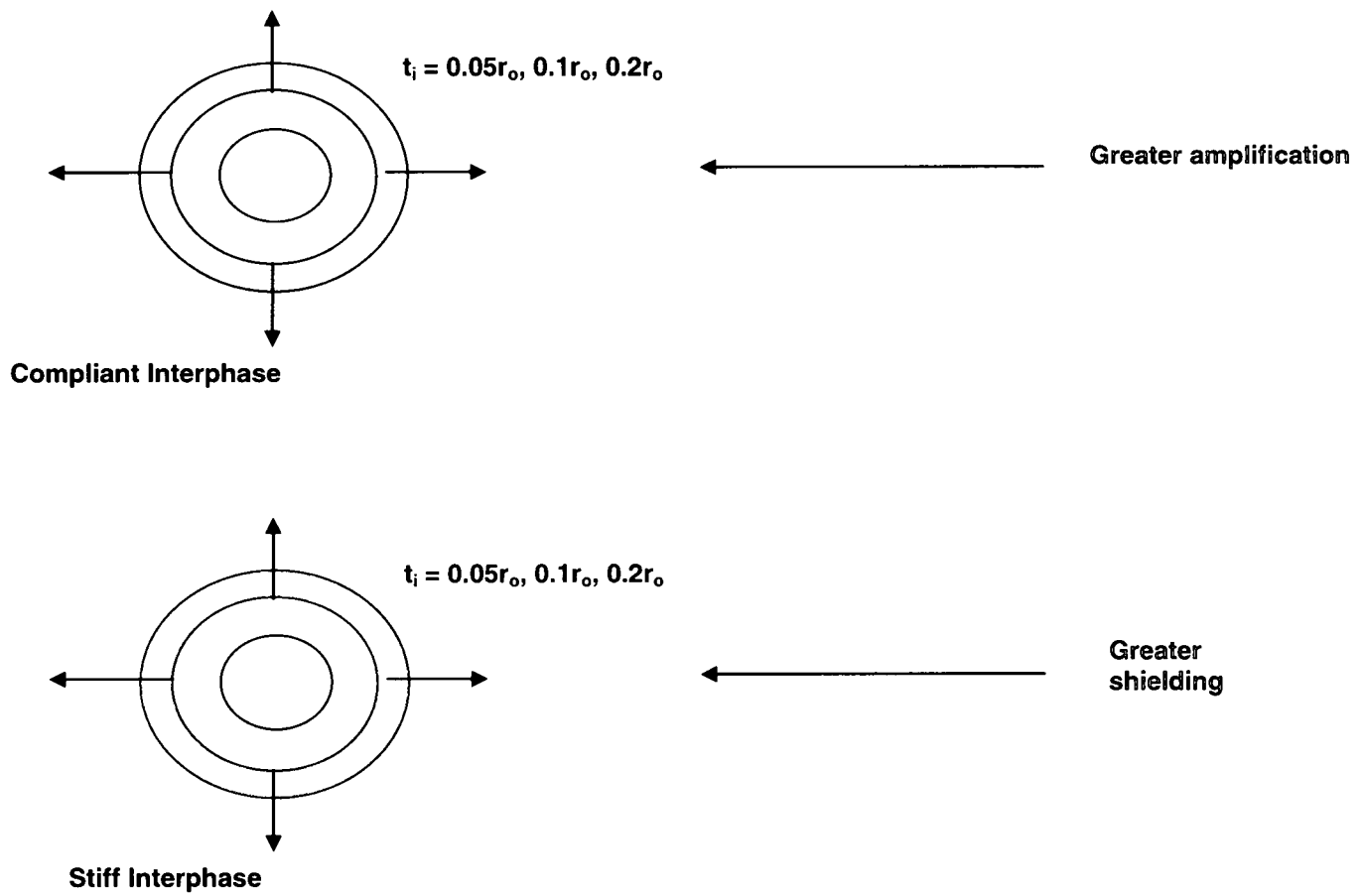


Figure 89. Schematic of the results for the investigation of the Influence of the interphase thickness on G_I/G_{I0}

more degrading influence on mode I crack energetics as its thickness is increased. Thus, energy release rate for a propagating crack experiences a larger amplification with the increasing interphase thickness.

The influence of increasing interphase thickness in the case of a stiff interphase is opposite of that in case of a compliant interphase. Figure 91 shows the influence of the interphase thickness when the interphase is stiff ($E_i/E_m = 10$). Now, having a larger interphase thickness enhances the toughening against mode I crack propagation. This is indicated by the energy release rate curves for various interphase thicknesses (t_i). With a larger interphase thickness, there is a greater reduction in the energy release rate as the crack propagates towards the nanofiber. The trend of the curves in figure 9 is exactly opposite of the trend for the curves in the figure 90.

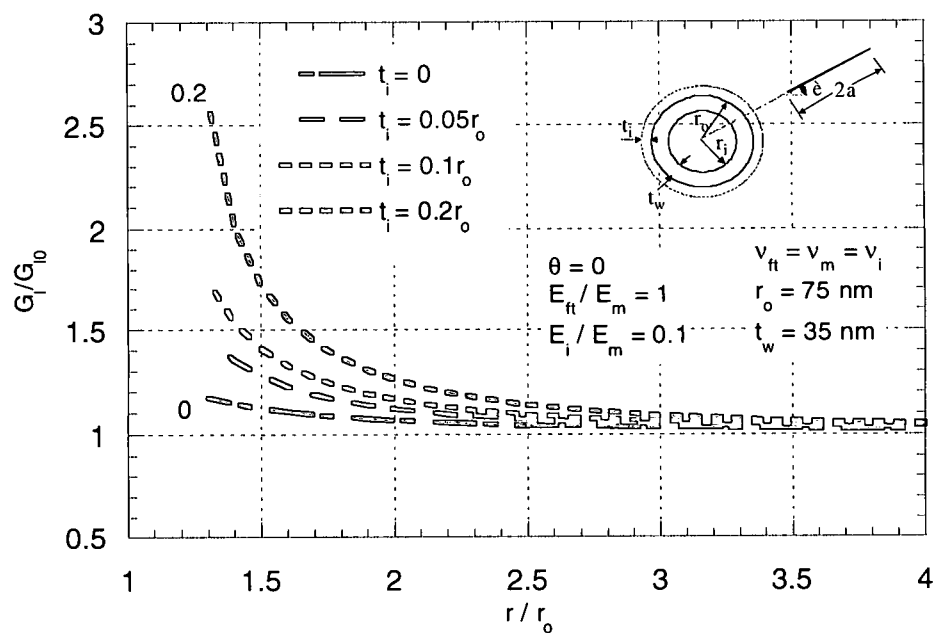


Figure 90. Influence of the interphase thickness on G/G_0 when the interphase is compliant than the matrix

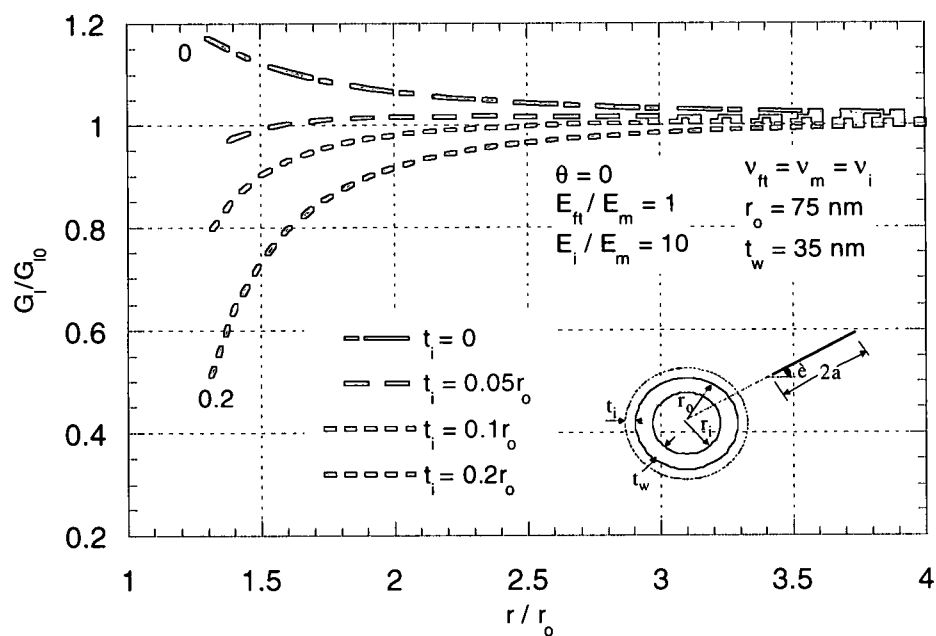


Figure 91. Influence of the interphase thickness on G/G_0 when the interphase is stiffer than the matrix

CHAPTER VII

CHARACTERIZATION OF THE INFLUENCE OF NANOFIBER DIAMETER

The nanofibers that are available today as composite reinforcement show a range of diameters that range from 100 to 200 nm. With the nanofiber geometry being hollow, question arises as to what influence the nanofiber diameter may have on nanofiber toughening. To investigate the same, three representative diameter values are considered and their influence on the energy release rate of a propagating crack studied. The nanofiber outer radius values used are,

$$R_o = 50, 75, 100 \text{ nm}$$

The nanofiber wall thickness is fixed and is 20 nm. The results are presented in the following sections.

Influence of Nanofiber Diameter on Mode I Behavior

Figures 1 to 3 show the influence of nanofiber diameter on the mode I energy release rate of a propagating crack. These figures indicate that with a relatively small wall thickness, an increase in nanofiber diameter results in an increased mode I energy release rate with which the crack approaches the nanofiber. At the same time, for all diameters considered, the crack experiences a decrease in the crack driving force as it approaches the nanofiber. thus, the crack seems to be responding to both the stiffness of the nanofiber and the hollow geometry. With the increasing diameter, the hollow core size increases for a fixed wall thickness. The increased energy release rate for a higher diameter seems to be the consequence of this increased hole size. Also, as figures 1 to 3 show, the trend observed for the mode I behavior seems to be insensitive to the crack orientation (θ).

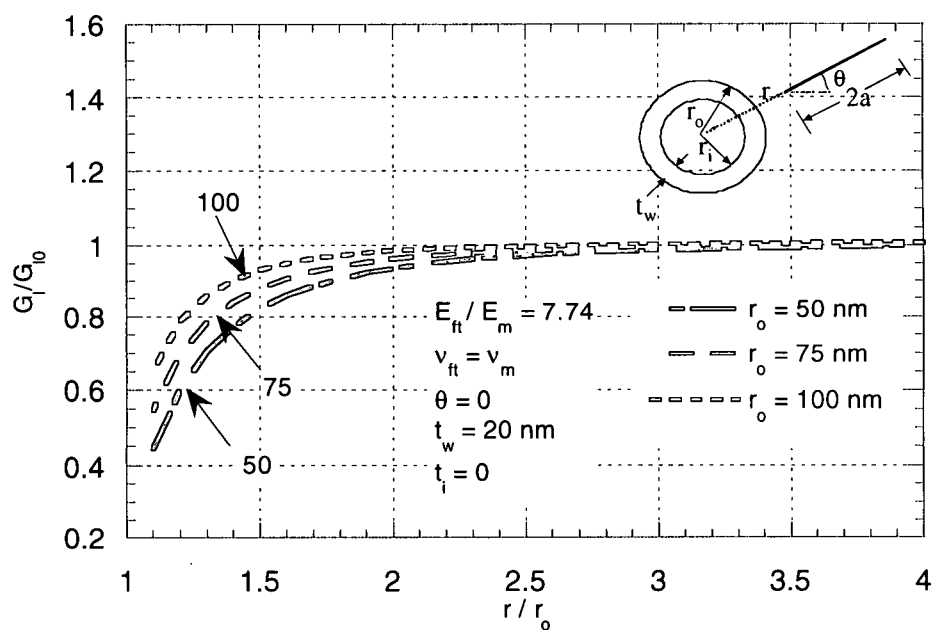


Figure 92. Influence of the nanofiber diameter on G/G_0

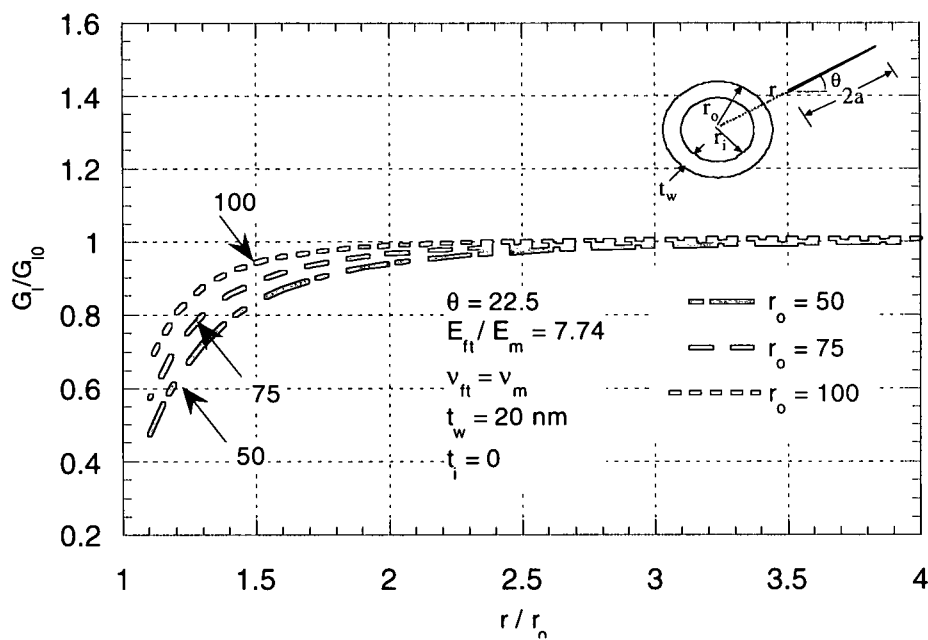


Figure 93. Influence of the nanofiber diameter on G/G_0

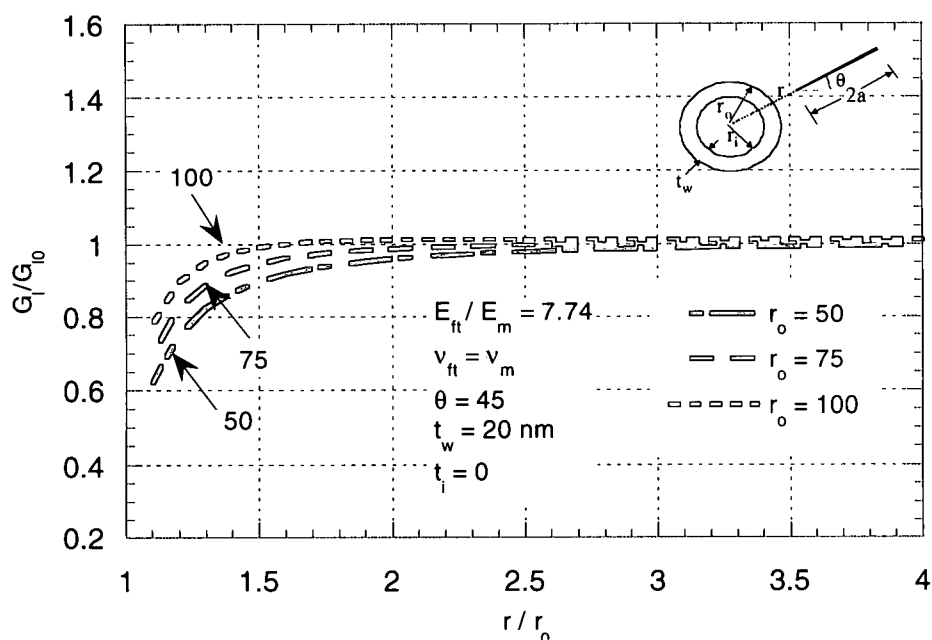


Figure 94. Influence of the nanofiber diameter on G_l/G_{l0}

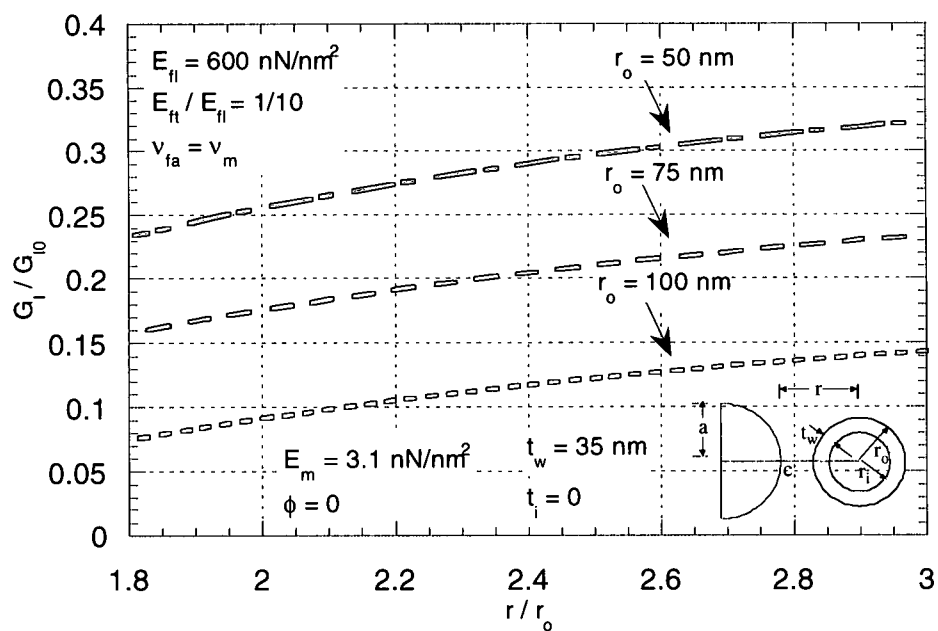


Figure 95. Influence of the nanofiber diameter on G_l/G_{l0}

Figures 4 to 6 show the results of the three-dimensional investigation to study the influence of nanofiber diameter on mode I crack energetics. In this case, the nanofiber wall thickness is increased and is 35 nm as compared to 20 nm used previously. As the figures show, the trend now seems to be reversed with the increased wall thickness. Now, the larger diameter enhances the mode I toughening by nanofiber. As a result, the mode I energy release rate is smaller for a larger nanofiber diameter. Thus, the influence of the nanofiber diameter on mode I energy release rate of the propagating crack is dependent on the nanofiber wall thickness. For a relatively small wall thickness, increasing the diameter seems to degrade the nanofiber toughening. On the other hand, for a relatively large wall thickness, the increasing diameter will result in the betterment of the resistance to crack propagation.

Influence of Nanofiber Diameter on Mode II Behavior

Figures 7 and 8 show the influence of the nanofiber diameter on the mode II crack propagation. It is clear from the figures that mode II behavior is more sensitive to the variation in the nanofiber diameter than corresponding mode I behavior. For the diameters of 150 nm and 200 nm, there is actually amplification in G_{II}/G_{II0} as the crack propagates towards the nanofiber. It is only when the crack is at its closest positions with respect to the nanofiber, that the energy release rate is checked. For the same values of nanofiber diameter and wall thickness, the mode I energy release rate experiences shielding effect of the nanofiber indicated by the decreasing G_I/G_{I0} for the crack propagating towards the nanofiber. Only the smallest diameter considered, that of 100 nm provides a pronounced shielding effect in the case of mode II propagation.

The influence of varying the nanofiber diameter on G_{II}/G_{II0} is similar to that on G_I/G_{I0} in that, in both cases increasing the diameter results in the higher shift for the energy release rate curve. But, whereas there is shielding effect of the fiber in the case of G_I / G_{I0} , there is an amplification effect in the case of G_{II} / G_{II0} for larger diameters considered. In this case the fiber diameter increase has a deteriorating effect. Figures 7 and 8 also indicate that, like the

trend observed in the case of mode I behavior, the mode II energy release rate trend in conjunction with the influence of nanofiber diameter is not sensitive to the crack orientation.

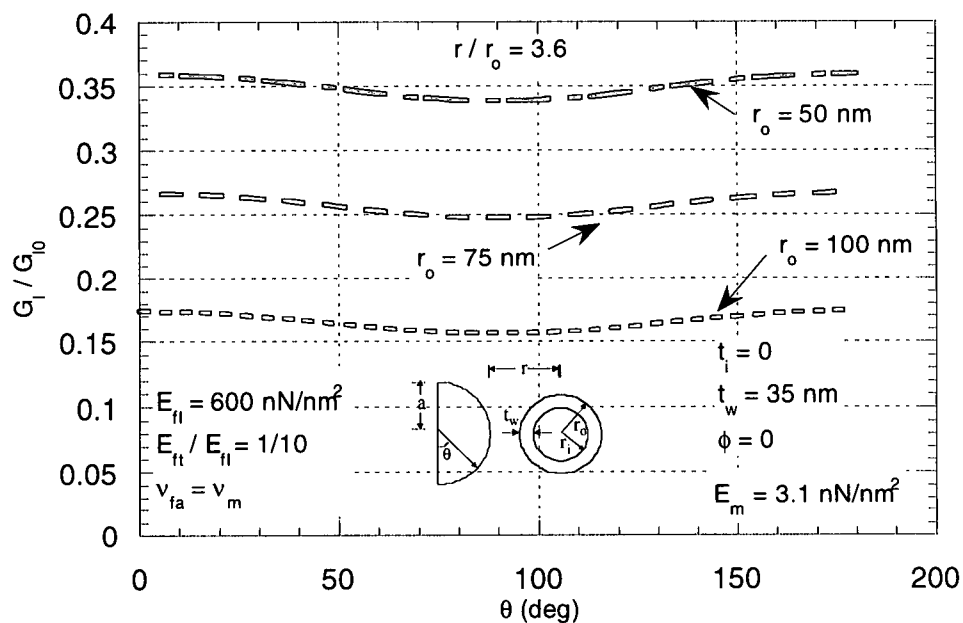


Figure 96. Influence of nanofiber diameter on Mode I energy release rate along the crack front

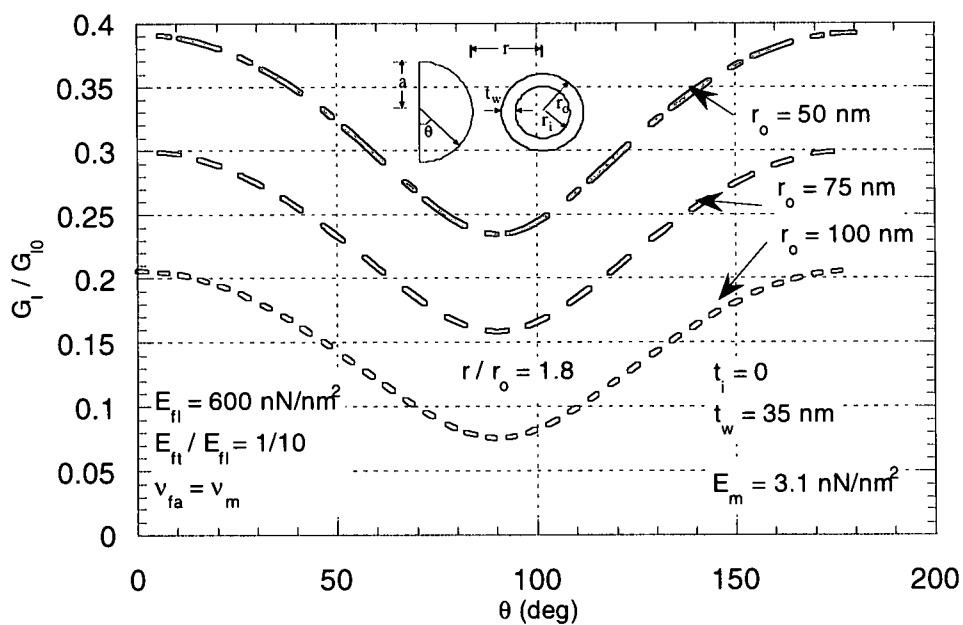


Figure 97. Influence of nanofiber diameter on Mode I energy release rate along the crack front

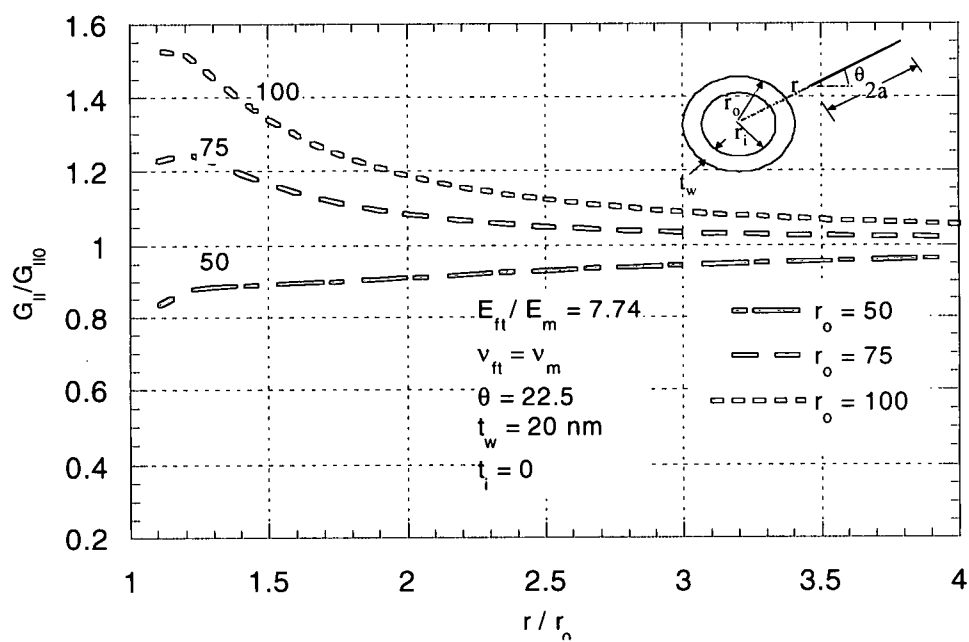


Figure 98. Influence of the nanofiber diameter on G_{II}/G_{II0}

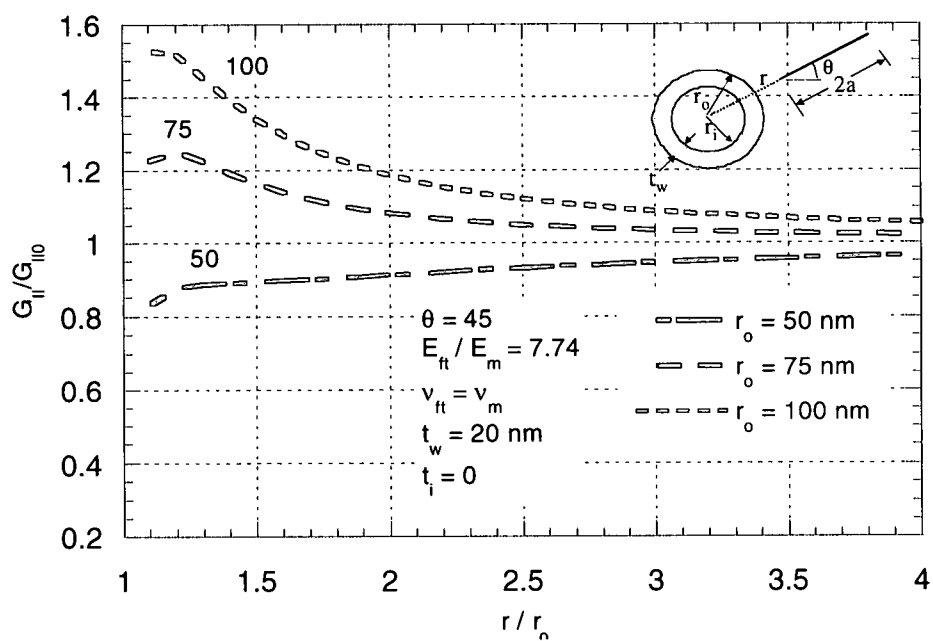


Figure 99. Influence of the nanofiber diameter on G_{II}/G_{II0}

CHAPTER VIII

CONCLUSIONS AND RECOMMENDATIONS

The present work is the first one to analytically investigate the influence of a hollow nanofiber on a propagating crack in the matrix, as the literature search does not reveal any other analytical work in conjunction with the nanofiber-crack interaction in a nanofiber reinforced composite. The nanofibers considered in this study are novel materials that are being currently explored as a reinforcement material in a structural composite. Such nanoscale materials have been reported to possess exceptional thermo-mechanical properties and thus hold tremendous potential to improve conventionally weak links in laminated composites like through the thickness properties and matrix-dominated properties. However, for all potential improvements predicted, the research work on the fracture characterization of materials like nanofiber reinforced composites remains mostly empirical. This study characterizes the fracture behavior of carbon nanofiber reinforced composites by considering the nanofiber-crack interaction. Mixed mode energy release rates are computed to study the influence of nanofiber on crack energetics. In addition, maximum values of normal interface tractions and shear interface tractions are computed along with their locations.

Summary of Variables

The nanofibers considered in this study make it necessary to model various features that are either not considered before in conjunction with crack-inclusion interaction, or are important in the context of the nanoscale nature of the problem. Following is a summary of variables that are considered to characterize the fracture behavior of the polymer matrix material reinforced with carbon nanofibers.

Nanofiber Elastic Moduli and Poisson's Ratio

The nanofibers considered in the present work are manufactured with a lack of controllability on their structure in terms of the orientations of graphitic planes that make up the nanofiber walls. As a consequence of this arrangement, the nanofibers are reported to show transversely isotropic elastic properties. However, the elastic moduli and the Poisson's ratio of nanofibers are a function of the orientation of the graphite planes that constitute the nanofiber geometry, and hence are expected to show significant variation in the absence of controllability in the processing. At the same time, the nanofiber longitudinal modulus is reported to be as large as 600 GPa. Therefore, for a material like nanofiber reinforced composite the fracture behavior should be studied not only for the influence of the modulus value, but also investigated for the sensitivity to the variation in the modulus values. The same can be said about the influence of the nanofiber Poisson's ratio.

Nanofiber Wall Thickness

The hollow geometry of nanofibers introduces a new variable in the characterization, which is the nanofiber wall thickness. The wall thickness of nanofiber varies and can be as large as 90 percent of the nanofiber outer radius. The nanofiber wall thickness represents an interesting factor to be considered in the fracture characterization. The question arises as to for a fixed nanofiber diameter, how the wall thickness will influence the crack energetics. There may be a case for having maximum resistance to crack propagation with the minimum possible wall thickness.

Interphase between Nanofiber and Matrix

Considering the effect an interphase region has on the crack energetics perhaps exemplifies the features that need to be accounted for when considering a fracture problem involving nanoscale material. Nanofiber dimensions are the same order of magnitude as the length of a polymer molecule chain. As a consequence, there is expected to be an interphase region in a material like carbon nanofiber reinforced composite that is more dominant than

the one in conventional composite. Thus, when studying the behavior of a crack propagating towards a nanofiber, the effect of the interphase region needs consideration. For instance, there may be an interphase region that is compliant, i. e., having elastic modulus smaller than that of the matrix. Now, if such interphase surrounds a very stiff nanofiber, the question arises as to how the crack energetics will be influenced. However, as of today little is understood about the interphase region in terms of its elastic behavior and thickness.

Nanofiber Diameter

The final variable investigated in the present study in conjunction with nanofiber-crack interaction is nanofiber diameter. Like the other nanofiber dimensions, nanofiber diameter shows a range of values between 100 to 200 nm. The nanofiber diameter becomes even more important to characterize in terms of its influence on crack energetics due to the hollow nanofiber geometry. The question to be addressed is that for a fixed nanofiber wall thickness, how will the nanofiber diameter affect its resistance to crack propagation. For example, is a large nanofiber diameter desirable? Or will it depend on the wall thickness?

Significant Results

The results of the investigation of nanofiber elastic properties in terms of its influence on nanofiber-crack interaction shows that although the crack driving force can be significantly affected by the nanofiber elastic modulus, it is the mode II behavior that shows a greater sensitivity to the variation in the nanofiber elastic modulus. Also, nanofiber provides a greater shielding effect against mode I propagation than mode II. Both, mode I and mode II trends observed are not sensitive to crack orientation. This means that crack orientation may not be an issue when one is concerned with aligning the nanofibers with respect to the expected path of crack extension.

The three-dimensional study shows that with a large nanofiber longitudinal modulus there can be a significant shielding effect of nanofiber if the nanofiber longitudinal axis is approximately perpendicular to the crack plane. Also, with a large longitudinal modulus the

influence of nanofiber is seemingly over a large region as indicated by a significantly small crack driving force exhibited by the farthest crack positions considered. These results from the three-dimensional modeling may represent an upper bound on the fracture behavior in the presence of nanofibers. On the other hand, the two-dimensional configuration wherein the nanofiber transverse modulus dominates the behavior may represent a lower bound on the fracture toughening provided by nanofibers.

The investigation of the influence of the Poisson's ratio on the crack energetics reveals that a smaller nanofiber Poisson's ratio results in the larger mode I crack driving force for a propagating crack. Also, for a relatively small nanofiber wall thickness, the crack always seem to experience mode I amplification regardless of the Poisson's ratio value. On the other hand, Poisson's ratio investigation is perhaps the only case where mode II behavior shows much less sensitivity to the variation of Poisson's ratio as compared to the mode I case. Overall, the investigation of the Poisson's ratio influence suggests that a nanofiber should have a large wall thickness and Poisson's ratio values.

The investigation of the influence of nanofiber wall thickness on the crack driving force of a propagating crack reveals that the wall thickness has a significant influence on the nanofiber toughening. As expected, a larger wall thickness results in a larger reduction in the energy release rate of a propagating crack. However, there seems to be a wall thickness value beyond which there seems to be no further significant advantage of increasing the wall thickness. This can be observed for both the mode I and mode II behavior. Again, it's the mode II behavior that shows a greater sensitivity to the variation in the wall thickness. The results of the study also indicate that the nanofiber wall thickness becomes more critical from the perspective of nanofiber toughening when the nanofiber modulus is small. Finally, with a relatively small wall thickness, the nanofiber offers better shielding effect in mode I as compared to mode II condition.

The influence of nanofiber wall thickness on the interface tractions also reveals a significant influence of nanofiber wall thickness. Maximum normal tractions show a reversal in trend with an increasing wall thickness, whereas the shear tractions show no such reversal

and are larger for a smaller wall thickness. The nanofiber wall thickness also affects the location of the maximum tractions. The locations of the maximum normal traction for the smallest wall thicknesses considered show a significantly different trend from that for the larger wall thickness values.

The results of the investigation of the influence of the interphase on crack energetics reveal the importance of understanding the interphase region in terms of its properties and dimensions. In the presence of an interphase region, the crack energetics is considerably altered. The crack seems to be responding more to the interphase than to the stiff nanofiber. A compliant interphase (stiffness less than that of the matrix) causes an amplification in the energy release rate, whereas a stiff interphase shields the crack propagation. A compliant interphase surrounding a stiff nanofiber still results in an amplification of crack driving force, indicating the tendency of the crack to respond to the nature of the interphase rather than that of the reinforcement. The mode II crack driving force seems to show a more complex behavior in the presence of an interphase. An interphase of given stiffness has a more degrading effect on mode II crack propagation.

The nanofiber diameter is another variable that shows the influence of the nanofiber hollow geometry on crack energetics. It is observed that with a relatively small wall thickness, a large nanofiber diameter actually results in a reduced resistance to the crack propagation as compared to a nanofiber of smaller diameter with identical wall thickness. On the other hand, the trend reverses with a relatively large wall thickness. Now, a larger diameter nanofiber causes a greater reduction in the crack driving force of a propagating crack for identical wall thickness.

Finally, the present work also investigated the nanofiber-matrix interface traction behavior. The maximum values of the normal and shear components of the traction are obtained along with their locations. It is observed that as a crack propagates towards a nanofiber, the maximum values of normal and shear tractions amplify. Overall, it is observed that the normal tractions show a greater degree of amplification. Thus, a failure like debonding seems to be a probable mode of secondary failure.

Maximum interface tractions are significantly influenced by the nanofiber wall thickness and for the closest crack positions are greater for a smaller wall thickness. However, maximum normal tractions show a reversal in the trend as for the farthest crack positions the greater wall thickness yields a greater normal traction value. Interface tractions show no sensitivity to the variation in the nanofiber modulus and in most cases to the crack orientations. The only exception is the maximum shear traction trends for various wall thicknesses considered. In this case, the trends show a variation with the change in the crack orientations. The locations of the maximum tractions show a shift as the crack propagates towards the nanofiber. The locations of maximum tractions seem to be shifting towards the projected point of intersection of the crack and the nanofiber. These locations are the possible points from where an interface failure may initiate.

Recommendations for Experimental Validation

Nanofibers considered in the present study are nanoscale materials and hence are extremely difficult in terms of controllability. As such, an experimental validation of the results obtained in this study may be a difficult task. However, an insight may be gained as to the validity of the predictions of this study, especially the characterization of the influence of nanofiber wall thickness on crack energetics. To this end, hollow rods of variable thickness can be used with a matrix material like epoxy. Experiments can then be performed in a controlled setting to evaluate the effect of nanofiber wall thickness on the energy release rate of a propagating crack. The hollow rods can be of a suitable material type (Aluminum, Steel, etc). Such experimentation may be utilized to corroborate the observation from this study that there seems to be a threshold value of the wall thickness beyond which there is no significant gain in the fracture toughness achieved by the nanofiber reinforcement.

Desirable Nanofiber Properties for Fracture

In the present study various investigations are performed to characterize the influence of a reinforcing nanofiber on the fracture behavior of a nanofiber-reinforced composite. The

results show that for some of the investigations a small nanofiber wall thickness resulted in amplifying the mode II crack driving force. For the corresponding mode I case the nanofiber seem to be providing a better resistance. Based on this observation it seems that a small nanofiber wall thickness can be afforded when the conditions are that of pure mode I. on the other hand, a relatively greater wall thickness may be needed in mixed mode conditions or pure mode II conditions. The other reason for preferring a wall thickness that is too small may be the interface tractions as they attain larger values for smaller wall thicknesses.

The results from the study show that, with a hollow geometry, the nanofibers should preferably have a large Poisson's ratio as the small value of the same results in amplifying the crack propagation irrespective of the other nanofiber features like wall thickness value. The three-dimensional study makes the case for a large nanofiber longitudinal modulus if nanofiber alignment can be controlled with respect to the direction of crack propagation. Finally, the variation in the nanofiber properties should be as small as possible when mode II conditions are present as the mode II behavior seems to be much more sensitive to these variations as compared to mode I.

Recommendation for future work

Based on the present study following recommendations are made to extend the research on the fracture behavior of the nanocomposite reinforced with carbon nanofibers.

1. Multitude of arbitrarily oriented nanofibers should be considered in order to better predict the bulk fracture behavior.
2. The most important characteristic of a system that contains nanoscale material is that there is a tremendous increase in the surface area and surface energy due to a dramatic increase in the interface/interphase between the bulk material and the nanoscale material. On the other hand, the research to date has reported that achieving the adhesion between the nanofibers and matrix is still a challenge and the actual property improvements fall well below those predicted due to a possible lack of adhesion between the nanofibers and matrix material. Thus, an effort should be

made to understand the mechanics of the interphase/interface effects in a nanofiber reinforced composite system in order to better predict the fracture behavior.

3. The present study is a continuum mechanics perspective on the nanofiber-crack interaction problem. Although a feature like an interphase between the nanofiber and matrix has been modeled, there may be need to include yet unknown nanoscale features. Thus, the continuum mechanics perspective should be complemented by other point of views like molecular mechanics to advance the knowledge of the fracture behavior in the presence of carbon nanofibers.
4. The present study assumes that the crack propagation occurs self-similarly under the action of a far field uniaxial stress. Studies should be undertaken to evaluate the fracture behavior in fatigue loading conditions.
5. The present study considers stiff nanofibers that create a mismatch in the elastic properties in the composite system. This mismatch alters the crack energetics relative to material not reinforced. Similarly, there can be mismatch between the coefficients of thermal expansion of matrix and nanofibers. This, and phenomenon like matrix cure shrinkage may result in the creation of residual stresses in the vicinity of fiber-matrix interface. These stresses can be tensile or compressive depending upon the nature of constituent materials. If the stresses are tensile, they may lead to interface separation. Residual stresses are not considered in the present study. This work thus can be extended to include the influence of residual stresses. For example, an interface crack subjected to internal pressure corresponding to residual stresses can be considered

Recommendations for Material Scientists

Based on the results of the two-dimensional and three-dimensional finite element studies of the interaction between a matrix crack and a nanofiber, following recommendations are put forth for the material scientists.

1. Effort should be made to understand the nature of the interphase between the nanofiber and matrix. Currently not much has been reported with regards to the nature of the interphase between a nanofiber and matrix. at the same time, the nature of the interphase influences the fracture behavior in various ways. An interphase that is just weak enough to allow debonding will help dissipate energy and hence may improve the fracture toughness. As this study demonstrates, the interphase properties significantly affect crack energetics and therefore warrant an effort to better understand the interphase.
2. Techniques should be developed to control the alignment of the nanofiber, as a nanofiber aligned perpendicular to the plane of the crack not only provides a strong shielding effect, it also ensures that the influence is present in a region that is very large compared to the nanofiber diameter.
3. The nanofiber wall thickness can be relatively small if the fracture conditions are mode I. On the other hand, if the loading on the structure is going to be that inducing the mode II crack propagation, the nanofiber wall thickness should be comparatively larger.

REFERENCES

1. Vaia, R. A., et al., "Polymer Nanocomposites: Status and Opportunities," MRS Bulletin, May 2001
2. Thostenson, E. T., et al., "Carbon Nanotube/Carbon Fiber Hybrid Multiscale Composites," Journal of Applied Physics, 91 (9): 6034-6037 (2002)
3. Saltysiak, B., et al., "Nanofiber Reinforcement of PMMA – The Hope and the Reality," In 17 th Technical Conference of American Society for Composites, 2002, Purdue University, West Lafayette, IN
4. Applied Sciences Incorporated, website at <http://www.apsci.com/ppi-pyro3.html>
5. Tandon, G. P., et al., "Influence of Vapor-Grown Carbon Nanofibers on Thermomechanical Properties of Graphite-Epoxy Composites," In 17 th Technical Conference of American Society for Composites, 2002, Purdue University, West Lafayette, IN
6. Whitney, Thomas, University of Dayton Research Institute, private communication
7. Tandon, G. P., University of Dayton Research Institute, private communication
8. Gao, H., et al., "Modeling Fracture in Nano-materials Via a Virtual Internal Bond Method," Engineering Fracture Mechanics, 70(14): 1777-1791 (2003)
9. Roy, A., et al., "Effective Thermoelastic Properties of Nanocomposites with Prescribed Random Orientation of Nanofibers"
10. Odegard, G. M., et al., "Constitutive Modeling of Nanotube-Reinforced Polymer Composites," Composites Science and Technology, 63: 1671-1687 (2003)
11. Odegard, G. M., et al., "Comparison of Two Models of SWCN Polymer Composites," Composites Science and Technology, 64: 1011-1020 (2004)
12. Wei, C., et al., "Nanomechanics of Carbon Nanofibers: Structural and Elastic Properties," Applied Physics Letters, 85 (12): 2208-2210 (2004)
13. Cottrell, A. H., "Continuum and Atomistic Theories of Mechanics of Materials," Fracture: A topical Encyclopedia of Current Knowledge, Krieger Publishing Company, 368-374 (1998)
14. Lake, M. L., et al., "Nanocomposites from Carbon Nanofiber," In 17 th Technical Conference of American Society for Composites, 2002, Purdue University, West Lafayette, IN

15. Private communication with an engineer from the manufacturer of vapor grown carbon nanofibers
16. Air Force Research Laboratory, website at <http://www.ml.afrl.af.mil/stories/mlb-00378.html>
17. Waddoups, M. E., et al., "Macroscopic Fracture Mechanics of Advanced Composite Materials," *Journal of Composite Materials*, 5: 446-554 (1971)
18. Nairn, J. A., "Fracture Mechanics of Composites with Residual Stresses, Traction-Loaded Cracks, and Imperfect Interfaces," *Composite Science and Technology*, 61, 2159-2167 (2000).
19. Shofner, M. L., et al., "Nanofiber-Reinforced Polymers Prepared by Fused Deposition Molding," *Journal of Applied Polymer Science*, 89: 3081-3090 (2003)
20. Wu, X., "Fracture of Advanced Laminated Composites with nanofiber Reinforced Interfaces," Ph. D. Thesis, University of Nebraska-Lincoln
21. Madhukar, M. S., et al., "Fiber-Matrix Adhesion and its Effect on Composite Mechanical Properties: IV. Mode I and Mode II Fracture Toughness of Graphite/Epoxy Composites," *J. Composite Materials*, 26, 7: 936-968 (1992)
22. Tsai, S. W., et al., "Role of Interface in the Strength of Composite Materials," Adhesion and Adsorption of Polymers, Part 8. New York, NY: Plenum Publishing Corp.
23. Anderson, T. L., *Fracture Mechanics Fundamentals and Applications*, Second Edition, CRC Press (1995)
24. Dugdale, D. S., "Yielding in Steel Sheets Containing Slits," *J. Mechanics and Physics of Solids*, 8: 100-104
25. Barenblatt, G. I., "The Mathematical Theory of Equilibrium Cracks in Brittle Fracture," *Advances in Applied Mechanics*, 7: 55-129 (1962)
26. Studer, M., et al., "Studies on Bridging Tractions-Simultaneous Bridging Tractions and COD Measurements," *Int. Journal of Fracture*, 114: 379-399 (2002)
27. Whitney, J. M., "Experimental Characterization of Delamination Fracture," in *Interlaminar Response of Composite Materials*, Composite Materials Series, 5, Edited by N. J. Pagano, 161-250 (1989)
28. Tamate, O., "The Effect of the Circular Inclusion on the Stresses Around a Line Crack in a Sheet Under Tension," *Int. J. Fracture Mechanics*, 4: 257-265 (1968)
29. Erdogan, F., "Stress Distribution in a Nonhomogeneous Elastic Plane with Cracks," *J. Applied Mechanics*, June 1963: 232-236
30. Liebowitz, J. S., et al., "Computational Fracture Mechanics: Research and Application," *Fracture: A topical Encyclopedia of Current Knowledge*, Krieger Publishing Company, 512-525 (1998)

31. Muskhelishvili, N. I., Some Basic Problems of the Mathematical Theory of Elasticity, P. Noordhoff Ltd (1953)
32. Becker, A. A., The Boundary Element Method in Engineering, McGraw-Hill Book Company (1992)
33. Meda, G., et al., "Path-independent J Integrals for Three-dimensional Fracture Mechanics," International Journal of Fracture, 94: 217 – 234 (1998)
34. Liebowitz, J. S., et al., "Smart Computational Fracture of Materials and Structures," Fracture: A topical Encyclopedia of Current Knowledge, Krieger Publishing Company, 526-540 (1998)
35. Cheeseman, B. A., et al., "The Interaction of a Curved Crack with a Circular Elastic Inclusion," International J. Fracture, 103: 259-277 (2000)
36. Helsing, J., et al., "On the Accuracy of Benchmark Tables and Graphical Results in the Applied Mechanics Literature," J. Applied Mechanics, 69: 88-90 (2002)
37. Wang, J., et al., "Benchmark Results for the Problem of Interaction Between a crack and a circular inclusion," J. Applied Mechanics, 70: 619-621 (2003)
38. Helsing, J., "Stress Intensity Factors for a Crack in Front of an Inclusion," Engineering Fracture Mechanics, 64: 245-253 (1999)
39. Muller, W. H., et al., "On the Behavior of R- and θ - Cracks in Composite Materials Under Thermal and Mechanical Loading," Int. J. Solids and Structures, 29: 1907-1918 (1992)
40. Patton, E. M., et al., "The Effect of Rigid Elliptical Inclusion on a Straight Crack," Int. Journal of Fracture, 46: 71-79 (1990)
41. Atkinson, C., "On the Stress Intensity Factors Associated with the Cracks Interacting with an Interface between Two Elastic Media," International Journal of Engineering Science, 13: 487-504 (1975)
42. Erdogan, F., Numerical Solutions of Singular Integral Equations, Vol. 1, Editor G. C., Noordhoff International, 1053-1067 (1972)
43. Romeo, A., et al., "A Crack Very Close to a Bimaterial Interface," journal of Applied Mechanics, 62: 614-619 (1995)
44. Selvadurai, A. P. S., "On Integral Equation Approaches to the Mechanics of Fiber-Crack Interaction," Engineering Analysis with Boundary Elements, 17: 287-294 (1996)
45. Mao, R., et al., "A Study of the Interaction between Matrix Crack and Matrix-Fiber Interface," Engineering Fracture Mechanics, 51(3): 469-477 (1995)
46. Steif, P. S., "A Semi-Infinite Crack Partially Penetrating a Circular Inclusion," Journal of Applied Mechanics, 54: 87-92 (1987)
47. Qin, Q. H., et al., "BEM for Crack-Inclusion Problems of Plane Thermopiezoelectric Solids," International Journal for Numerical Methods in Engineering, 48: 1071-1088 (2000)

48. Li, Z., et al., "The Near-Tip Stress Intensity Factor for a Crack Partially Penetrating an Inclusion," *Journal of Applied Mechanics*, 71: 465-469 (2004)
49. Li, R., et al., "Variation of the Energy Release Rate as a Crack Approaches and Passes through an Elastic Inclusion," *International Journal of Fracture*, 59: R69-R74 (1993)
50. Li, R., et al., "Energy Analysis of Crack Interaction with an Elastic Inclusion," *International Journal of Fracture*, 63: 247-261 (1993)
51. Knight, M. G., et al., "A Study of the Interaction between a Propagating Crack and an Uncoated/Coated Elastic Inclusion Using the BE Technique," *International Journal of Fracture*, 114: 47-61 (2002)
52. Xiao, Z. M., et al., "Stress Intensity Factor for a Griffith Crack Interacting with a Coated Inclusion," *International Journal Fracture*, 108: 193-205 (2001)
53. Cheeseman, B. A., et al., "The Effect of the Interphase on Crack-Inclusion Interactions," *International Journal of Fracture*, 109: 303-323 (2001)
54. Liu, Y., et al., "New Phenomena Concerning the Effect of Imperfect Bonding on Radial Matrix Cracking in Fiber Composites," *International Journal of Engineering Science*, 39: 2033-2050 (2001)
55. Bush, M. B., "The Interaction between a Crack and a Particle Cluster," *International Journal of Fracture*, 88: 215-232 (1997)
56. Yang, L., et al., "Crack-Inclusion Interaction for Mode II Crack Analyzed by Eshelby Equivalent Inclusion Method," *Engineering Fracture Mechanics*, 71: 1421-1433 (2004)
57. Shen, A., et al., "Analysis of the Singularity for the Vertical Contact Problem of Line Crack-Inclusion," *Applied Mathematics and Mechanics*, 22 (6): 630-636 (2001)
58. Lam, K. Y., et al., "Interaction between a Circular Inclusion and a Symmetrically Branched Crack," *Theoretical and Applied Fracture Mechanics*, 28: 197-211 (1998)
59. Chen, D., "The Effect of an Elliptical Inclusion on a Crack," *International Journal of Fracture*, 85: 351-364 (1997)
60. Noda, N. A., "Generalized Stress Intensity Factors in the Interaction within a Rectangular Array of Rectangular Inclusions," *Archive of Applied Mechanics*, 73: 311-322 (2003)
61. Dong, C. Y., et al., "An Integral Equation Approach to the Inclusion-Crack Interactions in Three-Dimensional Infinite Elastic Domain," *Computational Mechanics*, 29: 313-321 (2002)
62. Larson, M. C., "Experimental and Computational Models for Three-Dimensional Crack-Fiber Interactions," *Experimental Mechanics*, 37(4), 445-451 (1997)
63. Li, Z., et al., "Interaction between Three-Dimensional Crack and Near Piezoelectric Fiber, Sensors and Actuators A," 105: 10-22 (2003)

R702032129

HECKMAN

BINDERY, INC

T 022382 F 18 00



1/5/2006

64. ANSYS 8.1, SAS IP, Inc., 2002
65. ASM Handbook Vol 21, Composites
66. Nanotechnology, The Nanotech Report 2001
67. Gao, H., et al., "Modeling Fracture in Nano-materials Via a Virtual Internal Bond Method," *Engineering Fracture Mechanics*, 70(14): 1777-1791 (2003)
68. McKinney, J. M., "Mixed Mode Fracture of Unidirectional Graphite/Epoxy Composites," *J. Composite Materials*, 6: 164-166 (1971)
69. Haque, A., et al., "S2-Glass/Vinyl Ester Polymer Nanocomposites: Manufacturing, Structures, Thermal and Mechanical Properties," *Proceedings of 17 th Technical Conference of American Society for Composites*, 2002, Purdue University, West Lafayette, IN
70. Gerberich, W. W., et al., "Length Scales for the Fracture of Nanostructures," *International J. Fracture*, 119/120: 387-405 (2003)
71. Lourie, O., et al., "Evidence of Stress Transfer and Formation of Fracture Clusters in Carbon Nanotube-Based Composites," *Composite Science and Technology*, 59: 975-977 (1999)
72. Baker, R. T. K., "Synthesis, Properties and Applications of Graphite Nanofibers," http://www.wtec.org/loyola/nano/US.Review/09_03.htm
73. Paxton, J. P., et al., "Polymer Material Property Enhancement through Nanocomposite Technology," *Proceedings of the 16 th Technical Conference of American Society for Composites*, Virginia Tech, Blacksburg, Virginia
74. Paul, D. R., "Polymer Nanocomposites," *Proceedings of the 16 th Technical Conference of American Society for Composites*, Virginia Tech, Blacksburg, Virginia
75. Harik, V. M., "Ranges of Applicability for the Continuum Beam Model in the Mechanics of Carbon Nanotubes and nanorods," *Solid State Communications*, 120: 331-335 (2001)
76. Kelly, A., "Interface Effects and the Work of Fracture of a Fibrous Composite," *Proc. Royal Society of London A*, 319: 95-116 (1970)
77. Rice, J. R., "A Path Independent Integral and the Approximate Analysis of Strain Concentration by Notches and Cracks," *J. Applied Mechanics*, June 1968, 379-386
78. Griffith, A. A., "The Phenomena of Rupture and Flow in Solids," *Fracture: A Tropical Encyclopedia of Current Knowledge*, Krieger Publishing Company, 2-29 (1998)
79. Irwin, G. R., "Analysis of Stresses and Strains Near the End of a Crack Traversing a Plate," *Fracture: A Tropical Encyclopedia of Current Knowledge*, Krieger Publishing Company, 30-37 (1998)
80. Broek, D., *Elementary Engineering Fracture Mechanics*, Fifth Ed., Martinus Nijhoff Publishers (1987)